

**AN EXPERIMENTAL STUDY ON  
THE INTERFACIAL CHARACTERISTICS OF FIBER REINFORCED  
POLYMERIC COMPOSITES ENHANCED WITH NANO-SCALE MATERIALS**

**by  
Ece Belen**

**Submitted to the Graduate School of Engineering and Natural Sciences  
in partial fulfillment of the requirements for the degree of  
Master of Science**

**Sabanci University  
August, 2014**

AN EXPERIMENTAL STUDY ON  
THE INTERFACIAL CHARACTERISTICS OF FIBER REINFORCED POLYMERIC  
COMPOSITES ENHANCED WITH NANO-SCALE MATERIALS

APPROVED BY:

Assoc. Prof. Mehmet Yıldız

Assist. Prof. Serkan Ünal

Assoc. Prof. Bahattin Koç

Assoc. Prof. Fevzi Çakmak Cebeci

Prof. Yusuf Ziya Menceloğlu

DATE OF APPROVAL: 06.08.2014.....

© Ece Belen 2014

All Rights Reserve

# **AN EXPERIMENTAL STUDY ON THE INTERFACIAL CHARACTERISTICS OF FIBER REINFORCED POLYMERIC COMPOSITES ENHANCED WITH NANO-SCALE MATERIALS**

Ece Belen

MAT, Master of Science Thesis, 2014

Thesis Supervisor: Assoc. Prof. Mehmet Yıldız & Assist. Prof. Serkan Ünal

Keywords: Composite materials, carbon nanotubes, chemical functionalization, electrospraying, electrospinning, vacuum infusion, resin transfer molding

## **Abstract**

Fiber reinforced composites can be engineered to present excellent mechanical, thermal, electrical properties and corrosion resistance with low density if primary components are enhanced with the nano-phase materials. The nano-reinforcement should be integrated by using the industrially applicable and economically feasible method. Furthermore, the nano reinforcement strongly depends on the nanotube distribution at the interface between fiber and polymer matrix in the case of efficient load transfer from the matrix to the fiber. Therefore, we have to eliminate or even remove the common restrictions of carbon nanotube applications during our experiments. For this reason, chemical functionalization and surface characterization of multi walled carbon nanotubes (MWNTs) are significantly investigated prior to the electrospray deposition of functionalized CNTs at the interface of fiber reinforced polymeric composites which are manufactured by vacuum infusion method. The surface characterization of nanotube deposited reinforcing fibers and mechanical characterization of nano-integrated composites are presented in this thesis. Alternatively, RTM-manufactured electrospun nanofiber integrated glass-epoxy composites are also another approach in this thesis for testing the applicability and repeatability of the previous studies by performing comprehensive thermo-mechanical characterizations.

# NANO BOYUTTAKİ MALZEMELER İLE GÜÇLENDİRİLMİŞ ELYAF TAKVİYELİ POLİMERİK KOMPOZİTLERİN ARAYÜZ KARAKTERİSTİKLERİ ÜZERİNE DENEYSEL BİR ÇALIŞMA

Ece Belen

MAT, Yüksek Lisans Tezi, 2014

Tez Danışmanı: Doç. Dr. Mehmet Yıldız & Yrd. Doç. Dr. Serkan Ünal

Anahtar kelimeler: Kompozit malzemeler, karbon nanotüpler, kimyasal fonksiyonelleştirme, elektro-sprey, elektro-eğirme, vakum infüzyon, reçine iletim kalıplama.

## Özet

Elyaf takviyeli kompozit malzemeler kendilerini oluşturan ana bileşenlerin çeşitli nano fazlar ile takviye edilmesi yardımıyla mükemmel mekanik, termal, elektriksel özelliklere ve korozyon dayanımı ile düşük yoğunluklu yapıya sahip olacak şekilde işlenebilirler. Bu nano takviyeleri endüstriye uyarlanabilir ve ekonomik olarak uygulanabilir bir üretim metodu ile entegre edilmelidirler. Daha da fazlası güçlendirme prosesi büyük ölçüde elyaf ve polimer matris ara yüzeyindeki nanotüp dağılımına bağlıdır ki bu da matristen elyafa verimli yük taşınımını sağlayacaktır. Bu yüzden biz de karbon nanotüp uygulamalarının bilinen kısıtlarını ortadan kaldırmalıyız. Bu nedenle ki tez kapsamında çok duvarlı karbon nanotüplerin kimyasal fonksiyonelleştirilmesi ve karakterize edilmesi öncelikli olarak araştırıldı ve arkasından elektrosprey yöntemi ile fonksiyonelleştirilmiş nanotüpler elyaf takviyeli polimerik kompozitlerin ara yüzeyine entegre edilir. Nanotüp püskürtülen elyafların yüzey karakterizasyonları ile üretilen kompozitlerin mekanik testleri bu tezde bulunmaktadır. Alternatif olarak da elektro eğirme yöntemi ile nanofiberin elyaf takviyeli kompozitler içerisine dahil edildiği RTM kompozitler ile ilgili diğer bir çalışma da daha önceki araştırmaların uygulanabilirliği ve tekrar edilebilirliğini test etmek için daha kapsamlı olarak tezde incelenmiştir.

*To my grandmother*

## **Acknowledgements**

I would like to express my deep thankfulness to my supervisors;

Professor Mehmet Yıldız and Professor Serkan Ünal who have encouraged and supported my academic career during my master period while being always kind, systematic and having confidence in me. I appreciate Dr. Serkan Ünal for his patience and leading us to think about every problem with their reasons and solutions during our group meetings and even in our daily lives.

My jury members, Professors Bahattin Koç, Fevzi Çakmak Cebeci and Yusuf Ziya Menceloğlu, for their constructive comments on this thesis.

Marie Curie Career Integration Grants for funding during my two-year master education and research period,

Koç University Surface Science and Nanotechnology Research Center for their support in X-ray photoelectron spectroscopy analysis,

My colleagues at Advanced Composites and Polymer Processing and Structural Health Monitoring Laboratory (AC2PL-SHM) in FENS-L010 and group members in Nanotechnology Center (SUNUM), Ataman Deniz, Çağatay Yılmaz, Esat Selim Kocaman, Fazlı Fatih Melemez for their guidance and helps during the course of my thesis and Nihan Ongun, Nesibe Ayşe Doğan, Özge Çavuşlar for their friendships and patience to listen my presentations in every group meetings,

Dr. Serap Hayat Soytaş and MSc. Çağatay Yılmaz for their supports to the experiments and characterizations especially during the scanning electron microscope investigations,

My friends at Sabanci University, Ayça Ürkmez, Burcu Saner Okan, Burçin Üstbaşı, Dilay Ünal, Nihan Ongun, Tuğçe Akkaş and Zekiye Pelin Güven and all others,

My sister, Eda Belen for her life-long existence in all of my life,

My family especially to my grandmother, for their encouragement and support since opening my eyes to the world and for their long-lasting guidance to the right way in every moment of my life. I deeply appreciate them forever.

## Table of Contents

<b>Abstract</b> .....	<b>i</b>
<b>Özet</b> .....	<b>ii</b>
<b>Acknowledgements</b> .....	<b>iv</b>
<b>List of Figures</b> .....	<b>ix</b>
<b>List of Tables</b> .....	<b>xii</b>
<b>Abbreviations</b> .....	<b>xiii</b>
<b>1 INTRODUCTION</b> .....	<b>1</b>
1.1 Motivation .....	1
1.2 Outline of the Thesis .....	4
1.3 Objectives .....	4
<b>2 LITERATURE REVIEW</b> .....	<b>5</b>
2.1 Carbon Nanotubes (CNTs) .....	6
2.1.1 Structure .....	6
2.1.2 Properties of CNTs .....	8
2.1.3 Applications of CNTs.....	12
2.2 Processing of Carbon Nanotubes.....	13
2.2.1 Dispersion .....	13
2.2.2 CNT Integration Methods within the Polymeric Composites .....	14
2.2.3 Electrospray/Electrospin Processes.....	16
2.2.4 Chemical Functionalization of CNTs .....	19
<b>3 CHEMICAL FUNCTIONALIZATION AND ELECTROSPRAY DEPOSITION OF CNTS</b> .....	<b>29</b>
3.1 Introduction.....	29
3.2 Experimental .....	32
3.2.1 Ozone Oxidation of Multiwall Carbon Nanotubes (MWNTs).....	33
3.2.2 Dispersion .....	35
3.2.3 Electrospray Deposition of MWNT Solutions .....	36
3.2.4 Surface Analysis of Electrospray Deposited MWNTs over Glass Fiber.....	37
3.3 Results and Discussion.....	38
3.3.1 Ozone Oxidation Results.....	38

3.3.2	Thermo-gravimetric (TGA) Analysis.....	38
3.3.3	Raman Analysis.....	41
3.3.4	XPS Analysis.....	43
3.3.5	Dispersion.....	46
3.3.6	SEM Analysis.....	49
3.4	Conclusions.....	52
<b>4</b>	<b>PRODUCTION AND CHARACTERIZATION OF CNT INCORPORATED FRPCs.....</b>	<b>54</b>
4.1	Introduction.....	54
4.2	Experimental.....	57
4.2.1	Materials.....	57
4.2.2	Composite Production by Vacuum Infusion (VI).....	57
4.2.3	Mechanical Characterization.....	61
4.2.4	Surface Characterization.....	63
4.3	Results and Discussion.....	64
4.3.1	Composite Production.....	64
4.3.2	Static Tensile and Three Point Bending Test Results under UTM.....	64
4.3.3	Fracture Surface Characterization.....	71
4.4	Conclusions.....	72
<b>5</b>	<b>INTERFACE ANALYSIS of POLY(ST-CO-GMA) NANOFIBER INTEGRATED FRPCs.....</b>	<b>73</b>
5.1	Introduction.....	73
5.2	Experimental.....	75
5.2.1	Electrospun Poly[Styrene-co-Glycidylmethacrylate] Nanofibers.....	75
5.2.2	Electrospun Poly[Styrene-co-GMA] Interlayered Composites.....	76
5.2.3	Mechanical Characterization.....	77
5.2.4	Surface Characterization.....	79
5.3	Results and Discussion.....	79
5.3.1	Morphological Analysis of Electrospun Nanofiber.....	79
5.3.2	Static Flexural and Tensile Test Results.....	80
5.3.3	Dynamic Mechanical and Thermal Analysis (DMTA).....	84
5.4	Conclusions.....	86

<b>6 FUTURE WORK.....</b>	<b>87</b>
<b>Appendix.....</b>	<b>88</b>
<b>Bibliography.....</b>	<b>90</b>

## List of Figures

Figure 2.1 (a) Schematic honeycomb structure of a graphene sheet. Single-walled carbon nanotubes can be formed by folding the sheet along lattice vectors. The two basis vectors $a_1$ and $a_2$ are shown. Folding of the (8,8), (8,0), and (10,-2) vectors leads to armchair [14] .....	8
Figure 2.2 TEM images of (a) an arc-MWNT, (b) a CVD-MWNT. AFM images of (c) arc MWNT and (d) CVD-MWNT lying across a pore. Reproduced from (Coleman et al., 2006) .....	10
Figure 2.3 Schematic diagram of set up of electrospinning apparatus (a) typical vertical set up and (b) horizontal set up of electrospinning apparatus [33].....	16
Figure 2.4 Characteristic defects in a SWNT. (A) Instead of the normal six- member ring, five or seven member rings in the carbon backbone lead to a bend in the tube. (B) $sp^3$ -hybrideized defects (R=H and OH). (C) Disorder of carbon structure by oxidative conditions, which leaves a void lined with $-COOH$ groups. (D) Open end of the SWNT, terminated with $COOH$ groups. Besides carboxyl termini, the existence of which has been clearly introduced, other terminal groups such as $-NO_2$ , $-OH$ , $-H$ , and $=O$ are possible [44] .....	20
Figure 2.5 Schematic representation of the process by which CNTs are oxidized using acid and oxidative gas [45] .....	21
Figure 2.6 TEM images: (a) SWNTs rope; (b) acid treated SWNTs rope [51] .....	23
Figure 2.7 (a) XPS general spectra and high-resolution of C1s spectra of MWCNTs: (b) p-MWCNTs; (c) O-MWCNTs; (d) $H_2O$ -O-MWCNTs [53]. .....	25
Figure 2.8 SEM micrographs of two types of carbon nanotubes; (a) thick-walled CNTs and (b) thin- walled CNTs [54].....	26
Figure 3.1 Ozone oxidation set-up of MWNTs in dry phase (OD-MWNTs). .....	34
Figure 3.2 Ozone oxidation set-up including MWNTs in water (OW-MWNTs). .....	34
Figure 3.3 Schematic representation of the electrospray deposition of nanotubes over glass fiber mats. ....	37
Figure 3.4 TGA graph of pristine and 16 hour-ozone treated samples including OD-MWNTs, OW-MWNTs, and SOD-MWNTs versus temperature. ....	39
Figure 3.5 Weight loss of oxygenated groups versus oxidation time. ....	40

Figure 3.6 Overall Raman scattering spectra of pristine and 16 hour-ozone treated samples including OD-MWNTs, OW-MWNTs, SOD-MWNTs. ....	41
Figure 3.7 $I_D/I_G$ of MWNTs versus oxidation time for OD-MWNTs, OW-MWNTs, SOD-MWNTs. ....	42
Figure 3.8 a) XPS general spectra and C1s spectra of b) P-MWNTs, c) 2 h and d) 16 h OD-MWNTs .....	43
Figure 3.9 Change in surface composition of carbon atoms and functional groups attached to the carbon atoms after oxidation process as a function of process time. ....	45
Figure 3.10 SEM images of glass fiber surfaces prepared with various 16 h OD-MWNTs dispersions by electro spraying at constant 40 $\mu$ l/h flow rate and 15 kV applied voltage: a) 0.025 wt % of nanotube in NMP, b) 0.01 wt % of nanotube in NMP, c) 0.005 wt % of nanotube in NMP, d) 0.005 wt % of nanotube in NMP/H <sub>2</sub> O (50/50 wt %). ....	50
Figure 3.11 SEM images showing random orientation of nanotubes both horizontally and vertically to the glass fiber mat surface. Images correspond to trial number 5 <sup>th</sup> in Table 3.2. ....	50
Figure 3.12 SEM images of electro sprayed (60 $\mu$ l/h and 15 kV) glass fiber surfaces covered with a) P-MWNTs and b) 16 h OD-MWNTs. ....	52
Figure 4.1 Electro spray deposition of OD-MWNT into 50/50 wt. of NMP/H <sub>2</sub> O solution by using a two-axis router. ....	58
Figure 4.2 Vacuum in-fusion process .....	58
Figure 4.3 Symmetric 6-ply stack arrangement placed over the heating production region .....	60
Figure 4.4 Produced composite plate by vacuum fusion method .....	61
Figure 4.5 Flexure test specimens; a) neat and b) OD-MWNT reinforced composite specimens .....	62
Figure 4.6 Tensile test specimens; a) neat and b) OD-MWNT reinforced composite specimens .....	62
Figure 4.7 Deformation of a) three point bending and b) tensile test specimens .....	63
Figure 4.8 Tensile stress versus strain results of G1-B9 specimens .....	65
Figure 4.9 Flexure stress versus strain results of G1-B9 specimens including 0.01 wt. % of nanotubes within overall composite. ....	66
Figure 4.10 Flexure stress versus strain results of G1-B10 specimens including 0.01 wt. % of nanotubes within overall composite. ....	66

Figure 4.11 Flexure stress versus strain results of G1-B11 specimens including 0.02 wt. % of nanotubes within overall composite.....	67
Figure 4.12 SEM images of the fiber-matrix interface of a) neat; b, c and d) OD-MWNT (0) deposited composite specimens .....	71
Figure 5.1 Electrospun P(St-co-GMA) nanofiber over 0° directional surface of glass fiber layer deposited through 90° direction.....	76
Figure 5.2 Three point bending specimens; a) neat samples, b) copolymer integrated samples.....	78
Figure 5.3 Tensile fracture specimens .....	78
Figure 5.4 DMA samples; a) neat samples, b) copolymer included samples. ....	79
Figure 5.5 Nanofiber morphologies electrospun from 30% copolymer solution concentration.....	80
Figure 5.6 Three point bending test specimen under loading.....	81
Figure 5.7 Three point bending test results for a) 1 <sup>st</sup> and b) 2 <sup>nd</sup> experiment .....	82
Figure 5.8 Static tensile test results for 2 <sup>nd</sup> experiment .....	83
Figure 5.9 DMA results for neat and P(St-co-GMA) nanofiber reinforced glass- epoxy composites. ....	84

## List of Tables

Table 2.1 Theoretical and experimentally measured properties of carbon nanotubes....	11
Table 2.2 Different polymers used in electrospinning, characterization methods and their applications [33] .....	17
Table 3.1 Total O atomic percentage and surface composition of the P-MWNTs and OD-MWNTs versus treatment time .....	44
Table 3.2 Experiments on the dispersion of 16 h OD-MWNTs in various organic solvents using probe sonication. ....	48
Table 3.3 Electro-spray experiments with stable dispersions from Table 3.2 under various process conditions. ....	49
Table 4.1 Three different composite plates including P-MWNTs and 16 h OD-MWNTs deposited with variable parameters.....	59
Table 4.2 Average tensile strength and Young's modulus obtained from G1-B9 .....	65
Table 4.3 Average flexure strength and Young's modulus results for overall specimens	68
Table 5.1 Average flexural strength and Young's modulus values of two different composite plates with 30 % Poly (St-co-GMA) and different production configuration. ....	81
Table 5.2 Average tensile strength and Young's modulus of composites for 2 <sup>nd</sup> experiment with 30 % Poly (St-co-GMA).....	83

## Abbreviations

BET	Brunauer-Emmett-Teller
CF	Carbon fiber
CFRC	Carbon fiber reinforced composite
CNF	Carbon nanofiber
CNT	Carbon nanotube
CVD	Chemical vapor deposition
DMTA	Dynamic mechanical and thermal analyzer
EPD	Electrophoresis deposition
FTIR	Fourier transform infrared spectroscopy
GF	Glass fiber
GFRC	Glass fiber reinforced composite
ILSS	Interlaminar shear strength
MWNT	Multi walled carbon nanotube
OD	Oxidation in dry phase
OW	Oxidation in aqueous phase
SOD	Oxidation in dry phase using “pre-sonicated” MWNTs
PMMA	Polymethylmetachrylate
RTM	Resin transfer molding
SEM	Scanning electron microscopy
SWNT	Single walled carbon nanotube
TGA	Thermo-gravimetric analysis
UTM	Universal testing machine
VI	Vacuum infusion
XPS	X-ray photoelectron microscopy

# CHAPTER 1

## 1 INTRODUCTION

### 1.1 Motivation

Fiber reinforced polymeric composite materials (FRPC) are load bearing structures owing to their superior properties such as excellent mechanical, thermal, structural properties and corrosion resistance with low density and they have recently been of great interest to different areas such as aircraft industry, transportation, marine sector, wind turbines [1] . FRPCs have been used as structural engineering materials which are typically fabricated by combination of a polymer matrix and reinforcing materials such as carbon or glass micro fibers with metallic or organic fillers [2] . Recently the industrial needs especially in airplane sector are changing rapidly to obtain stronger, more durable and lighter polymeric composites; hence the micro scale composites need to be further improved with the nano-phase integrations. The primary reinforcements are known as micro scale glass or carbon fiber fillers while the nano-phase structures such as carbon nanotubes (CNTs) or nanofibers of different polymers are introduced as secondary fillers within the fiber reinforced polymeric composites. It has been claimed that 40 wt % of reinforcing materials are used in the traditional micro scale composites while very few amount of nano-phase reinforcements are sufficient in order to observe reasonable improvement in the mechanical, thermal and electrical properties leading to the development of multifunctional composite materials [3] . In the case of industrial applicability, FRPCs reinforced with nano structures are economically feasible, processed easily with the appropriate production methods. In view of this, our investigations and inventions related to the incorporation of nano phase materials within

the FRPCs offer a new era to be able to scale up the productions to the industrial applications especially in airplane sector. For example, the Airbus Military patent application includes electrospinning process in order to integrate nanofibers of epoxy resin and also nanofibers doped with carbon nanotubes onto each carbon fiber plies by a two axes electrically moving device. Finally, the electromagnetic characteristics of the aero-structures are significantly improved particularly for the protection against lightning impact [4] .

In the literature various incorporation techniques of the nano structures into the neat polymer or polymeric composites have been widely studied. The most remarkable ones have been stated as in resin infusion, CVD growth production, electrophoretic deposition and interlayer placement. However, in all of the aforementioned methods, there have been some problems while integrating the nano phase materials into the fiber reinforced polymeric composites at a large scale. These inevitable central challenges of the experiments which are associated with dispersion, alignment, compatibility with polymer matrix etc. have yet to be overcome. Accordingly, in this thesis content, electrospinning has been chosen as a versatile methodology for the integration of carbon nanotubes individually and uniformly within the fiber reinforced polymeric composites fabricated with the vacuum infusion method.

Following the first study reported by Ajayan in 1994 [5] , the production of carbon nanotube (CNT) reinforced polymeric composites became one of the most attractive research areas. Although there have been various current studies about carbon nanotubes, still very few startup companies based on CNT applications related to nanotechnology exist. Additionally, chemically modified CNTs have been significantly considered in different researches in order to achieve much improvement in mechanical properties of nanocomposites forming the reactive sites with the polymer matrix [6] . This process has been generally defined as chemical functionalization. Moreover, the interfacial characteristic of these fiber reinforced polymeric composites enhanced with nano materials has been emphasized between nanotube-matrix, nanotube-reinforcing fibers, polymer matrix-reinforcing fibers and the efficient load transfer needs to be achieved through the interface. Therefore, functionalization of CNTs is believed to increase interfacial properties within the FRPCs [7] . Furthermore dispersion quality of

CNTs can be aided with chemical modification of nanotube surface structure so as to obtain strong interactions with the dispersion medium [8] .

Three related experimental studies are stated in detail within each corresponding chapter of this thesis including the chemical functionalization and characterization of multi walled carbon nanotubes (MWNTs) and then the electrospray deposition of chemically functionalized CNT solutions over the glass fiber reinforcements; and the composite production by vacuum infusion process and characterization of functionalized CNT integrated fiber-epoxy composites. In the last chapter electrospinning of copolymer solution has been studied for the enhancement of interfacial properties between fiber and epoxy matrix. For this reason, polystyrene-co-glycidyl methacrylate was previously developed as a compatible copolymer with the cross linking epoxy systems and used as an interlayer for the carbon fiber-epoxy pre-preg composites [9]. Alternatively, RTM-manufactured electrospun nanofiber integrated glass-epoxy composites has been another approach in this thesis for testing the applicability and repeatability of the previous studies by performing comprehensive thermo-mechanical characterizations. In this work, we have developed a novel method that is feasible in the industrial scale for the incorporation of nano structures into the FRPCs.

## **1.2 Outline of the Thesis**

The work has been organized as follows. Chapter 2 gives the general background information and describes the state of art for fiber reinforced polymeric composites (FRPCs), carbon nanotubes, dispersion, functionalization of carbon nanotubes, their incorporation methodology into the FRPCs, electrospraying/electrospinning process. Three experimental studies together with their results and discussions are provided in detail separately but in an interrelated manner with each other in Chapter 3, Chapter 4 and Chapter 5. At the end of this thesis, future work and recommendations are given in Chapter 6.

## **1.3 Objectives**

This current work aims to prepare chemically functionalized multi walled nanotubes (MWNTs) and their integration into the FRPCs in order for enhancing the interfacial interactions between the constituents of the composites, namely fiber and polymer matrix thereby improving load transfer through the interface. In addition, the functional species over the nanotube surfaces are expected to provide strong interactions both with the thermoset polymer matrix and also the glass fiber reinforcement. Finally, it is also targeted to achieve noticeable improvements in the mechanical strength of the produced nano incorporated FRPCs by modifying the surfaces of fiber reinforcement with lowest amount of functional MWNTs.

The mechanical performance of FRPCs are also attempted to be improved through integrating polystyrene-co-glycidyl methacrylate P(St-co-GMA) nanofiber into fiber-epoxy composites by means of in-house developed electrospinning process. It is shown that, both mechanical and the thermo-mechanical responses of this nanofiber integrated FRPCs significantly increase due to the fact that the presence of nanofiber interlayer augments the interfacial interactions between fiber and polymer matrix.

## CHAPTER 2

### 2 LITERATURE REVIEW

Considering their unique characteristics and properties, CNT integrated fiber reinforced polymeric composites has recently been in high demand for most of the studies. Ajayan [4] reported that the efficient load transfer between fiber and the surrounding matrix can be achieved through creating strong interfacial interactions within fiber reinforced polymeric composites such as by means of CNT deposition at the interface of fiber and matrix. Volder et al. [10] discussed that engineering nanoscale stick-slip among CNTs and CNT-polymer interactions can enhance material damping properties, which are preferable to improve sport goods such as baseball bats, tennis racquets, and bicycle frames.

Recent examples for utilizations of carbon fiber reinforced polymeric composites enhanced with CNTs include strong, lightweight wind turbine blades and hulls for maritime security boats. However, in some cases good interface bonding and hence efficient load transfer, which are extremely important to produce high strength composites, cannot be achieved easily due to the sliding effect of each layers of MWNTs or shearing effect of individual tubes in SWNT bundles, which were substantiated by Micro-Raman spectroscopy [11, 12]. In order to benefit from CNTs integration, the aggregates of CNTs should be removed by using appropriate methods [12], some of which are also considered within this thesis. In some other studies, nanotubes have been mixed with polymer resins such as epoxy to increase its strength and stiffness. Upon mixing ~1 wt % MWNT with the epoxy resin, it was shown in literature that the stiffness and toughness of the resin can be increased up to 6% and

23%, respectively without deteriorating other mechanical properties. It was also concluded that the associated improvements are directly related to the diameter, aspect ratio, alignment, dispersion quality and interfacial interaction of CNTs with the polymer matrix [10, 11].

## **2.1 Carbon Nanotubes (CNTs)**

### **2.1.1 Structure**

In 1991, carbon nanotubes were found as a needle-like material while Iijima was observing them with an electron microscope. Having been determined that these materials consist of a simple graphitic structure, they were called “carbon nanotubes” because of their tubular, cylindrical sheets with the micron-sized length and thickness of up to 100 nm [13]. Carbon nanotubes (CNTs) have been of great interest to most researchers within a wide range of fields of science and engineering due to their unique properties such as high conductivity, mechanical strength, stiffness, chemical inertness, and good thermal and electrical properties with low density. Because of these features, scientists foresee that they will be promising materials for building the future of nanotechnology.

CNTs are comprised of folded graphitic sheets that are rolled into a concentric, cylindrical and hexagonal lattice structure. Graphite and diamond are two allotropes of the carbon atom as solid phases. Isotropic strong diamond is obtained by sharing the four valence electrons equally in carbon atom. Graphite is created by sharing three of these valence electrons with the neighbor atoms through the covalent structure in a plane while the fourth electron is slant to be shared among all atoms. The type of  $sp^2$  bonding creates strong intrinsic forces in the plane sheets while it produces weak van der Waals bonding forces out of the plane graphitic sheet. Nanotubes also consist of  $sp^2$  bonded carbon structure. Concentric structures of graphitic layers can be formed as a result of the definite topological defects of nanotubes. All carbons in well-organized CNTs are bonded in a hexagonal lattice except at their ends whereas disorders in bulk CNTs produce pentagons, heptagons, and other defects within the sidewalls that usually

destroy desired unique properties of CNTs [10]. Nanotubes are divided into two types depending on their number of inner graphene layers with open or closed ends. One of them is the multi-walled carbon nanotube (MWNT), which was discovered firstly as the shape of the concentric cylinders located around the same axis and similar to hollow graphite fibers. The invention of MWNT has more regular structure than these graphite fibers. The distance between each graphite layer into the MWNTs is 0.34 nm, which is slightly greater than the single crystal value, 0.335 nm. This smaller value is because of a various geometrical limitations in forming concentric cylinders without seam while keeping and protecting the space between each graphite sheet [11]. The hexagonal honeycomb graphene structure, located into a cylindrical shape whose boundary conditions identified with (m,n) lattice vector forms a single-walled carbon nanotube (SWNT) (as seen in Figure 2.1). Since each nanotube has the main symmetrical structure, this schematic of graphene structure characterizes the important properties of each nanotube [11, 14]. This second type of CNTs have uniform diameter in between 1-2 nm, while MWNTs' one is typically between 5 and 20 nm, respectively. Also, MWNT diameters can exceed 100 nm [10]. In addition to this, the orientation of the graphene lattice with respect to the tube axis, chirality, and diameter are important features for nanotubes [10, 14]. They are specified with aforementioned lattice vector indices (m, n), and the nanotubes are also classified with respect to their folding features. When  $n=0$ , (m,0), CNTs are defined as “zigzag”, in case of  $m=n$  (m,m), CNTs are identified as “armchair.” In other cases, they are named “chiral” [14, 15]. A graphene layer is illustrated in Figure 2.1 combined with the unit vectors of the hexagonal lattice. The chiral angle between the tube axis and hexagons determines metallic properties such as whether each CNT wall is metallic or semiconducting [14]. As an example, individual SWNTs can have a thermal conductivity of  $3500 \text{ W m}^{-1} \text{ K}^{-1}$  at room temperature with respect to the surface area; this value is higher than the thermal conductivity of a diamond [10].

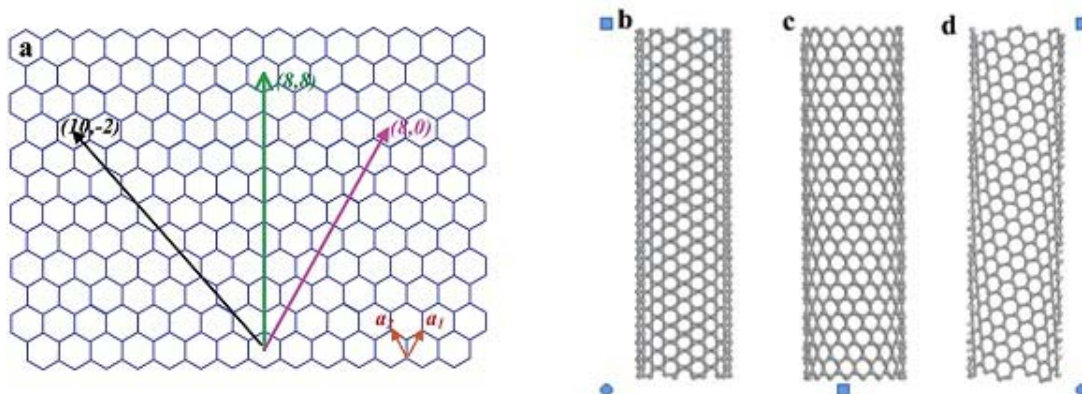


**Figure 2.1** (a) Schematic honeycomb structure of a graphene sheet. Single-walled carbon nanotubes can be formed by folding the sheet along lattice vectors. The two basis vectors  $a_1$  and  $a_2$  are shown. Folding of the  $(8,8)$ ,  $(8,0)$ , and  $(10,-2)$  vectors leads to armchair [14] .

In many literature reviews, three different synthesis methods of nanotubes such as arc-discharge, chemical vapor deposition and laser ablation method have been explained in detail [16] . In the following part of this chapter, significant properties that are separate from other materials and special application areas have been briefly stated.

### 2.1.2 Properties of CNTs

Nanotubes are special materials for most researchers because of their unique properties resulting from the combination of structure, dimension and chemical geometry of the CNTs. The strength of C=C covalent double bond over the nanotube main structure produces one of the strongest and stiffest linkage in nature. In addition to the distinguishing properties of nanotubes from other materials, these nano-dimensional materials also have a large surface area, which is advantageous for chemical and mechanical applications. The surface area of MWNT has been measured as 10-20  $\text{m}^2/\text{g}$  by BET techniques. This value is larger than that of graphite and smaller than that of activated porous carbons. It is expected for SWNT to be order of magnitude higher than that of the graphite. Additionally, nanotube density has to be lower than that of graphite. According to the literature, the density of SWNT must be at around  $0.6 \text{ g/cm}^3$ , and for

MWNT, it can be in the range of 1-2 g/cm<sup>3</sup> depending on the chemical combination of samples [11] .

### **2.1.2.1 Electrical and thermal conductivity**

Generally, electron transport properties are well defined around the outer layer of tubes according to some MWNT researchers [17] . McEuen and coworkers used atomic force microscope (AFM) for deposition of SWNTs on a surface area and then placed metal electrodes to contact the nanotubes [18] . This is why electronic features of CNTs are significantly changed by the surface modification of these nanotubes. Depending on the chiral angle, unique conductivity properties of nanotubes have been probed in recent years by the electron transport system, which is called ‘ballistic’ observed in each MWNT at room temperature [11, 19] and they behave as metals or extremely small band gap semi-conductors. The electronic properties of SWNT have been identified rather than that of MWNT, because measurements of the electron transfer mechanism are much more observable on each SWNT [11] . Band gaps for semi-conducting nanotubes are measured to be inversely proportional with diameter. In the case of small diameter nanotubes, it is about 1.8 eV and 0.18 eV for the largest diameter of stable SWNT. The conductivity of pristine nanotubes is extremely high and has minimum resistance because of their one-dimensional structure. This causes it to carry the charge through the nanotubes without scattering; hence, there is a minimization of heat accumulation. Nanotubes can transport extremely high current densities up to 100 MA/cm<sup>2</sup> [20] .

Thermal conductivity of nanotubes is also considerably high at a room temperature up to 6000 W/mK; however the measured value is at about 200 W/mK, whereas 3000 W/mK can be also observed for MWNT according to the available reports [19] .

### **2.1.2.2 Mechanical properties**

Mechanical properties such as elastic modulus, strength, stiffness etc. have the same importance as the electronic properties of CNTs. The axial elastic modulus of CNTs which is called as Young’s modulus is estimated to be at least 1 TPa relative to the in-plane elastic modulus of graphite. On the other hand, the strength of CNTs is also order of magnitude higher than high strength carbon fibers. New methods have been available in recent experiments to predict specific elastic properties and stiffness such as scanning

probe microscopes (SPM) or AFM . The mean value for the MWNT modulus obtained by SPM was shown to be 1.8 TPa which was higher than that of in-plane modulus of graphite [11] . Yu et al. in 2000 obtained stress–strain measurements on individual arc-MWNTs by an electron microscope. They attained 0.27–0.95 TPa for elastic modulus and they showed strength in the range 11–63 GPa. This allows for the prediction of nanotube toughness at about 1240 J/g [21] . However, Salvetat et al. achieved Young’s modulus values between 12 and 50 GPa by the AFM during bending and manipulation in the first measurements for CVD growth MWNT as shown in Figure 2.2 [19] . After that Xie et al. obtained a modulus of 0.45 TPa and 4 GPa of tensile strength according to stress–strain measurements on bundles of CVD growth MWNT [9].

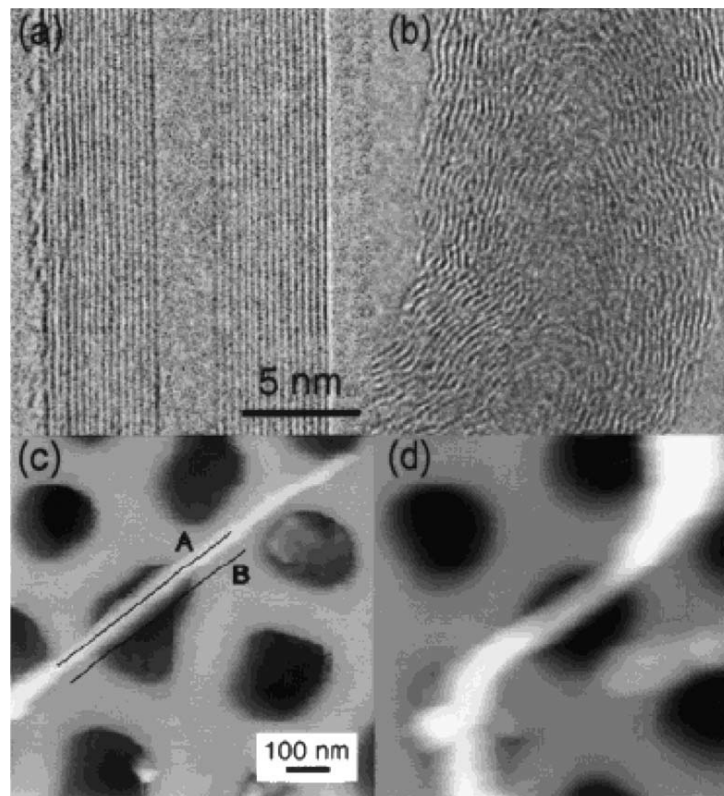


**Figure 2.2** TEM images of (a) an arc-MWNT, (b) a CVD-MWNT. AFM images of (c) arc MWNT and (d) CVD-MWNT lying across a pore. Reproduced from (Coleman et al., 2006) .

In the case of compelling fracture and deformation, nanotubes can sustain up to 40% strain in tension without showing any brittle behavior, plastic deformation or bond rupture. Some of the properties of CNTs albeit not being exactly the same for all types of nanotubes are tabulated in the following Table 2.1.

**Table 2.1** Theoretical and experimentally measured properties of carbon nanotubes

Property	CNTs	Graphite
Lattice Structure	Rolls of hexagonal lattice	Planar hexagonal structure
Specific gravity	0.8 g/cm <sup>3</sup> for SWNT 1.8 g/cm <sup>3</sup> for MWNT (theoretical)	2.26 g/cm <sup>3</sup>
Surface area	10-20 m <sup>2</sup> /g	
Elastic modulus	~1 TPa for SWNT ~0.3-1 TPa for MWNT	1 TPa (in-plane)
Strength	50-500 GPa for SWNT 10-50 GPa for MWNT	
Resistivity	~5-50 μΩ cm	50 μΩ cm (in-plane)
Thermal conductivity	3000 W m <sup>-1</sup> K <sup>-1</sup> (theoretical)	3000 W m <sup>-1</sup> K <sup>-1</sup> (in-plane) 6 W m <sup>-1</sup> K <sup>-1</sup> (c axis)
Thermal expansion	Negligible (theoretical)	-1 × 10 <sup>-6</sup> K <sup>-1</sup> (in-plane) 29 × 10 <sup>-6</sup> K <sup>-1</sup> (c axis)
Oxidation in air	>700 °C	450-650 °C

### 2.1.2.3 Chemical inertness

Carbon nanotubes are inert materials because of comprising of non-reactive based graphite lattice structure. According to the oxidation studies, reactivity of end caps which are opened by using several kinds of etching process increases more than that of the side walls of nanotubes. Then pentagonal defects cause dimensional curvature and strain and so create tip reactivity. In recent experiments, electron transfer over nanotube surfaces can be extremely possible by using electrodes in chemical reactions [11].

### **2.1.3 Applications of CNTs**

Because of all exceptional properties briefly introduced above, CNTs can be used in a wide range of commercial application areas such as field emitters, conducting plastics, thermal conductors, energy production and storage media, enhancement fillers in composite structures, novel probes and sensors and components of biosensors and medical devices.

Due to nanotubes' high aspect ratio to produce a percolation network even at low concentrations, MWNTs were initially used as electrically conductive fillers in plastics. In addition, conductive CNT plastics have enabled electrostatic-assisted painting of mirror housings, as well as fuel lines and filters that dissipate electrostatic charge in the automotive industry [10].

Field emission is an attractive source for electrons compared to thermionic emission, which is a quantum effect. For CNTs, electron field emission has recently been intriguing area which has found widely commercial and technological applications such as flat panel displays, electron guns in electronic microscopes, microwave amplifiers. Moreover, low threshold emission fields and stability at high current density are important requirements for electron emissive materials. Including compatibility of properties-structure such as diameter, integrity, chemical stability, high electron transfer and conductivity, CNTs show desired electron emission capability with a lower threshold electric field than conventional emitters. However, nanotubes can have different capability of current transfer and emission stability depending on their manufacturing mechanism and conditions [12]. Another application area in which CNTs have been used owing to their nano-meter sized diameter, good conductivity, high mechanical strength and elastic modulus includes nanoprobe, which can be employed in high-resolution imaging, nanoelectrodes, sensors and field emitters as well.

CNTs have also been considered for energy production and storage. Carbon fiber electrodes have been used for fuel cells, battery and other electrochemical applications before. Nowadays, nanotubes are preferred in electron transfer reactions especially due to their high surface area in lieu of the carbon fibers. In these reactions, CNTs can

provide higher reaction rates and better reversibility compared to the other carbon electrodes [11].

## **2.2 Processing of Carbon Nanotubes**

### **2.2.1 Dispersion**

Dispersion state of carbon nanotubes in either solvents or polymeric media indicates the structural quality and performance of the CNT reinforced polymeric composites. In other words overall mechanical and thermal properties of these reinforced composite structures are demonstrated to be strongly depending on the dispersion state of nanotubes, functionalization process, nature and concentration of the surface agents if necessary to use, interfacial interactions and re-agglomeration behavior of the nanotubes in the matrix during the curing of the resin [22]. CNTs are known as chemically inert nano-materials which tend to agglomerate and entangle easily in any media owing to their inherent morphology and attractive van der Waal's forces between nanotubes. These drawbacks result in the considerable dispersion difficulties in either any solvents or polymeric media. In the literature, there exist two different dispersion methods, namely, mechanical and chemical methods. Milling, ultrasonication (bath or probe), high shear mixing, and grinding have been considered as mechanical methods while acidic treatment, fluorination or using surfactant systems as chemical techniques. In literature, many works have been dedicated to investigate the effects of these methods on the aspect ratio of nanotubes and the interactions between CNTs and the surrounding media [23].

### **2.2.2 CNT Integration Methods within the Polymeric Composites**

CNT-based fiber reinforced polymeric composites are produced basically with two different strategies [24] that is, mixing nanotubes into the polymeric resin followed by the impregnation of the CNT-resin mixture into the primary fiber reinforcements or incorporating CNTs directly onto the microfibers. Considering these basic strategies, in the literature there are four well-known CNT-incorporation methods into neat polymers and polymeric composites, namely, in-resin infusion, CNT growth over carbon fiber substrates, interlayer placement and electrophoretic deposition.

Since in-resin infusion is the most scalable and practical integration process in the industrial applications, it has been widely used method which includes an initial dispersion process into the resin followed by the infusion of the CNT-resin mixture into the fiber assembly by liquid injection molding for the production of final composite structure. On the other hand, nanotube loading concentration has been limited due to the dispersion or local filtration problems. Additionally, the CNT addition with relatively high loading concentrations dramatically increases the viscosity of the resin, thus leading unimpregnated regions/dry spots in the fiber perform owing to the agglomeration during the manufacturing of composite part. Specifically higher than 1 vol.% of nanotube concentration consequently exacerbate the mechanical performance of the final composites and in turn causing the significant degradation in reinforcement ability [25] . Therefore, among all integration methods, this method is deemed to be most problematic ones.

CNTs can be directly grown onto the reinforcing fiber substrates by CVD method in the presence of a catalyst in order to improve interfacial properties of the composites. This assembly is then impregnated by the polymeric resin using the suitable composite manufacturing method. In this method, the dispersion and alignment of nanotubes can be controlled along with the composite properties through the thickness direction. However, there exist difficulties during the CNT growth process such as limitations of CNT growing in large volumes, catalyst usage restrictions, functionalization problems of nanotubes grown onto the primary reinforcing fiber surfaces and also deterioration of the micro fibers because of the excessive growing conditions of the CVD method [26] .

Thostenson et al. [27] showed that the presence of carbon nanotubes at the fiber/matrix interface improves the interfacial shear strength of the composites. However, the application of catalyst on the fiber surface resulted in significant degradation (32%) on the interfacial strength.

Since the primary micron-sized fiber has a potential to be damaged by CNT growth process and the homogeneity and purity cannot be easily controlled, the third nanotube integration method, named as “interlayer placement”, has been developed as direct placement of nanotubes between the primary reinforcing fiber plies before the composite production process. This method has an advantage of alignment of nanotubes vertically providing the improvement of out-of plane properties [26] . Most influential study belongs to Garcia et al. [28] who had a success to align CNTs on a silicon substrate and transferred them onto the primary fiber ply along the thickness direction. Hence, 2.5 fold of increase in initial Mode I value and 3 fold of increase of initial Mode II values are reported on unidirectional prepreg carbon fiber composite. Contrary to the advantages, this method has disadvantage of being an impractical process in the industry due to the limitations in production of large volumes, being an expensive process and also thickness changes in the fabricated composite structures.

The fourth CNT integration method is the electrophoresis deposition (EPD) technique which is based on application of an electrical field to the charged particles dispersed in a liquid medium. Usually CNTs are used as particles in solution and they're charged through a certain bias voltage. As a result, charged particles can move and get deposited onto the carbon fabric or glass fabric substrate. EPD of both untreated and functionalized CNTs on the fiber substrate has been investigated and shown to be providing a uniform deposition along with being a practical, scalable and economically feasible process [29] . On the other hand difficulties of control of the CNT alignment and insufficient chemical interaction with the carbon fibers have been stated as the encountered drawbacks of this EPD method [26] . In a recent research of Zhang et al. [30], EPD of carboxylic acid functionalized MWNTs onto the electrically insulating primary glass fiber substrate showed a significant increase in the interfacial shear strength in comparison with that of the neat glass fiber composite materials. Additionally, it was shown that EPD of carboxylated CNTs onto carbon fiber has no affect on the in-plane properties in contrary to the CNT growth [31] .

### 2.2.3 Electrospray/Electrospin Processes

Electrospinning (electro + spinning) has been known as a useful and versatile method which combines both electrospray and spinning. This technique mainly contains three components as high voltage source, syringe tip and collecting metal surface as seen in the schematic in Figure 2.3. Upon subjecting an electric field to the droplet of a liquid solution (which might be a solution or a polymeric melt flowing) at the tip of a nozzle, the charged droplet forms a cone shaped jet therein, which will move towards the grounded collecting metallic surface, thereby leading to the continuous nanofiber formation [32].

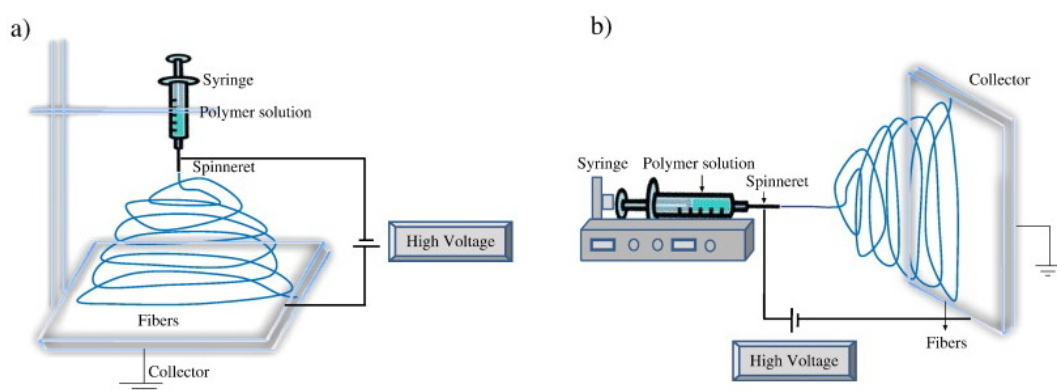


**Figure 2.3** Schematic diagram of set up of electrospinning apparatus (a) typical vertical set up and (b) horizontal set up of electrospinning apparatus [33]

Extremely high surface-to-volume ratio, tunable porosity, malleability to conform to a wide variety of sizes and shapes and the ability to control the nanofiber composition make this method a widely-used and well-known nanofiber manufacturing process which has recently been attracting interest from different fields such as biotechnology, water and air purification, technical textiles, optical electronics or polymeric composite industry due to its multi-functionality. This method additionally has been studied for years in the textile industry for producing non-woven fabrics. A number of electrospinning applications in various fields are presented in Table 2.2.

**Table 2.2** Different polymers used in electrospinning, characterization methods and their applications [33]

Polymers	Applications	Characterizations	References
Poly(glycolide) (PGA)	Nonwoven TE <sup>3</sup> scaffolds	SEM <sup>b</sup> , TEM <sup>c</sup> , <i>in vitro</i> rat cardiac fibroblast culture, <i>in vivo</i> rat model	Boland et al. (2004a)
Poly(lactide-co-glycolide)(PLGA)	Biomedical applications, wound healing	SEM, WAXD <sup>d</sup> , SAXS <sup>e</sup> , degradation analysis	(Zong et al., 2003; Katti et al., 2004)
Poly( $\epsilon$ -caprolactone) (PCL)	Bone tissue engineering	SEM, <i>in vitro</i> rat mesenchymal stem cell culture	Yoshimoto et al. (2003)
Poly(L-lactide) (PLLA)	3D cell substrate	SEM, <i>in vitro</i> human chondrocyte culture	Fertala et al. (2001)
Polyurethane (PU)	Nonwoven tissue template wound healing	SEM, <i>in vivo</i> guinea pig model	Khil et al. (2003)
Poly(ethylene-co-vinyl alcohol) (PEVA)	Nonwoven tissue engineering scaffold	SEM, <i>in vitro</i> human aortic smooth muscle cell and dermal fibroblast cultures	Kenawy et al. (2003)
Polystyrene (PS)	Skin tissue engineering	SEM, <i>in vitro</i> human fibroblast, keratinocyte, and endothelial single or cocultures	Sun et al. (2005)
Syndiotactic 1,2-polybutadiene	Tissue engineering applications	ESEM <sup>f</sup> , XRD <sup>g</sup> , FTIR <sup>h</sup>	Hao and Zhang (2007)
Fibrinogen	Wound healing	SEM, TEM, mechanical Evaluation	Wnek et al. (2003)
Poly(vinyl alcohol)/cellulose acetate (PVA/CA)	Biomaterials	SEM, FTIR, WAXD, mechanical evaluation	Ding et al. (2004)
Cellulose acetate	Adsorptive membranes/felts	SEM, FTIR	Zhang et al. (2008b)
Poly(vinyl alcohol)	Wound dressings	SEM, EDX <sup>i</sup>	Jia et al. (2007)
Silk fibroin, silk/PEO <sup>j</sup>	Nanofibrous TE scaffold	SEM, FTIR, XPS <sup>k</sup>	Jin et al. (2002)
Silk	Biomedical Applications	SEM, TEM, WAXD	Zarkoob et al. (2004)
Silk fibroin	Nanofibrous scaffolds for wound healing	SEM, ATR-IR <sup>l</sup> , <sup>13</sup> C CP/MAS NMR, WAXD, NMR <sup>m</sup> , <i>in vitro</i> human keratinocyte culture	Min et al. (2004a,b)
Silk/chitosan	Wound dressings	SEM, viscosity analysis, conductivity measurement	Park et al. (2004)
Chitosan/PEO	TE scaffold, drug delivery, wound healing	SEM, XPS, FTIR, DSC <sup>n</sup>	Duan et al. (2004)
Gelatin	Scaffold for wound healing	SEM, mechanical evaluation	Huang et al. (2004)
Hyaluronic acid, (HA)	Medical implant	SEM	Um et al. (2004)
Cellulose	Affinity membrane	SEM, DSC, ATR-FTIR <sup>o</sup>	Ma et al. (2005b)
Gelatin/polyaniline	Tissue engineering scaffolds	SEM, DSC, conductivity measurement, tensile testing	Li et al. (2006a)
Collagen/chitosan	Biomaterials	SEM, FTIR	Chen et al. (2007)

To be able to electro spray a liquid solution, the electric field applied at the fluid droplet needs to overcome the surface tension of the solution, which consequently results in the formation of a charged jet. Taylor [34] solved the stability problem of the surface shape of the charged liquid droplet and emphasized the existence of a critical angle from the droplet tip named as “Taylor cone”. In this process strong electrical repulsive forces overcome the surface tension force of the charged flow and lead to the deformed droplet forming a conical shape. The applied electric field reaches a critical value which results in jet formation. This jet is whipped out from the tip of the Taylor cone and then the formed jet leads to evaporation of the solvent between the syringe tip and ground collector surface, enabling the nanofiber formation on the collector surface [35].

The electrospinning process is directly affected by variety of parameters classified as solution properties, process conditions and ambient parameters which considerably affect the nanofiber morphology. Solution concentration and viscosity, surface tension, conductivity and charged carried by the liquid are key parameters that have to be taken into account in the solution properties while the working distance (distance between tip die and the collecting surface), applied electric voltage and flow rate need to be considered as key processing parameters explained in detail by Bhardwaj et al. [33].

The most influential solution property on the nanofiber morphology has been shown to be the solution concentration which can directly influence the viscosity of the solution to be electrospun. Sukigara et al. [36] stated that there should be an optimum solution concentration for the electrospinning process, as at low concentrations beads are formed instead of fibers and at high concentrations the formation of continuous fibers are prohibited because of the inability to maintain the flow of the solution at the tip of the needle resulting in the formation of larger fibers. It was found that the fiber diameter is increasing with the increase in solution concentration [37]. Indeed, the range of concentrations from which continuous fibers can be obtained by electrospinning can be determined by solution surface tension and viscosity parameters. Secondly surface tension plays an important role in the electrospinning process and decreasing the surface tension of a solution creates nanofiber formation without beads. Moreover integration of fillers into the polymer solution can also provide bead-free nanofibers [38]. Higher surface tension than the critical value inhibits the electrospinning process due to instability of the jets and produces droplets while lower surface tension helps the electrospinning process to be performed at a lower electric field. Additionally Doshi and Reneker [39] found out that higher net charge density of the polymer solution could also yield thinner fibers with no beads.

Regardless of the polymer concentration, decreasing the applied voltage or increasing the working distance reduces bead formation. Deitzel et al. [40] found out that the spinning voltage affects mainly the formation of beads whereas the polymer concentration has effect on the fiber size. Frenot et al. [41] investigated the effect of solution concentration, capillary tip-collector distance (working distance), electric potential at the tip, and the flow rate on electrospinning Esthane® 5720, a segmented polyether urethane. They found out that bead-like structure appears and average fiber diameter increases when the working distance decreases. On increasing the concentration, the average diameter raises and the bead-like structure turns into blobs at smaller tip to collector distance. Low flow rate is required in order to have enough time to evaporate the solvent and high flow rate induces the bead formation during the electrospinning process due to the insufficient drying time allowed for fibers before reaching the collector surface.

#### **2.2.4 Chemical Functionalization of CNTs**

One of the applications of CNTs that has been mentioned previously is their incorporation into FRPCs for enhanced properties. Since CNTs have large length to diameter ratio (aspect ratio) and chemical inertness, they easily form agglomerates in any organic solvent or polymer matrix, which is a considerable challenge commonly encountered during dispersion process of CNTs and their incorporation into composite materials for potential industrial applications. These drawbacks directly cause interfacial failure between the reinforcement material and the polymer matrix by hindering the efficient load transfer through the interface. Therefore, poor incorporation of these nanomaterials in fiber reinforced polymeric composites can result in considerable deficiency in mechanical properties of these materials and can directly bring about limited lifetime for related composite part of applications especially in airplane industry.

Due to these challenges, CNTs need to be delicately processed when incorporated into the interface of FRPCs to ensure homogeneous and individual distribution of them, taking the diameter of carbon or glass fibers (usually in the range between 6 and 12 micron) into consideration. If they are not distributed homogeneously and individually, which means the presence of CNT bundles, the diameter of these CNT bundles remains closer to the micron sized primary fibers. In such a case, these bundles may act as inclusion and imperil the integrity and interfacial strength of the FRPCs. As emphasized in this thesis and studied in detail, in addition to incorporation method of CNTs, improvement of interfacial interactions between primary reinforcing fiber and the polymer matrix in FRPCs via the incorporation of CNTs at this interface depends on the nature and concentration of chemical functional groups attached to the surface of CNTs, which directly affects the dispersibility and miscibility of CNTs in a variety of organic solvents or polymer matrices and chemical compatibility at the interface region [42]. As already reported in the literature, strong interface in FRPCs can be only achieved by individually separated carbon nanotubes [43]. In order to eliminate stated limitations of CNTs hence disperse them uniformly, and increase their interactions with the constituents of composite materials, extensive research efforts have been devoted to the chemical modification of the surface of CNTs, which is referred as ‘chemical functionalization’. The surface modification methods can be simply divided into

covalent and non-covalent functionalization resulting in a controlled degree of interaction between CNTs and the surrounding materials depending on the type of functionalization.

#### 2.2.4.1 Covalent functionalization

It is well known in the literature that the end caps of nanotubes are more prone to chemical reactions than that of the side walls due to tendency of nanotubes to form highly curved fullerene like hemispheres at tube ends. Hirsch indicated in their study that  $sp^3$ -hybridized defects, pairs of pentagon- heptagons called Stone-Walls defects, and voids in the nanotube walls are considered as defect sites of the tube ends and sidewalls illustrated in Figure 2.4 [44] .

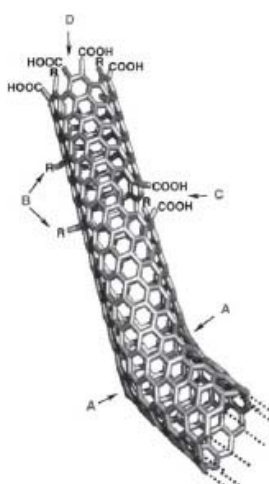


**Figure 2.4** Characteristic defects in a SWNT. (A) Instead of the normal six- member ring, five or seven member rings in the carbon backbone lead to a bend in the tube. (B)  $sp^3$ -hybridized defects (R=H and OH). (C) Disorder of carbon structure by oxidative conditions, which leaves a void lined with  $-COOH$  groups. (D) Open end of the SWNT, terminated with  $COOH$  groups. Besides carboxyl termini, the existence of which has been clearly introduced, other terminal groups such as  $-NO_2$ ,  $-OH$ ,  $-H$ , and  $=O$  are possible [44] .

Covalent functionalization of CNTs occurs at the end caps of the tubes and/or at their sidewalls, whereas non-covalent functionalization mainly consists of weak interactions, such as van der Waals,  $\pi$ -  $\pi$  and hydrophobic interactions, between CNTs and commutative moieties usually along CNT walls.

Covalent surface modifications involve the chemical attachment of molecules with functional groups such as  $-\text{COOH}$ ,  $-\text{COH}$ , and  $-\text{OH}$  on the sidewalls and termini of the CNTs by covalent bonds[45]. This process can occur by different types of reactions with the aid of highly reactive molecules. Chemical reactions to modify the surface properties of CNTs by fluorination [46], direct oxidation, amidation [47], and thiolation [48] have been previously reported in detail in the literature.

In the literature, ‘defect-site functionalization’ has been investigated to obtain defect sites in the CNT framework, in which the hybridization changes from  $\text{sp}^2$  to  $\text{sp}^3$ . This transformation within the CNT structure generally causes a structural loss on graphitic sheet. Kim et al. demonstrated that intrinsic damages are formed in the nanotube structure after being treated by oxidative procedures using strong acids such as boiling nitric acid, a mixture of sulfuric acid and nitric acid, or “piranha” (sulfuric acid–hydrogen peroxide) solution treatment as shown in Figure 2.5. These etching oxidants leave holes over CNTs while introducing oxygenated functional groups such as carboxylic groups, hydroxyl, carbonyl, ester, and nitro compounds. According to this oxidation process, initially tube ends open and subsequently these oxygenated functional moieties can be generated onto these ends and/or defect sites of these nanotubes [45].

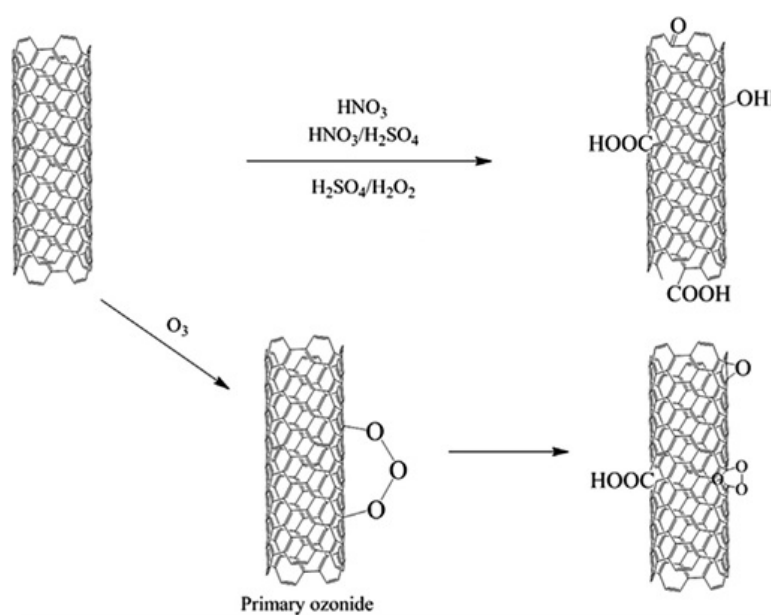


**Figure 2.5** Schematic representation of the process by which CNTs are oxidized using acid and oxidative gas [45]

After oxidation treatment, active CNTs can be used for subsequent chemical reactions including silanation, polymer grafting, esterification, thiolation, and attachment of even some biomolecules [42].

Particularly, in order for adding carboxylic groups over graphitic structure of MWNTs, Xing et al. investigated the oxidation of MWNTs (95% purity, ~30 nm in diameter) in a mixture of equimolar  $\text{HNO}_3$  and  $\text{H}_2\text{SO}_4$  solution which is bath sonicated at 60 °C. Sonication was performed for the duration of 1, 2, 4 and 8 hours. Treated MWNTs were then separated from acids in a centrifuge [49]. Functional MWNT-COOH were washed and dried in vacuum before structural analysis. As a consequence, it was shown that hydroxyl (OH), carbonyl (C=O), and carboxyl (COOH) groups could be attached by a combination of sonochemical and acid treatments. In another study, Theodore et al. prepared 3:1  $\text{H}_2\text{SO}_4/\text{HNO}_3$  solution to modify the surface of MWNT by using ultrasonic bath for 3 hours at room temperature. After sonication in acidic environment, post-processes such as dilution and filtration with distilled water were performed until reaching neutral conditions. Subsequently, MWNTs were removed from acidic solution through drying in a vacuum. Even though this oxidation method increased the number of reactive carboxyl groups (COOH) at the defect sites of MWNTs, amorphous carbon structure of MWNTs was burnt out leading to decrease in length and diameter as well [6]. Canto et al. has indicated that nitric acid is a commonly used strong acid to purify nanotubes from residual catalysts and amorphous carbons while also allowing covalent interaction of different amounts of oxygenated functional groups (mainly carbonyl and carboxylic acid groups) with the defect sites [50].

Covalent methods to functionalize the CNTs enable nanotubes to be miscible in various organic solvents because of the introduction of many polar and non-polar functional groups over CNT surfaces. On the other hand, it is important to note that the acidic oxidation causes opening of the end of nanotubes along with a large number of defects on nanotube sidewalls to yield carboxylated functionality even sometimes entailed with fragmentation of CNTs into the smaller pieces as seen in the Figure 2.6 depending on the extent of the oxidation process [51]. Although the acid oxidation of CNTs seem chemically straightforward, deleterious liquid waste generated from the solution-phase acidic oxidation of CNTs and lengthy purification processes would diminish their

benefits for large scale industrial applications. Consequently, alternative efforts have been put forward to develop methods that are convenient to use, low cost and render less damage to CNT structure and the environment [42].

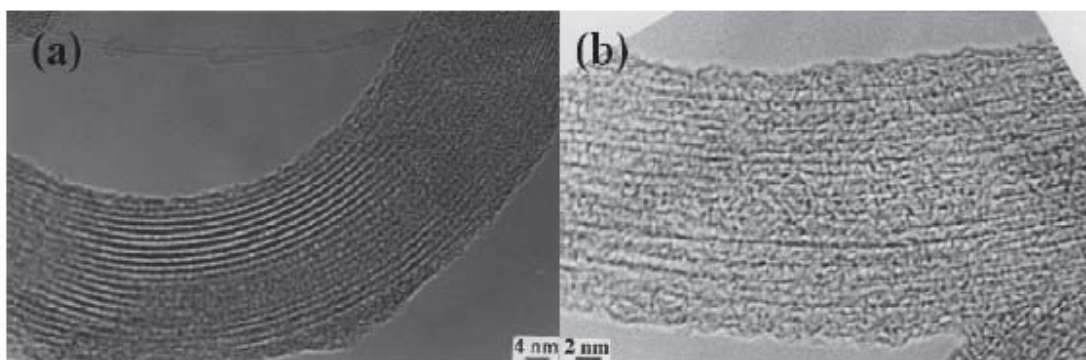


**Figure 2.6** TEM images: (a) SWNTs rope; (b) acid treated SWNTs rope [51]

As an alternative to vigorous acidic treatments of CNTs for defect site functionalization purposes, gas phase oxidation, which is widely known as “ozonolysis”, stand out as the most efficient surface modification technique in terms of being environmentally and economically friendly with no destructive effects on the CNT structure. Kim et al. illustrated that the ozonide group is produced intermediately on CNTs by ozone oxidation, and then that preliminary ozone group turns to secondary ozonide and/or other functional groups [45] as shown in Figure 2.5. In addition Banerjee et al. indicated in their study that oxidative procedure involved three main characteristics expressed as purification of SWNTs to get qualified product, chemical functionalization of nanotube sidewalls, and at last process development systematically to obtain specific arrangements of oxygenated functional groups. Finally, they achieved the production of carboxylic acids, aldehydes/ketones or alcohols over the purified nanotube side walls with the post-reactions of primary ozonide species with hydrogen peroxide ( $H_2O_2$ ), dimethyl sulfide (DMS), or sodium borohydride ( $NaBH_4$ ), respectively [52].

The research work on the ozone treatment of CNTs for establishing the functionalization process presented in this thesis was inspired by the study Peng et al. reported, [53] who have recently studied the oxidation of 1 g of pristine MWNTs (P-MWNTs) (produced by a chemical vapor deposition method) through using pure  $O_3$  (5 wt.% in  $O_3/O_2$

mixture), and water vapor assisted H<sub>2</sub>O-O<sub>3</sub> mixture at room temperature. The gas flow rate was at 150 L/h for both treatment, but humidity was changed from 2% to 60% relatively. The reaction time was varied from 0.5 to 6 h. The oxidized MWNTs were characterized by both FTIR spectrum qualitatively and X-ray photoelectron spectroscopy (XPS) quantitatively. They compared typical FT-IR spectra of MWNTs before and after O<sub>3</sub> treatment and also relative intensity ratio of  $\nu(\text{C}=\text{O})/\nu(\text{C}=\text{C})$  between the O<sub>3</sub> treated and H<sub>2</sub>O-O<sub>3</sub> treated MWNTs. According to the intensity ratio obtained from FT-IR and XPS results, the degree of oxidation of nanotubes as a result of H<sub>2</sub>O-O<sub>3</sub> treatment was observed to be higher than that of O<sub>3</sub> treatment and more functional groups were introduced onto MWNT surfaces after the H<sub>2</sub>O-O<sub>3</sub> treatment in comparison with the O<sub>3</sub> treatment. Furthermore, they analysis of XPS results indicated and increased amount of oxygen for oxidized MWNTs by H<sub>2</sub>O-O<sub>3</sub> treatment as illustrated in Figure 2.7 (a). Referring to high-resolution C1s XPS spectra of pristine MWNTs, O<sub>3</sub> treated MWNTs and H<sub>2</sub>O-O<sub>3</sub> treated MWNTs represented in Figure 2.7 (b), (c) and (d), they observed higher increase in the relative percentage of surface oxygenated moieties for H<sub>2</sub>O-O<sub>3</sub> treated MWNTs quantitatively which was consistent with FT-IR results.

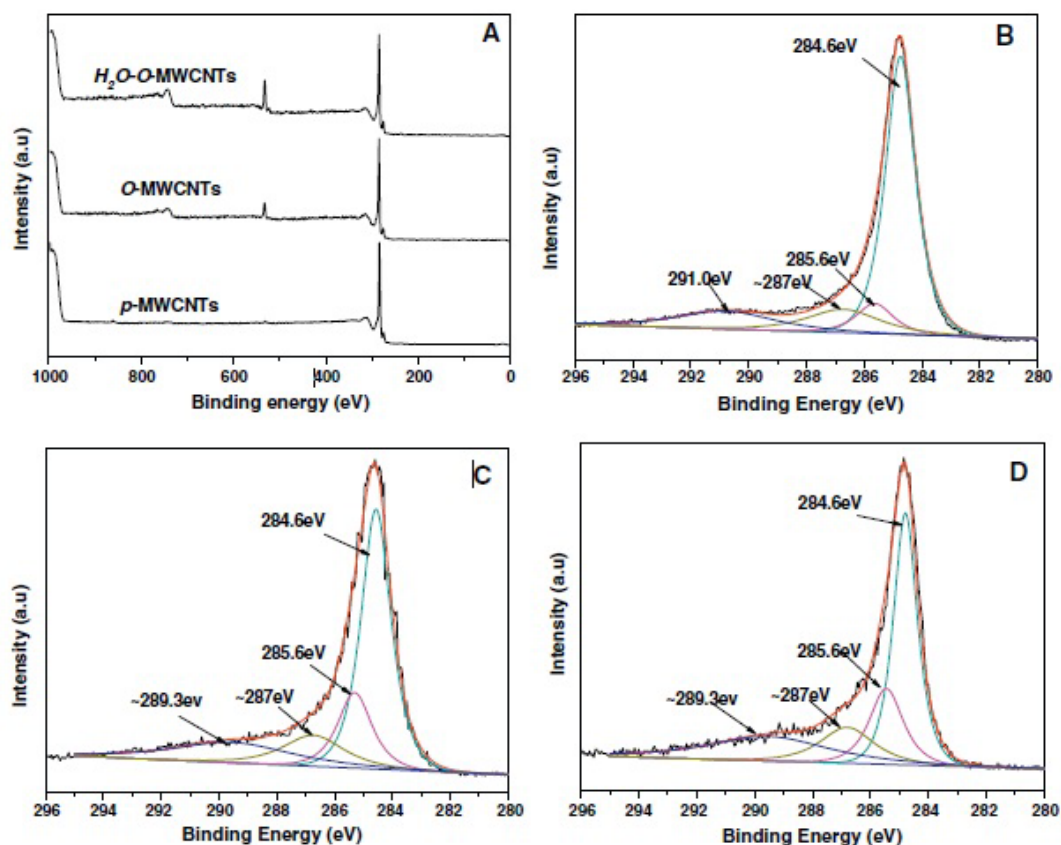


**Figure 2.7** (a) XPS general spectra and high-resolution of C1s spectra of MWCNTs: (b) p-MWCNTs; (c) O-MWCNTs; (d) H<sub>2</sub>O-O-MWCNTs [53].

In another study, with the aim of improving the interfacial properties in epoxy-based nanocomposites, two types of multi-walled CNTs with different outer diameter and length were purified by ultrasonication in a bath (Branson 150) with acetone. Then, both CNTs were subjected to a UV/Ozone treatment for different durations and changes in surface functionality and morphology were characterized by XPS (PHI 5600), Raman spectroscopy (Renishaw, RM 3000) and scanning electron microscope (SEM)[54]. According to SEM) analysis, thick-walled nanotubes (Figure 2.8-a) were much less aggregated and individual carbon nanotubes could be clearly seen. On the other hand, it was noticed that closely packed, highly entangled bundles of thin-walled CNTs as illustrated in Figure 2.8-b.

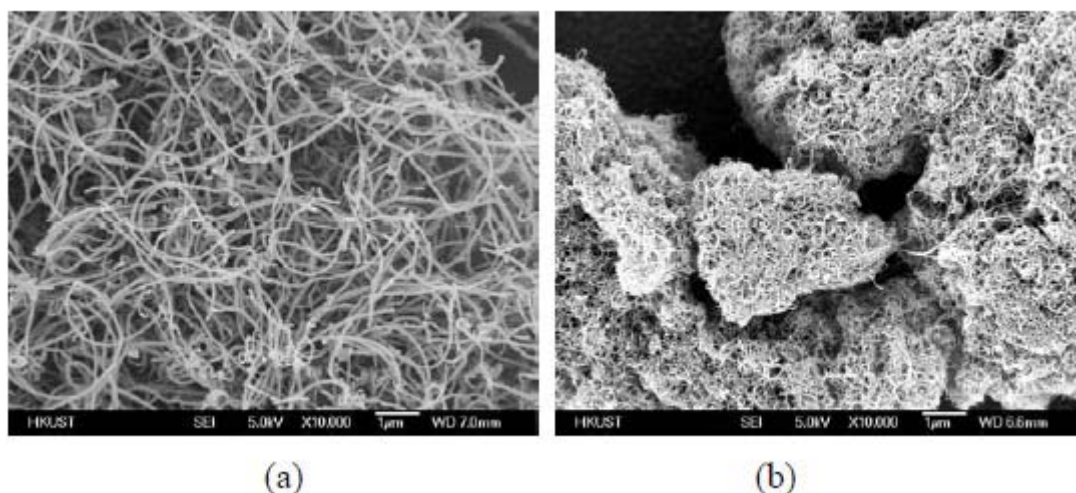


**Figure 2.8** SEM micrographs of two types of carbon nanotubes; (a) thick-walled CNTs and (b) thin-walled CNTs [54].

In XPS general spectra for both CNT types, oxygenated moieties were identified by the -C-O- linkage. Based on XPS atomic concentrations (%), both carbon nanotubes similarly showed a large increase in oxygen surface functionalities (O/C ratio) for the first 30 minutes of oxidation. The difference in O/C ratio of the two different carbon nanotubes began after an hour (h) of oxidation time. In conclusion, thick-walled CNTs had higher reactivity than that of thin-walled CNTs due to turbo static carbon layers reported by Naveed et al. according to D/G intensity ratios (used for evaluation of the disorder density of the nanotube walls) in Raman spectroscopy. There was an increase in defect sites for thick nanotubes up to 2 h whereas no change was observed for thin-walled CNTs. As a result of this study, improved interfacial interactions were achieved within polymeric composites due to possible covalent bonding between the functionalized CNTs and epoxy resin [54].

A few reports have shown that by sonication of MWNTs in water and bubbling O<sub>3</sub> through the dispersion, oxidation levels up to 3-7% oxygen incorporation can be achieved [55]. Li, M. and co-workers claimed that processes which are environmentally-friendly, economically-feasible and can be scaled up easily should be developed to obtain modified CNTs. Because of this reason, they studied oxidation of SWNTs with ozone in aqueous phase under ambient conditions. They also investigated the effect of ultrasonication on the ozone oxidation and evaluated the stability and solubility properties depending on interactions between water and oxidized nanotubes

simultaneously in their research. As a result, they proved that oxidation with ozone and ultrasonication simultaneously was more effective than ozone only in order to resist settling in aqueous suspensions. In addition, with ozonized/ultrasonicated SWNTs they obtained much finer colloidal suspensions that were stable for a longer time with the increasing oxidation time compared to only ultrasonicated SWNTs [56].

Moreover, Danny and his colleagues studied a fluidized ozone oxidation reaction system with O<sub>3</sub>/O<sub>2</sub> mixture in order to remove non-graphitic impurities from MWNTs and to oxidize sidewalls of two types of commercially available nanotubes without using any solvents or acidic treatments. Dimensions and purity levels of carbon species were same for both nanotubes but the defect density was different from each other. Their ultimate goal was also to develop industrially scalable functionalization methods for MWNTs. They exposed nanotubes to ozone for 5 to 90 min at a relative humidity of 50% in a vertical fluidized bed reactor. They reported SEM and Raman spectroscopic analyses for the characterization of structural changes along with FTIR and XPS. According to detailed characterization of oxidized MWNTs, initially and predominantly formed -OH groups were further oxidized to C=O and COOH groups with longer ozone treatment [57].

#### **2.2.4.2 Non-covalent surface modifications**

The advantage of non-covalent surface modification approach is the fact that the sp<sup>2</sup> hybridization is preserved within the graphene structure of CNTs and therefore electronic properties of them can be conserved while their solubility increases significantly. The methodology of non-covalent chemistry is based on adsorption molecules onto CNTs surfaces such as a polymer wrapping action.

Surfactants, amphiphilic copolymers and polyaromatic molecules can be adsorbed over surfaces of nanotubes by  $\pi$ - $\pi$  stacking interactions. Therefore, non-covalent functionalization is considered as the simplest and most effective way to improve the miscibility and solubility of CNTs without any disruptions within the main graphitic structure of nanotubes. For instance, surfactants are used because their hydrophilic ends interact with polar solvent compounds and hydrophobic parts adsorb onto nanotube surfaces [58]. Therefore, the length of the hydrophobic regions and types of hydrophilic groups of the surfactant play a key role in the separation of nanotubes individually from

bundles, aggregates or ropes while dispersing them in organic solvents [45]. In other case, the tendency of CNT aggregation in a solvent can be remarkably reduced by the adsorption of surfactant molecules over CNT sidewalls while lowering the surface tension and improving wettability and adhesion characteristics of nanotubes. Moreover, strong van der Waals interactions between nanotubes can be overcome with electrostatic or steric repulsive forces by non-covalent functionalization. The properties of surfactants, medium chemistry and polymer matrix are main factors to determine the efficiency of this modification method [42]. Sodium dodecyl sulfate (SDS), lithium dodecyl sulfate (LDS) and sodium dodecylbenzene sulfonate (SDBS) are among the simplest and most popular surfactants used for non-covalent functionalization and dispersion of CNTs. However, it should be noted that adsorption of small surfactant molecules onto CNTs may also negatively affect mechanical features of end products such as polymeric composites. On the other hand, polymers, especially conjugated polymers, have also been shown to serve as excellent wrapping materials for the non-covalent functionalization of CNTs as a result of  $\pi$ - $\pi$  stacking and van der Waals interactions between the conjugated polymer chains containing aromatic rings and the surfaces of CNTs [59].

## CHAPTER 3

### 3 CHEMICAL FUNCTIONALIZATION AND ELECTROSPRAY DEPOSITION OF CNTS

#### 3.1 Introduction

Since Iijima [60] discovered carbon nanotubes (CNTs) and made a milestone in the development of CNTs in 1991, these nano structures have been of great interest by most several researchers in a wide range of fields in science and engineering due to their eye catching properties such as high conductivity and mechanical strength, stiffness, chemical structure, inertness, good thermal and electrical properties with low density resulting from the combination of structure, dimension and chemical geometry of the CNTs. The strength of carbon-carbon double bond (C=C) as the main backbone constituted of graphitic sheets within the nanotube structure provides one of the strongest and stiffest linkage in nature. In addition to unique properties of nanotubes, these nano-scale materials have also large surface area to volume ratio which provides an advantage for applications such as nano-composite production. Ajayan [11] determined the surface area of multi-walled carbon nanotubes (MWNT) in his study as 10-20 m<sup>2</sup>/g by Brunauer-Emmett-Teller (BET) theory. This value is larger than that of graphite whereas smaller than that of activated porous carbons and is expected to be an order of magnitude higher for single-walled carbon nanotubes (SWNT). Additionally, CNTs' density is lower than that of graphite. These features make them as promising materials for the scientists in nanotechnology area.

In spite of their widely reported superior features, there are some obvious challenges in incorporating CNTs into fiber reinforced polymeric composites (FRPCs), which are related to difficulties in obtaining a homogeneous dispersion of individual nanotubes avoiding the bundle formation. Agglomerated nanotubes once incorporated into FRPCs act as micron-size defects and do not yield efficient mechanical load transfer from individual nanotubes to polymeric matrix [61]. In order to obtain efficient CNT incorporation into FRPCs, new and novel approaches are needed such as modifying surface properties of CNTs widely referred to as ‘surface modification’ or ‘functionalization’. Surface modification of MWNTs with oxygenated functional groups could be achieved by different functionalization concepts such as covalent or non-covalent methods [62] which have been widely investigated in the last two decades for proper dispersion, purification, or application of CNTs in nano-composite production. Covalent functionalization leading to the attachment of oxygenated functional groups on MWNT surfaces can be achieved with high degree of modification by conventional acid etching, solution processing, or thermal treatment techniques [63]. These methods result in modified nanotubes that are highly miscible with various organic solvents because of introduced polar and non-polar functional groups onto CNT surfaces. Contrary to the advantages, particularly acidic oxidation has two main drawbacks, namely, the first one is to bring about fragmentation of CNTs into the smaller pieces [51] or destruction of graphitic structure of nanotubes, thus; reducing mechanical and conductivity properties of CNTs, while the second one is associated with environmental concerns and high cost due to necessity of post-purification processes. Existing acidic treatments at elevated temperature on the surface characteristic of nanotubes have been commonly studied in the literature. Among them Theodore et al. [6] work can be given as a good and comprehensive example where 3:1 sulphuric acid/nitric acid ( $\text{H}_2\text{SO}_4/\text{HNO}_3$ ) solution was prepared for the treatment of MWNTs at room temperature by using ultrasonic bath for 3 h, which was then subjected to post-processes such as dilution and filtration with distilled water until achieving neutral conditions. Even though this oxidation method increased the number of reactive carboxyl groups (COOH) at the defect sites of MWNTs, amorphous carbon part of MWNTs was burnt out, leading to decrease in the length and diameter. Ziegler et al. [64] have focused on the oxidation of SWNTs with sulphuric acid/hydrogen peroxide ( $\text{H}_2\text{SO}_4/\text{H}_2\text{O}_2$ ), namely ‘piranha mixture’. They have found out that piranha attacks to the defect sites of

nanotubes by leaving some voids in the main structure of CNTs and induces the consumption of oxidized regions producing shorter nanotubes at elevated temperatures. Datsyuk et al. [65] worked on both conventional refluxed nitric acid ( $\text{HNO}_3$ ) and piranha treatment of pristine MWNTs and prepared their dispersion with specified conditions. Both treatment mechanisms required time consuming post-processes such as dilution and filtration, washing the solid part until neutral conditions are reached and vacuum drying. As a consequence of the oxidative treatment by different reagents, oxidation with nitric acid solution increase number of defect sites over CNT sidewalls because of a decrease in the length of nanotubes observed by Raman and XPS analysis, thus leading to increased concentration of carboxyl and hydroxyl groups on the graphitic framework in comparison with the piranha oxidation which results in the absence of further defects onto CNTs. Considering apparent disadvantages of various acidic treatments, gas phase oxidation, which is widely known as “ozonolysis” also, is a more preferable approach since it provides a high degree of functionalization with minimum damage to CNT chemical structure under economically and environmentally feasible conditions. Moreover it is prudent to state that ozone oxidation can lend itself easily to industrial scalability. In this gas phase approach, oxidation is more likely to occur on the reactive defect sites of CNT walls. Therefore, the most probable location to find the attached functional groups along CNT sidewalls was demonstrated to be where defects naturally were present [66].

Having provided the reader with relevant background information concisely, we will here introduce the experimental part of this study which consists of chemical functionalization of MWNTs which will be explained in sufficient detail. Following the oxidation step, thermo-gravimetric analysis (TGA) and Raman spectroscopic characterization methods were used to determine expected oxygenated species over MWNTs qualitatively while the nature of surface composition was quantitatively characterized by utilizing X-ray photoelectron spectroscopy (XPS).

Once all functionalization steps were designed and optimized, different dispersion experiments of both as-received (pristine) and surface modified MWNTs were performed by using ultrasonication method with a probe type sonicator in various organic solvents. Qualified MWNT dispersions were determined and electrosprayed over glass fiber substrates, which were then investigated by scanning electron microscope (SEM) for the distribution of individual nanotubes.

Recalling that the main objective of this study is to incorporate functionalized CNTs as nano level reinforcement into FRPCs as uniformly as possible at the polymer-fiber interface by electrospray deposition method on dry glass fiber reinforcement layers, all processing parameters, leading to enhanced interfacial interactions, and thus improving FRPCs properties have been scrutinized in detail.

### **3.2 Experimental**

The experimental part of this study includes ozone oxidation of MWNTs which is the initial step of the functionalization process providing attachment of oxygenated functional groups over CNT walls. After the optimization of functionalization reaction conditions, different dispersion trials were facilitated to be able to achieve uniform electrospray deposition of MWNT suspensions by systematically varying different process parameters.

### **3.2.1 Ozone Oxidation of Multiwall Carbon Nanotubes (MWNTs)**

Surface functionalization of MWNTs kindly provided by Bayer MaterialScience (produced by a chemical vapor deposition method (CVD) with the a purity greater than 95 wt.%, average diameter between 10– 20 nm, and length of 1–10  $\mu\text{m}$ ) was initially carried out using a gas phase treatment by flowing continuous ozone gas generated by an ozone generator (A2Z Ozone Systems Inc.) through a vertically positioned reactor containing dry nanotubes or bubbling through aqueous dispersion of nanotubes in a glass Erlenmeyer containing 2 and 0.5 g of pristine MWNTs, respectively, at a rate of 3 L/min at room temperature. Ozone treatment was employed with three different processing methodologies, namely as oxidation in dry phase, oxidation in aqueous phase and oxidation of ‘pre-sonicated’ MWNTs in dry phase, which are represented by OD-MWNTs, OW-MWNTs and SOD-MWNTs, respectively, in the thesis. The reactions were performed for various oxidation times; 2, 4, 6, 8, 12, 16 h. Firstly OD-MWNT samples were produced by placing as received dry nanotubes in a vertically positioned column as shown in Figure 3.1. A discharge pipe was connected to the top outlet of the reactor to direct the excess ozone gas into potassium iodide (KI)/distilled water solution and hence to avoid release of the discharged ozone gas to the atmosphere.



**Figure 3.1** Ozone oxidation set-up of MWNTs in dry phase (OD-MWNTs).

Secondly, the ozone gas was supplied into a mixture of MWNTs and distilled water (OW-MWNTs) at a concentration of 1wt% MWNTs while being stirred by a magnetic stirrer in a glass Erlenmeyer flask with oxidation times from 2 to 16 h as shown in Figure 3.2.



**Figure 3.2** Ozone oxidation set-up including MWNTs in water (OW-MWNTs).

Thirdly, as received MWNTs were pre-sonicated in methanol for 1 h, followed by vacuum filtration and drying in an oven at 60 °C overnight before exposing to ozone gas in the vertical fluidized bed in order to prepare SOD-MWNT samples.

The aforementioned ozone treated nanotube samples were characterized qualitatively by thermo-gravimetric analysis (TGA) with a heating rate of 10 °C/min in nitrogen atmosphere on Shimadzu DTG-60H Instrument between room temperature and 1000 °C and Raman spectroscopy in order to determine the expected oxygenated functionalities over MWNT surfaces while the nature of surface composition was quantitatively characterized by utilizing X-ray photoelectron spectroscopy (XPS) performed at Koç University Surface Science and Technology Center.

### **3.2.2 Dispersion of MWNTs**

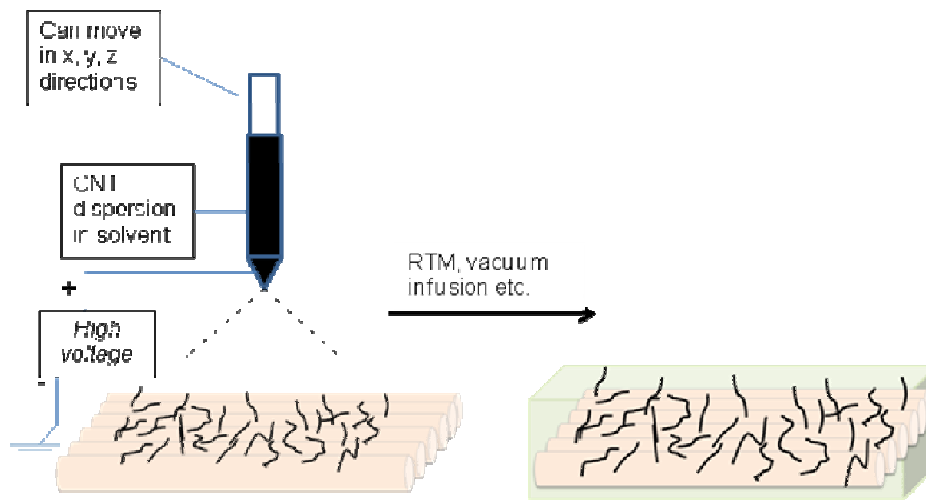
In order for identifying appropriate solvents to obtain most stable MWNT dispersions, oxidized MWNTs were dispersed in a variety of solvents at different concentrations with the aid of a probe sonicator (SONICA Q700 equipment) operated with at previously optimized settings (67 % amplitude with 9 seconds pulse on and 4 seconds pulse off

Table 3.2, as illustrated in the following characterization part, tabulates all of the dispersion attempts with 16 hour ozone treated MWNT samples (OD-MWNTs), in order to determine optimum solvent type, MWNT concentration and sonication time.

### **3.2.3 Electropray Deposition of MWNT Dispersions**

Having achieved a desirable quality of stable MWNT dispersions using the procedure number 12 given in Table 3.2, electropray deposition of carbon nanotubes was carried out over glass fiber substrates as schematically seen in Figure 3.3. To be able to optimize electrospraying conditions for oxidized nanotubes, key electrospraying parameters such as flow rate and applied voltage were systematically investigated as summarized in

Table 3.3. Electrospray deposition experiments were also performed for pristine MWNTs (P-MWNTs) utilizing optimized dispersion and electrospray conditions determined for 16 h-treated OD-MWNTs sample in order to investigate the effect of chemical functionalization on the interfacial interactions between fiber and polymer matrix, and hence the mechanical properties of nanotube integrated composites. These two systems containing pristine and 16 hr oxidized MWNTs were also compared with that of neat composites without nanotubes.



**Figure 3.3** Schematic representation of the electrospray deposition of nanotubes over glass fiber mats.

### 3.2.4 Surface Analysis of Electrospray Deposited MWNTs over Glass Fiber Mats

Scanning electron microscopy (SEM) analysis was performed with LEO Supra VP35 Field Emission Scanning Electron Microscope using secondary electron detector at 2 kV after sputter deposition of a thin conductive carbon coating onto the nanotube electrosprayed glass fiber substrates. The state (individually dispersed or agglomerated) and distribution of nanotubes on the glass fiber surfaces was analyzed in order to determine the best MWNT dispersion suitable for electrospraying and optimum parameters that were mentioned above.

### **3.3 Results and Discussion**

#### **3.3.1 Ozone Oxidation of MWNTs**

Three different oxidation processes were performed by utilizing ozone gas yielding OD-MWNT, OW-MWNT and SOD-MWNT samples. As an immediate advantage of gas phase treatment, environmentally friendly and economically feasible conditions were employed without any extreme post-processes. The dry oxidation approach (OD) was the simplest and easiest among all three methods since the other two approaches required relatively more works such as mixing MWNTs with water or methanol, pre-sonication, filtration and drying processes. In the aqueous oxidation method (OW), nanotubes were stirred in distilled water during the ozone oxidation process with the purpose of having much higher concentration of oxygenated groups over nanotube surfaces due to the presence of water molecules. In the case of pre-sonicated dry phase oxidation method (SOD), MWNTs were pre-sonicated in methanol with the purpose of breaking bundles of nanotubes thereby increasing CNT surface area accessible by ozone gas molecules in the vertical reactor in dry phase as much as possible. As a result of the chemical characterization MWNTs obtained from all three oxidation methods, dry phase oxidation determined to be the most efficient and easiest one for the ozone oxidation process as discussed in the following sections.

#### **3.3.2 Thermo-gravimetric (TGA) Analysis**

Thermo-gravimetric analyses were performed on both pristine and oxidized MWNT samples as a function of the ozone treatment time. As shown in Figure 3.4, which presents the characteristic graph of TGA weight loss for pristine and 16-hour oxidized MWNTs with three different techniques as a function of temperature, MWNT samples showed weight losses in three different temperature ranges. In the first temperature region spanning from room temperature to approximately 100 °C, the small weight loss was attributed to the evaporation of residual moisture absorbed on nanotube surfaces. The second temperature range covering 100°C up to 400 °C corresponds to the degradation and disappearance of organic oxygenated functional groups such as

hydroxyl, carbonyl or carboxylic species formed over the MWNTs by ozone treatment. As for the third region extending up to 800 °C, there is a weight loss attributed to the degradation of CNTs including the amorphous carbon impurities and main graphitic carbon backbone.

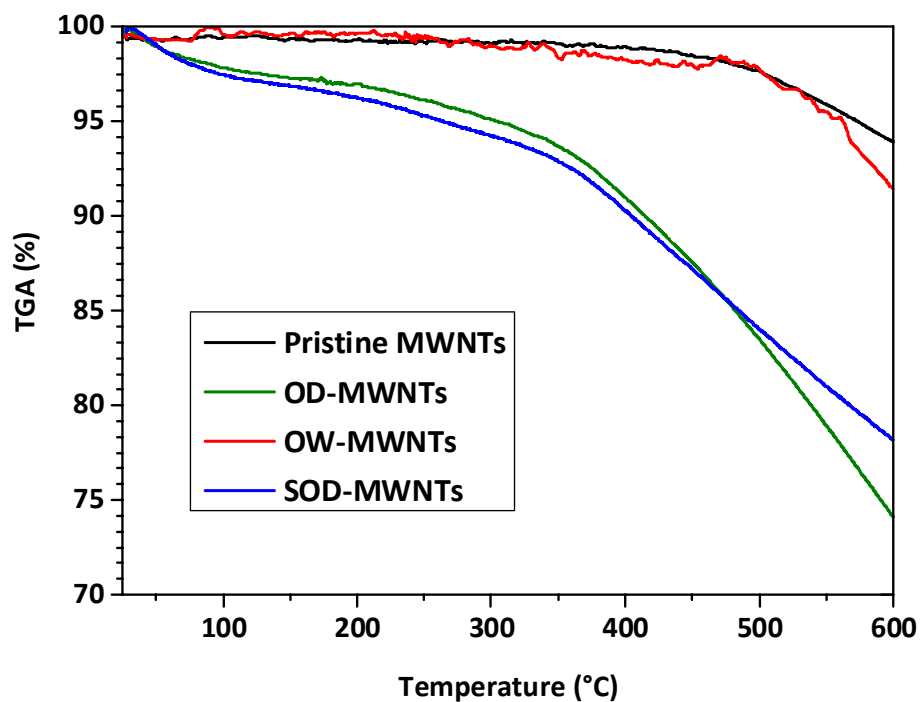


**Figure 3.4** TGA graph of pristine and 16 hour-ozone treated samples including OD-MWNTs, OW-MWNTs, and SOD-MWNTs versus temperature.

The weight loss analyses of both untreated and ozone treated nanotube samples by three different mechanisms were illustrated in Figure 3.5, which specifically shows weight loss values between 100 and 400 °C with increasing ozone treatment time.

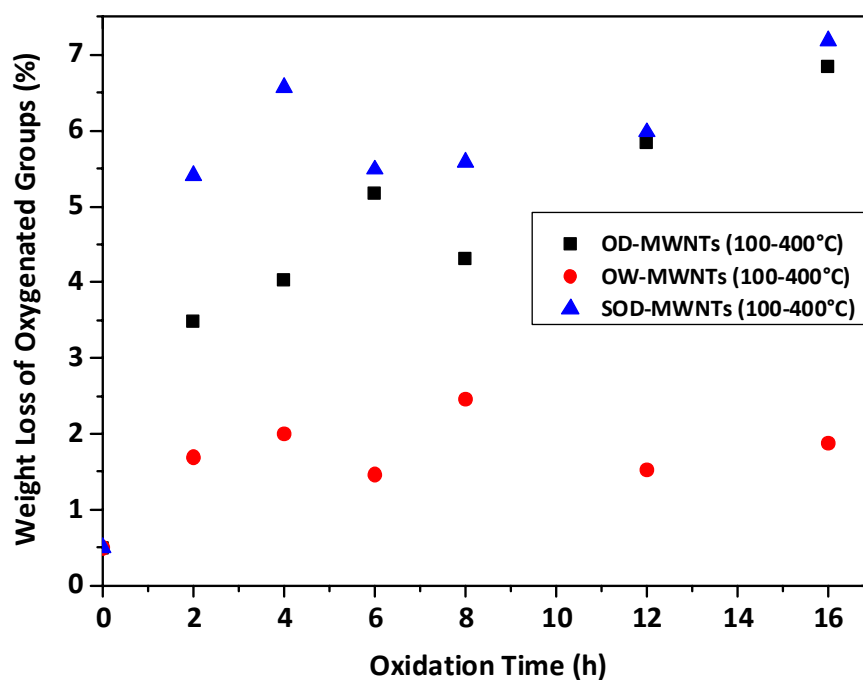


**Figure 3.5** Weight loss of oxygenated groups versus oxidation time.

Referring to Figure 3.5, one can easily notice that unlike initially expected, the OW method does not provide an adequate degree of oxygen functionality on MWNTs in comparison to both OD and SOD methods as a function of ozone exposure time. This conclusion can be easily extracted from the figure by paying specific attention to the weight loss, which is roughly 0.5 to 1.4 % between 100 and 400 °C from 0 to 16 hr oxidation. Achieving nearly 7 % weight loss in OD-MWNTs with respect to the pristine sample over the duration of 16 hour-oxidation time as seen Figure 3.5, the OD technique delivers the highest degree of functionality for MWNTs while being the simplest and easiest method which does not require any extensive pre- and post-processes. SOD-MWNTs shows similar trend (from 0.5 to 7.2 % of weight loss) to OD method in the same temperature range, which clearly shows that the penetration of the ozone gas into as received MWNT bundles was efficient enough and did not improved when MWNT bundles were pre-broken. Thus, in light of these TGA results, the 16 h oxidized MWNT sample in the dry phase was chosen and used in this thesis for all forthcoming functionalization, dispersion, electrospraying and composite manufacturing studies.

### 3.3.3 Raman Spectroscopic Analysis

The most characteristic peaks obtained from Raman spectroscopy of pristine and oxidized MWNTs are demonstrated in Figure 3.6. The intensive peak between 1320 and 1360  $\text{cm}^{-1}$  represents the disorder mode (D line) while the high-frequency peak between 1500 and 1600  $\text{cm}^{-1}$ , called graphite mode (G band), corresponds to distinctive graphitic carbon framework of nanotubes [67]. This peak could be superimposed with the G-line of residual graphite with a second order mode between 2450 and 2680  $\text{cm}^{-1}$  assigned to the first overtone of the D mode and often called G' mode.

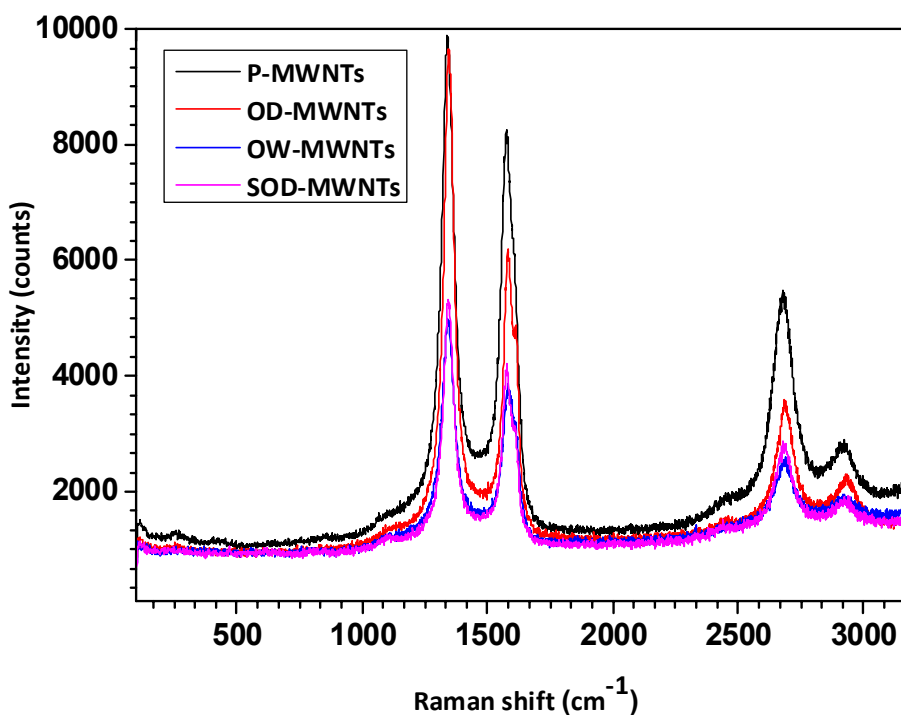


**Figure 3.6** Overall Raman scattering spectra of pristine and 16 hour-ozone treated samples including OD-MWNTs, OW-MWNTs, SOD-MWNTs.

The degree of functionalization was quantified using the relative intensity ratio of D to G bands ( $I_D/I_G$ ) which is the intensity of the disorder mode at 1345  $\text{cm}^{-1}$  divided by the intensity of graphitic mode at nearly 1578  $\text{cm}^{-1}$  [68]. The change in  $I_D/I_G$  ratios corresponding to the OD-MWNTs, OW-MWNTs and SOD-MWNTs as a function of oxidation time ranging from 2 to 16 h in this study was shown in Figure 3.7.

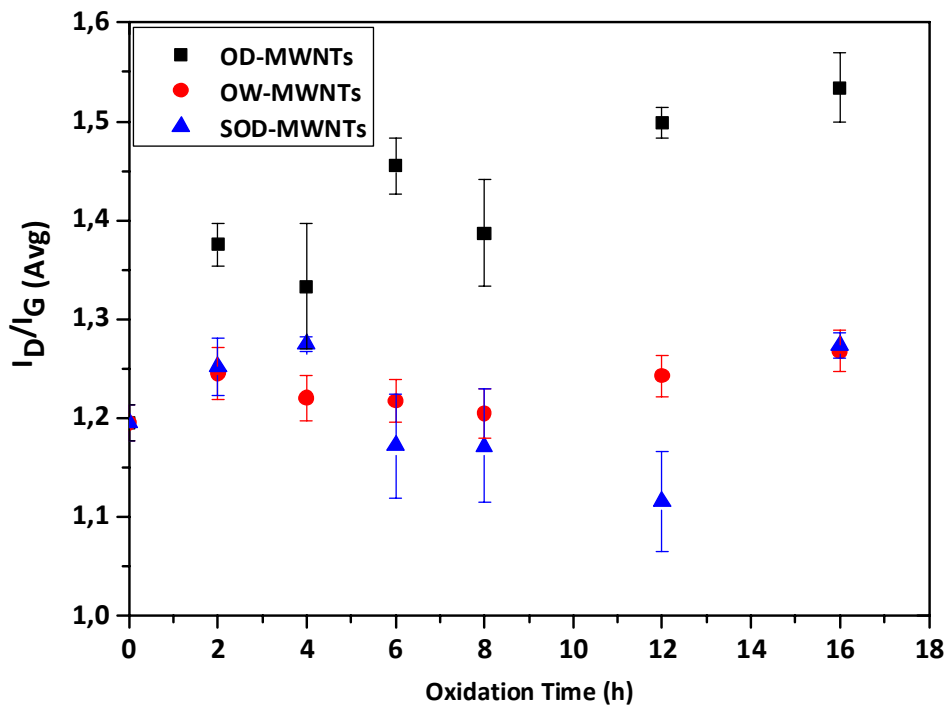


**Figure 3.7**  $I_D/I_G$  of MWNTs versus oxidation time for OD-MWNTs, OW-MWNTs, SOD-MWNTs.

All OD-, OW- and SOD-MWNT samples show similar oxidation trends as shown in Figure 3.7. Initially, there exist a steep increase in  $I_D/I_G$  upon 2 h oxidation and it proceeds with a very slight increase until 16 h. Since the sidewalls or end caps of MWNTs, on which the defects are most probably found, are highly active sites, ozone exposure is highly effective on these regions and large portion of functional groups including  $-OH$  groups forms over the CNT sidewalls in the early stages of oxidation. Following the initial oxidation step, most of the defects disappear and hydroxyl species over CNT structure are further oxidized to the carbonyl groups so that the rate of oxidation and  $I_D/I_G$  show a slight gradual increase with forming carboxylic groups over CNT surfaces. According to Figure 3.7, the aforementioned oxidation profile could be seen remarkably for the 16 h oxidized OD-MWNT sample with the highest concentration of oxygenated functionalities among all other oxidized samples. Raman spectroscopic analysis clearly supported TGA results, which enables the qualitative determination of oxygenated functional groups over CNT surfaces.

### 3.3.4 X-Ray Photo-Electron Spectroscopic (XPS) Analysis

XPS is one of the most effective characterization tool for the quantitative analysis of functionalized MWNTs. XPS analysis can detect exactly the type of introduced functional groups, based on the change in carbon atomic structure which results in a shift at the corresponding binding energies of each modified carbon atoms to the higher energy levels, and provides better understanding of the change in the overall surface composition on the nanotube outer walls. XPS general spectra and high-resolution C1s spectra before and after dry phase ozone oxidation process (OD-MWNTs) are represented in Figure 3.8.

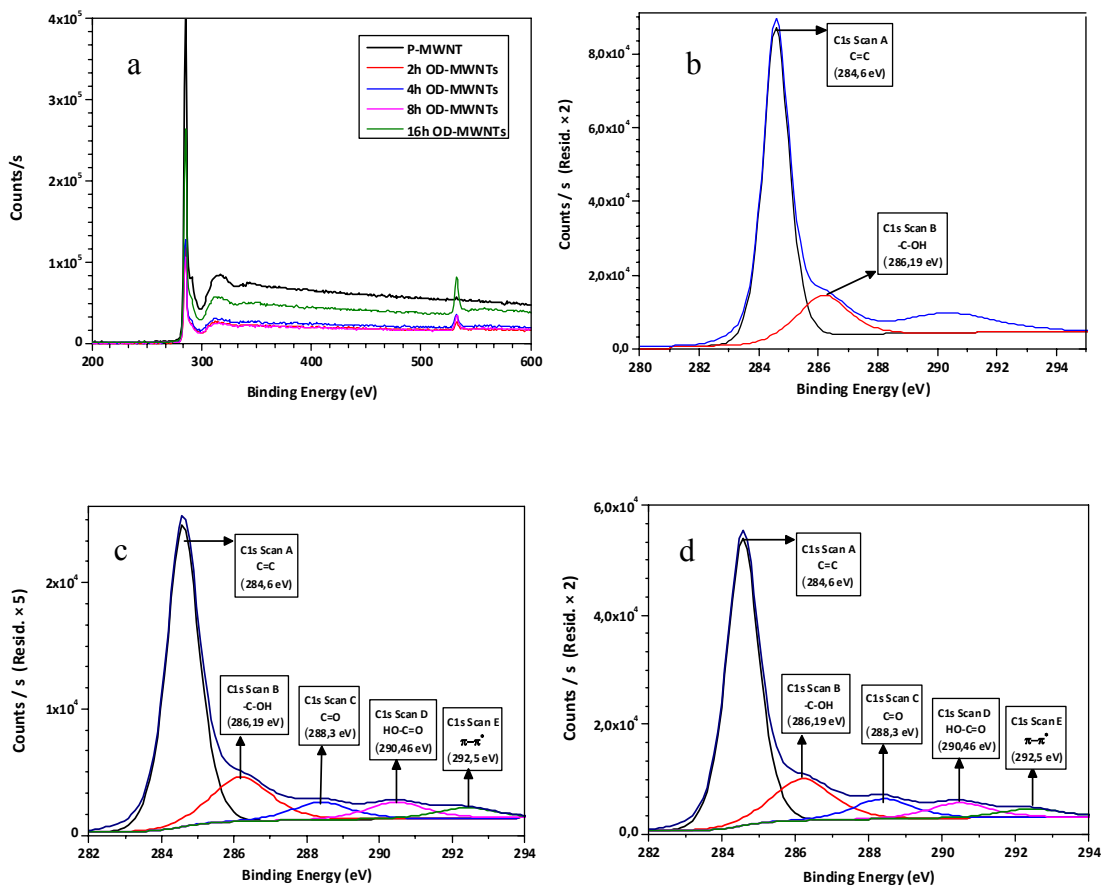


**Figure 3.8** a) XPS general spectra and C1s spectra of b) P-MWNTs, c) 2 h and d) 16 h OD-MWNTs

As shown in Figure 3.8, the main carbon peak can be observed in the C1s based XPS spectra at around a binding energy of 284.6 eV which represents carbon-carbon double bonds ( $-C=C-$ ) detected from the characteristic structure of pristine MWNTs [53]. The

electron density of the carbon atoms changes locally by transferring charge to the surrounding oxygen atoms introduced with increasing ozone oxidation times. Therefore, the specific binding energy of carbon atoms bound oxygen atoms slightly shifts to the higher energy levels on the MWNT outer surface. Accordingly, C1s based spectra for the ozone treated nanotubes (OD-MWNTs) could be de-convoluted by curve fitting of each convoluted five peaks basically representing -C=C- at binding energy of ~284.6 eV and -C-OH, -C=O, HO-C=O at ~286.19 eV; ~288.3 eV and ~290.46 eV, respectively by taking the study of Peng et al. as a reference [53] for the deconvolution process. There also exist  $\pi-\pi^*$  transition peaks at about ~292.5 eV for all nanotube samples. Furthermore, in accordance with the O1s based XPS spectra -C=O and C-O groups were assigned to be approximately at 531.53 and 533.21 eV, respectively.

Quantitative results revealing the composition of surface functionalities and atomic oxygen content of oxidized MWNTs obtained from XPS analyses were summarized in Table 3.1 and Figure 3.9. It can be observed that there is a residual amount of oxygen (0.46 wt%) in P-MWNT sample, which is a commercial available product, Baytubes C 150 P, manufactured by Bayer MaterialScience, Germany.

**Table 3.1** Total O atomic percentage and surface composition of the P-MWNTs and OD-MWNTs versus treatment time

Sample	Total O At. %	C=C (284.6 eV) %	C-OH (286.19 eV) %	-C=O (288.38 eV) %	HO-C=O (290.46 eV) %
P-MWNTs	0.46	80.75	18.79	-	-
2h OD-MWNTs	4.47	65.41	17.05	6.69	6.38
4h OD-MWNTs	5.30	64.71	17.33	6.84	5.82
8h OD-MWNTs	7.42	62.74	16.77	7.36	5.71
16h OD-MWNTs	7.62	62.2	16.42	7.82	5.94

Both Table 3.1 and Figure 3.9 demonstrate the change in composition of carbon double bonds and functional species of carbon atoms as a function of ozone treatment duration. There can be clearly seen a rapid increase in oxygenated groups of carbon atoms mostly in the form of carbonyl and carboxylic groups, whereas a considerable decrease occur

simultaneously in the fraction of C=C structures arising from the graphitic  $sp^2$  hybridized carbon framework upon 2 h ozone oxidation process. After 2 h ozone oxidation, contents of C=O, HO-C=O and even C=C groups reach a plateau until the end of the oxidation process. This means that we could achieve a significant amount of attachment of oxygenated functional groups onto the nanotube surfaces at the end of the 2 hr treatment. However according to Table 3.1, due to the presence of the highest amount of oxygenated species, 16 h OD-MWNT sample were chosen to incorporate into the glass fiber reinforced epoxy based composite structures.

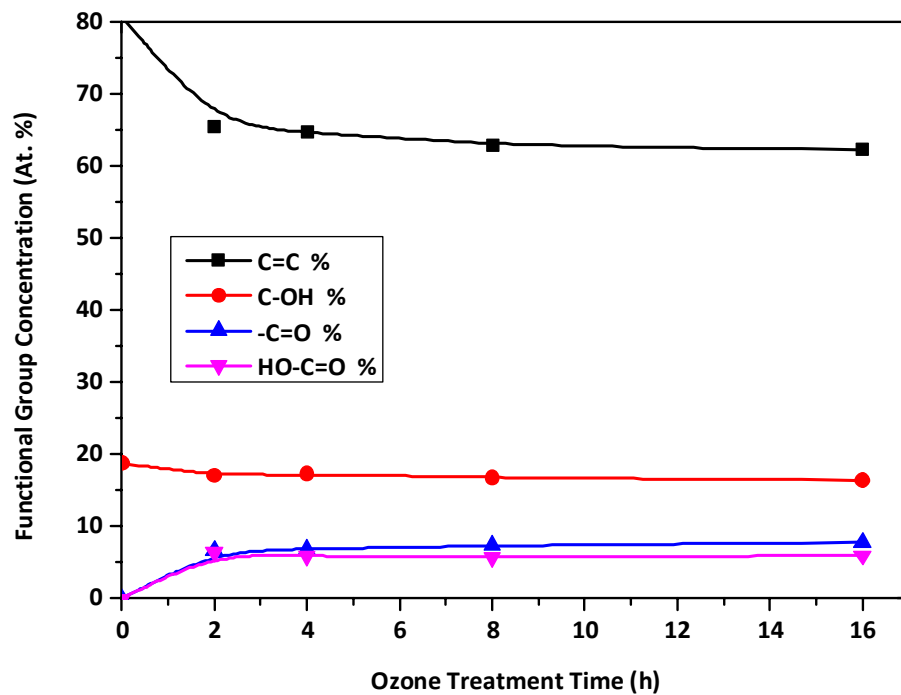


**Figure 3.9** Change in surface composition of carbon atoms and functional groups attached to the carbon atoms after oxidation process as a function of process time.

### 3.3.5 Dispersion

Dispersion quality of MWNTs in an organic solvent prior to the electrospaying process is a critical parameter which plays a role in the relation between optimum interfacial characteristics and properties of the CNT-incorporated composites. Thus, an immense amount of effort has been devoted to prepare uniform and also stable dispersions of MWNTs, which is considered as preservation of the homogenous distribution of nanotubes in their dispersions without any phase separation for a given period. Homogeneous distribution of MWNTs in the dispersion was believed to play a direct role on homogeneous and uniform distribution of them on fiber mats upon electrospaying. Ethanol and acetone were initially evaluated to disperse oxidized nanotubes due to their non-deteriorating nature. However, after several dispersion trials even with very low nanotube concentrations, it was observed that these two solvents were very far from providing good and stable dispersions even with 16 h OD-MWNT samples. On the other hand, organic solvents such as N,N-dimethylformamide (DMF) and N-Methyl-2-pyrrolidone (NMP) are well-known in the literature as candidate solvents to disperse MWNTs much more efficiently and uniformly than ethanol and water. Even though DMF was considered as an effective solvent to disperse nanotubes, our trials summarized in Table 3.2

unfortunately did not lead to stable dispersions without any phase separation, which was observed within a few minutes after the probe sonication process. The most useful organic solvent was found to be NMP, which was presumed to be due to its unique chemical structure which can interact with the oxygenated functional groups attached over CNT surfaces through non-covalent interactions such as hydrogen bonding. A 50:50 mixture of NMP and distilled water was also evaluated, which resulted in a good dispersion containing 0.005 wt % of 16 h OD-MWNTs (trial #12 in Table 3.2). The reason behind mixing NMP and water was to diminish the detrimental effect of NMP in the working environment.

**Table 3.2** Experiments on the dispersion of 16 h OD-MWNTs in various organic solvents using probe sonication.

#'s					Observations	
	Solvent	CNT Concentration (wt%)	CNT deposition (mg/m <sup>2</sup> )	Solvent (g)	Dispersion Quality	CNT Deposited Surface
1.	Ethanol	0.005	16.66	10	Poor	-
2.	Acetone	0.005	-	30	-Poor -Presence of bundles	-
3.	DMF	0.010	-	10	-Good -Unstable	-
4.	NMP	0.010	66	20	Good	Presence of CNT bundles
5.	NMP	0.010	33	10	Good	Presence of CNT bundles
6.	NMP	0.010	16.6	5	Good	Presence of CNT Bundles
7.	NMP	0.010	16.6	5	Good	Presence of CNT bundles
8.	NMP	0.0250	33	4	Poor	Presence of CNT bundles
9.	NMP	0.005	16.66	10	Good	Uniform CNT distribution
10.	H <sub>2</sub> O	0.005	16.66	10	Good	Sprayability issues
11.	NMP/H <sub>2</sub> O (50:50wt %)	0.005	16.66	10	Good	Uniform CNT distribution
12.	NMP/H <sub>2</sub> O (25:75 wt %)	0.005	16.66	10	Good	Sprayibility issues

**Table 3.3** Electro-spray experiments with stable dispersions from Table 3.2, #12

#'s	Materials		Concentration (wt%)	Process conditions	Results	Time (min)
1.	NMP/H <sub>2</sub> O (50:50wt %)	16h OD-MWNT	0.005	80μL/h, 15kV	Problem in electrospray	5
2.	NMP/H <sub>2</sub> O (50:50wt %)	16h OD-MWNT	0.005	60μL/h, 15kV	Good dispersion and best condition	5
3.	NMP/H <sub>2</sub> O (50:50 wt %)	16h OD-MWNT	0.005	60μL/h, 24kV	Nothing changed from 2 <sup>nd</sup> trial	5
4.	NMP/H <sub>2</sub> O (50:50 wt %)	16h OD-MWNT	0.005	60μL/h, 15kV	Nothing changed from 2 <sup>nd</sup> trial	10

### 3.3.6 SEM Analysis

A homogenous dispersion and uniform distribution of nanotubes in the surrounding media has to be evaluated and ensured in order to translate key multifunctional properties of nanotubes to the properties of the corresponding composite structure. For this purpose, surface coverage of nanotube deposited glass fiber mats produced under different dispersion and electrospray process parameters was evaluated by probing under SEM. Firstly the solvent type, nanotube concentration, sonication time and amount of nanotube deposition over glass mats were optimized by performing the electrospray process at a constant 40 μl/h flow rate and 15 kV applied voltage. SEM images of deposited 16 h OD-MWNT deposited glass fiber surfaces corresponding to all of the dispersion trials which were summarized in Table 3.2 and Table 3.3 are shown in Figure 3.10 and Figure 3.11.

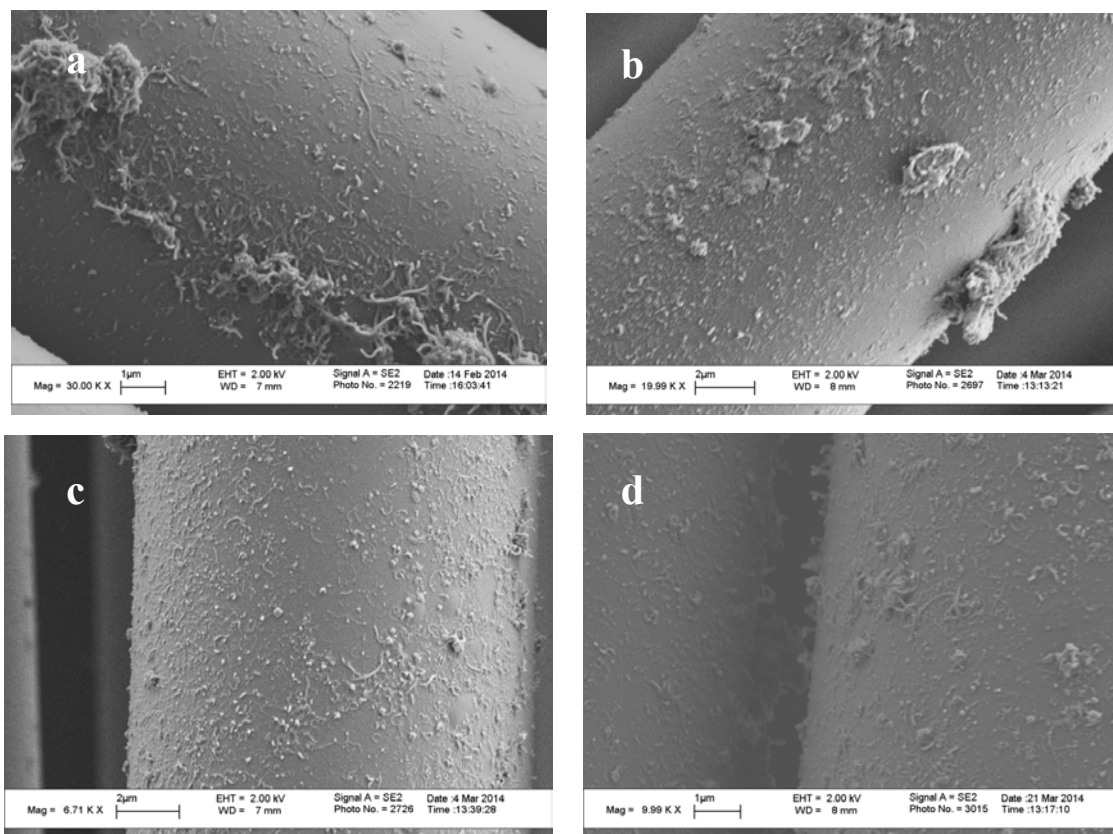


**Figure 3.10** SEM images of glass fiber surfaces prepared with various 16 h OD-MWNTs dispersions by electrospaying at constant 40  $\mu\text{l/h}$  flow rate and 15 kV applied voltage: a) 0.025 wt % of nanotube in NMP, b) 0.01 wt % of nanotube in NMP, c) 0.005 wt % of nanotube in NMP, d) 0.005 wt % of nanotube in NMP/ $\text{H}_2\text{O}$  (50/50 wt %).

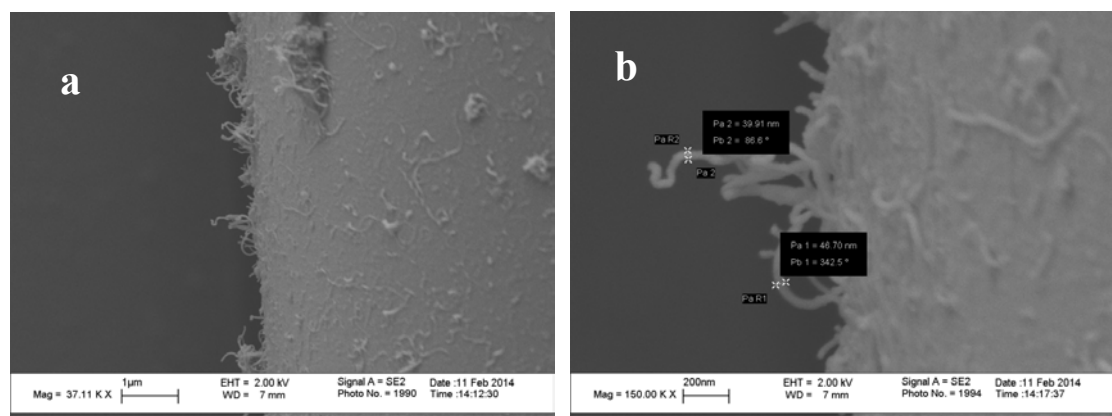


**Figure 3.11** SEM images showing random orientation of nanotubes both horizontally and vertically to the glass fiber mat surface. Images correspond to trial number 5<sup>th</sup> in Table 3.2.

Although it was expected that ozone oxidation could lead to homogenous dispersion and uniform distribution of functional nanotubes, large amount of agglomeration and non-uniform nanotube distribution over glass fiber substrates could clearly be seen in Figure 3.10a and b, for samples electro sprayed from 0.025 wt. % and 0.01 wt% of 16 h OD-MWNTs containing dispersions in NMP, respectively. However, the presence of these agglomerations was clearly minimized once the nanotube concentration in the dispersion was decreased to a lower level, 0.005 wt%. As shown in Figure 3.10c and d, the agglomeration formation was mostly handled by attaining the most homogenous and stable dispersion, thus resulting in the most uniform electro spray deposition with individual distribution of nanotubes over glass fiber mats was achieved at a 0.005 wt% concentration of 16 h OD-MWNT in NMP and NMP/H<sub>2</sub>O dispersions, respectively. Based on these results, we decided to use NMP/H<sub>2</sub>O medium for nanotube dispersions in order to eliminate the adverse effect of NMP on both glass fiber mats and also the working environment. Uniformly distributed and randomly oriented nanotubes both vertical and horizontal to the fiber mat surface observed in Figure 3.11 that were deliberately placed between polymer-fiber interface are expected to efficiently interact with both components in the composite structure with the aid of chemical functionalities over CNT structures.

In the case of achieving uniform distribution of individual nanotubes over glass layers, electro spraying conditions such as flow rate and voltage supply were also optimized as 60 $\mu$ l/h and 15 kV, respectively, using SEM analyses shown in Figure 3.12b. On the other hand, electro spray deposition of P-MWNTs under the optimized dispersion and electro spray conditions was also performed comparatively to the oxidized nanotubes as presented in Figure 3.12a.

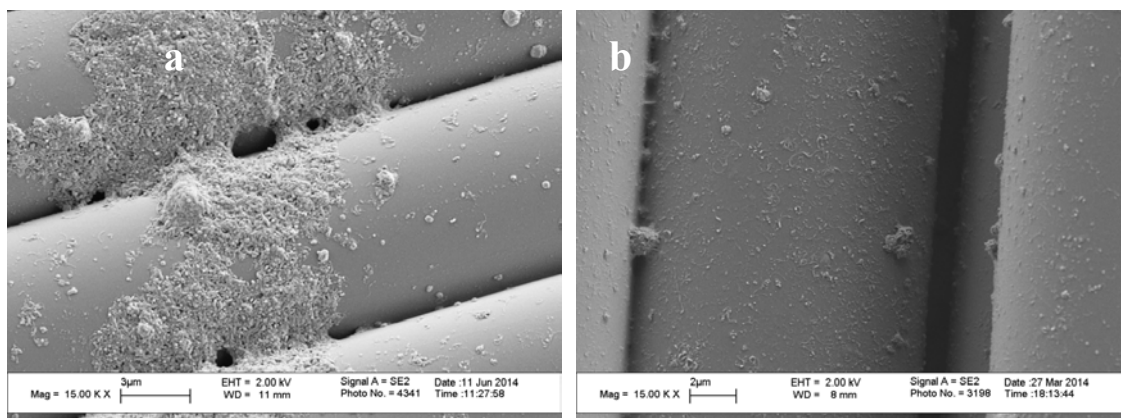


**Figure 3.12** SEM images of electrospayed (60  $\mu\text{l/h}$  and 15 kV) glass fiber surfaces covered with a) P-MWNTs and b) 16 h OD-MWNTs.

In Figure 3.12, the formation of much larger aggregates was observed after the electrospay deposition of 0.005 wt% P-MWNTs containing NMP/ $\text{H}_2\text{O}$  (50:50 wt%) dispersion under optimum electrospay conditions. It can clearly be stated that the ozone oxidation process utilized and optimized in this study significantly improved both dispersibility and electrospayability of MWNTs as evidenced by corresponding SEM images.

### 3.4 Conclusions

Gas phase ozone oxidation was demonstrated as an effective oxidation method due to its applicability without any solvent or any post purification processes. Ozone oxidation experiments were carried out with three different techniques; OD-MWNTs, OW-MWNTs and SOD-MWNTs. TGA and Raman spectroscopic analyses confirmed that the highest amount of oxygenated functional groups such as hydroxyl, carbonyl or carboxylic groups could be introduced over nanotube outer surfaces by using a dry oxidation process on pristine MWNTs for up to 16 h. In addition the highest rate of oxidation process could be observed from zero to 2 h ozone oxidation duration.

For further analysis, XPS was used to quantify the composition of surface functionality and atomic oxygen content attached to OD-MWNTs as a function of ozone oxidation time. From the analysis of XPS results, the highest amount of atomic oxygen content

was observed in the 16 h OD-MWNT sample and these results were found to absolutely support TGA and Raman spectroscopy results, which enabled us to determine the best sample in the following experiments.

To be able to obtain homogenous and stable dispersions of MWNTs to be electro sprayed, several dispersions were evaluated by trial and error approach using a variety of solvents with varying nanotube concentration and sonication time. On the other electro spray parameters such as flow rate and voltage supply were also optimized by probing SEM analysis of distribution of 16 h OD-MWNTs electro sprayed onto glass fiber mats. Consequently, based on surface investigations of glass fiber mats by SEM analysis, the most effective dispersion trial leading to the most uniform distribution of individual nanotubes with minimized amount of aggregations over the glass fiber layers was accomplished by dispersion of the 0.005 wt% of 16 h OD-MWNTs in NMP/H<sub>2</sub>O (50:50 wt%) by an electro spray process at 60  $\mu$ l/h of flow rate and 15 kV of voltage supply prior the composite production and testing experiments.

Moreover, SEM images of P-MWNTs deposited glass fiber surfaces show not only the presence of much larger agglomerates but also a non-uniform distribution of CNTs on the glass fiber mat surface compared to that of experiments performed with the 16 h OD-MWNTs under the same conditions.

## CHAPTER 4

# 4 PRODUCTION AND CHARACTERIZATION OF CNT INCORPORATED FRPCs

### 4.1 Introduction

Advanced glass or carbon fiber reinforced polymeric composites (FRPCs) are load bearing structures utilized in different industrial and energy-related applications. Each component retains its original structure and contributes its own unique properties such as lightweight, high specific strength, corrosion and chemical resistance, durability, conductivity that results in a new and multifunctional composite material with extreme overall performance. For instance, carbon fiber reinforced polymeric (CFRPs) composite materials provide a greater structural strength-to-weight ratio over many traditional metallic materials. Specifically Davis et al. [69] indicates that CFRP composites have been recently used in airplane structural components for their high ultimate tensile strength and modulus (stiffness) properties along with high resistance to fatigue loadings. Recently industrial needs especially in aerospace sector are changing rapidly to obtain stronger, more durable and lighter polymeric composites; hence the micro scale composites need to be further improved with nano-phase integrated materials. Jiang et al. [70] studied laying up of carbon fiber pre-pregs which were produced from the 1 wt% of acid functionalized MWNT integrated epoxy resin and they investigated interfacial characteristics of hybrid carbon fiber/MWNT/epoxy composite laminates. They reported that the main failure mechanisms were described as crack initiation and propagation and also fiber-matrix interface delamination at the defect

located stress concentration regions. According to their investigation the most beneficial approach was the incorporation of functionalized MWNTs near the fiber-matrix interface in order to prevent crack initiation or propagation by means of nanotube bridging effect. They also proved better interfacial properties within MWNT reinforced composites by observing significant improvements in interlaminar shear strength (ILSS) via three point bending tests. Zhou et al. [71] studied incorporation of as high as 2 wt% of carbon nanofibers (CNFs) into the epoxy matrix, and then they produced CNF incorporated epoxy based carbon fiber composites by vacuum assisted resin transfer molding method. They showed 22% and 11% improvement in the flexural and tensile strengths, respectively. They also observed that the crack propagation resistance was improved by the bridging effect of CNFs.

Glass fiber reinforced polymeric (GFRPs) composites have lower cost than carbon fibers with their enhanced multifunctional properties such as high mechanical, chemical resistance and insulating properties [72]. Even if they are not as stiff or strong as CFRP composites, they always find great attention in the industry due to a better cost-performance ratio than CFRP composites. Thus, the integration of promising nano-phase reinforcement in order to create high performance GFRP composites with improved performance is still a challenging and attractive topic in the composites world. Carbon nanotubes have been commonly utilized as nano fillers in FRPCs due to their high strength with high aspect ratio leading to the property improvements by enhancing fiber-matrix interfacial properties of when they are incorporated individually and uniformly at the interface. Gojny et al. [73] investigated the application of amine functionalized double walled carbon nanotube (DWNT-NH<sub>2</sub>) reinforced epoxy matrix for GFRP composites manufactured by resin transfer molding process. They used a calendaring process in order to disperse DWNT-NH<sub>2</sub> in the neat epoxy resin. Since tensile properties were dominated through in-plane directions by glass fiber reinforcement, they could not see any improvement in tensile strength and modulus for 0.3 wt% of functionalized nanotube (into the epoxy resin) incorporated GFRP composites. On the other hand they were able to see approximately 18% and 20% increase in fracture toughness and interlaminar shear strength (ILSS), respectively, performed under three point bending loads. Such an improvement with DWNT-NH<sub>2</sub> in GFRP composite properties was due to strong interfacial interactions between amino functionalized nanotube and epoxy resin as well as between nanotube and glass fibers

due to the further cross linking ability of epoxy matrix and sizing material of the glass fibers which include epoxy functionality.

FRPCs are produced with various manufacturing techniques by considering the type of matrix and fibers, required temperature to cure the matrix and form composite parts, and the cost, quality and effectiveness of the process. The manufacturing process is the most critical step for the design of a composite material which can be produced for different application areas such as in aerospace, construction, transportation or marine industry. These composite materials have been recently found special interest in luxury automobile, compressed gas storage tank and wind turbine applications. For instance, longer and even lighter turbine blades with increased generation of wind power were developed with rigid, high strength and fatigue resistant CFRP composites[10]. Furthermore, the main features of composite materials can be designated by the relevant manufacturing methods which have to be considered simultaneously with their advantages, restrictions, costs, production rates and capacities and also typical usages [74] . Literally, common production methods include hand lay-up, pre-preg lay-up, autoclave processing, vacuum infusion, and resin transfer molding (RTM). Detailed information about manufacturing steps of composites is comprehensively covered in the literature [74]. Among these methods, RTM and vacuum infusion are economically and environmentally feasible methods, providing safe working conditions. Vacuum infusion process allows for the fabrication of larger capacity and lower cost composite materials than that of other methods. An advantage of the ability to remove excess amount of resin out of the production area by vacuum bag and producing larger fiber reinforcement to resin ratio results in lighter composite structures with higher strength so that vacuum infusion process is used as the composite manufacturing technique within the content of this study.

In this study, deliberate incorporation of chemically oxidized carbon nanotubes (OD-MWNTs) into the polymer-fiber interface in FRPCs by depositing them on each surface of layered glass fiber mats using a novel electrospray system prior to the vacuum infusion process to manufacture CNT integrated GFRP composites is reported. The effect of key structural and process parameters such as the CNTs' functionality, CNT dispersion concentration, solvent type and CNT content on the mechanical properties of final FRPC materials was systematically investigated. If the term reinforcement

efficiency is defined as the degree of property improvement as a function of the CNT content in the final composite material, very high reinforcement efficiencies up to 20% improvement in the flexural strength of composite materials with as low as 0.01 wt% OD-MWNT content in the overall composite achieved in this study have never been reported in the literature and will be reported for the first time in this thesis.

## **4.2 Experimental**

### **4.2.1 Materials**

As-received pristine MWNTs (P-MWNTs), Baytubes C150 P, produced by a chemical vapor deposition method with higher purity than 95 wt.% and average diameter 10–20 nm and length 1–10  $\mu\text{m}$  were kindly from Bayer MaterialScience AG. The fiber mat used is Metyx LT300 E10A 0/90 biaxial E-glass stitched fabric with 161 gsm in the 0° orientation, and 142 gsm in the 90° orientation, summing to 329 gsm total. The epoxy resin component, ARALDITE LY 564 epoxy resin and XB 340 hardener, were produced from Huntsman Corporation, and mixed with the ratio of 100 and 36 parts by weight respectively.

### **4.2.2 Composite Production by Vacuum Infusion (VI)**

Following the electrospray deposition (seen in Figure 4.1) of pristine and OD-MWNTs with different dispersion concentration or variable spraying capacity over each of the glass fiber surfaces, the overall 6-ply symmetric composite laminates were manufactured by vacuum infusion process represented in Figure 4.2. We achieved three different composite productions labeled as G1-B9, G1-B10 and G1-B11 were manufactured with varying parameters as summarized in Table 4.1. In each label, G1-Bx, G1 represents the type of glass fiber reinforcement; B and the number x represent biaxial reinforcement and the order of the production respectively.

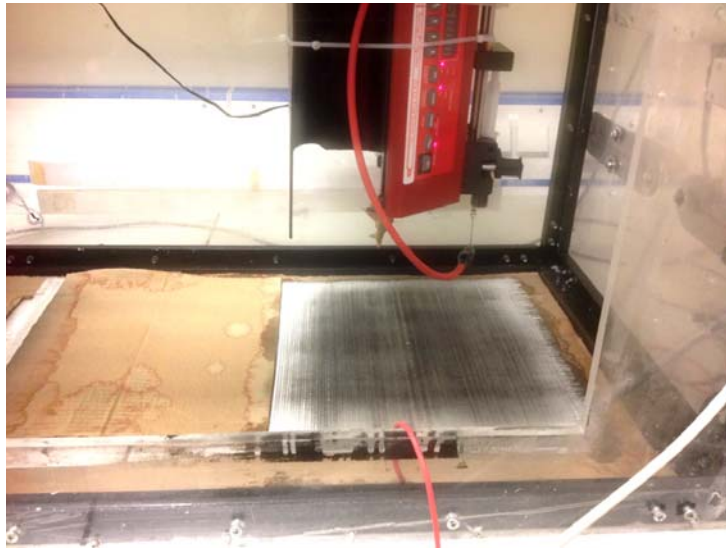


**Figure 4.1** Electrospray deposition of OD-MWNT into 50/50 wt. of NMP/H<sub>2</sub>O solution by using a two-axis router.

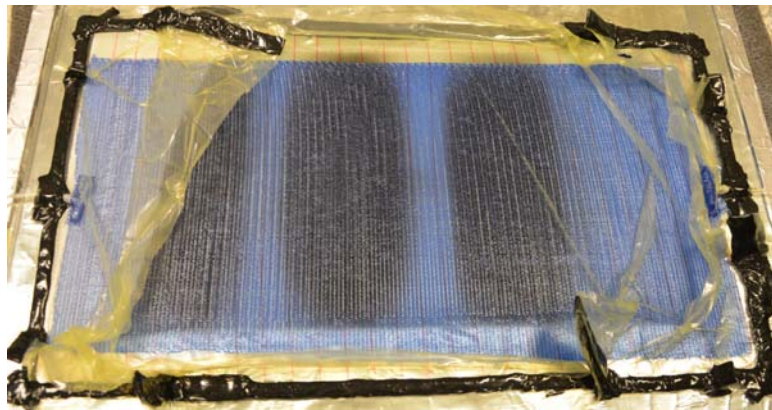


**Figure 4.2** Vacuum in-fusion process

**Table 4.1** Three different composite plates including P-MWNTs and 16 h OD-MWNTs deposited with variable parameters

Composite Name	G1-B9	G1-B10	G1-B10-1	G1-B10-2	G1-B11-3	G1-B11-4
Type of CNTs	OD-MWNT (0)	P-MWNT	OD-MWNT (1)	OD-MWNT (2)	OD-MWNT (3)	OD-MWNT (4)
Solvent	NMP/H <sub>2</sub> O	NMP/H <sub>2</sub> O	NMP/H <sub>2</sub> O	NMP/H <sub>2</sub> O	NMP/H <sub>2</sub> O	NMP
Dispersion Concentration (wt %)	0.005	0.005	0.005	0.01	0.01	0.01
Spray Direction	x-y	y	y	y	y	y
Amount of CNTs on fiber mat surface (mg/m <sup>2</sup> )	400	400	400	400	800	800
CNT content in the final composite (wt %)	0.01	0.01	0.01	0.01	0.02	0.02

According to the Table 4.1 each electro spray process in different conditions was labeled with numbers such that OD-MWNT (0) one represents the initial spraying process which was performed through x and y axis. On the other side the others were achieved only through y axis.

Figure 4.3 presents symmetrical stacking arrangement of the electro sprayed glass reinforcements, and then they were placed over the production region such that 90° directional surfaces of glass fiber layers faced towards the outside of the laminate midplane while 0° direction of the plies was aligned along the resin flow direction. After

placing the glass fabrics, Teflon film was put below the ply stacks to be able to remove the manufactured composite plate easily from the molding area. In addition flow mesh used for making the glass fiber mats wet by leading uniform resin infiltration process and peel ply to prevent sticking problem of the plies to the flow mesh are the main components of vacuum in-fusion process. Then a vacuum bag was used in order to cover the glass layers over the production region by the help of sealing tape in order to keep all the system into the vacuum.

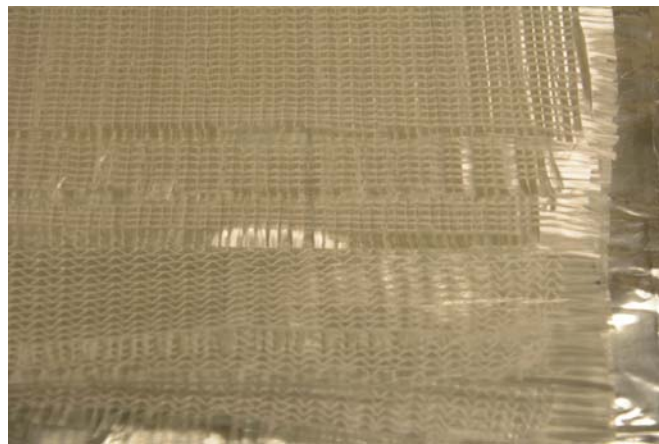


**Figure 4.3** Symmetric 6-ply stack arrangement placed over the heating production region

The epoxy resin and hardener were mixed sufficiently and degassed for 15 minutes before the vacuum injection process which was performed by using atmospheric pressure at 75 °C for curing during 20 hours. Final composite plate was removed from the production area as seen in Figure 4.4 as a representative example.

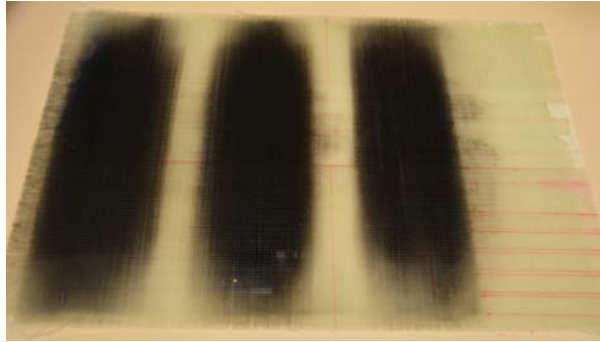


**Figure 4.4** Produced composite plate by vacuum fusion method

### **4.2.3 Mechanical Characterization**

Tensile and three point bending tests were performed with the Zwick Roell Z100 Universal Testing Machine (UTM) in accordance with the ASTM D3039 and ASTM D790 respectively. Figure 4.5 and Figure 4.6 show flexure and tensile test specimens respectively. All test samples were cut from manufactured composite panels such that the length of the specimens was adjusted along the  $0^\circ$  direction. Specimen length and width for tensile test were  $250 \text{ mm} \times 25 \text{ mm}$  and for the flexural tests these quantities are determined as  $80 \text{ mm} \times 15 \text{ mm}$ . The span length was also determined in accordance with the ASTM standard as  $150 \text{ mm}$  for tensile tests. Furthermore the span length of three point bending specimens were determined as 16 times of the thickness values for each manufactured composite plate according to the related standard. Tensile tests were applied to only the specimens which were cut from the preliminary composite plate (G1-B9) and the tests were performed with the head displacement rate of  $2 \text{ mm/min}$ . Flexural tests were conducted for all of the composite samples at the rate of cross head motion of approximately  $0.8 \text{ mm/min}$  calculated as a function of span length and depth of the composite. At least three test specimens cut from each of the nanotube integrated and their corresponding neat composite were tested and average strength and modulus values were calculated and reported.

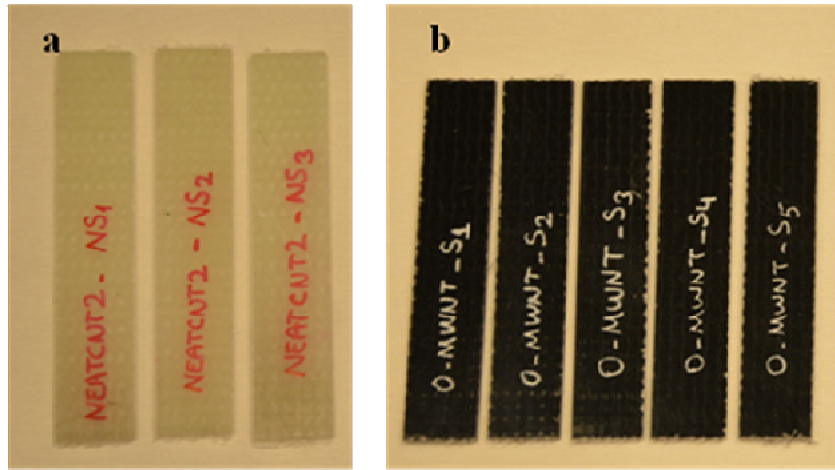


**Figure 4.5** Flexure test specimens; a) neat and b) OD-MWNT reinforced composite specimens

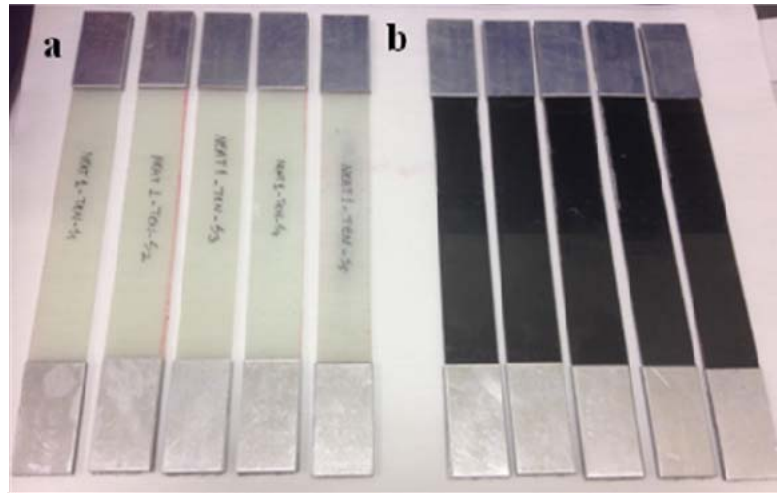


**Figure 4.6** Tensile test specimens; a) neat and b) OD-MWNT reinforced composite specimens

Deformed specimens under flexural and tensile loads were represented in Figure 4.7.

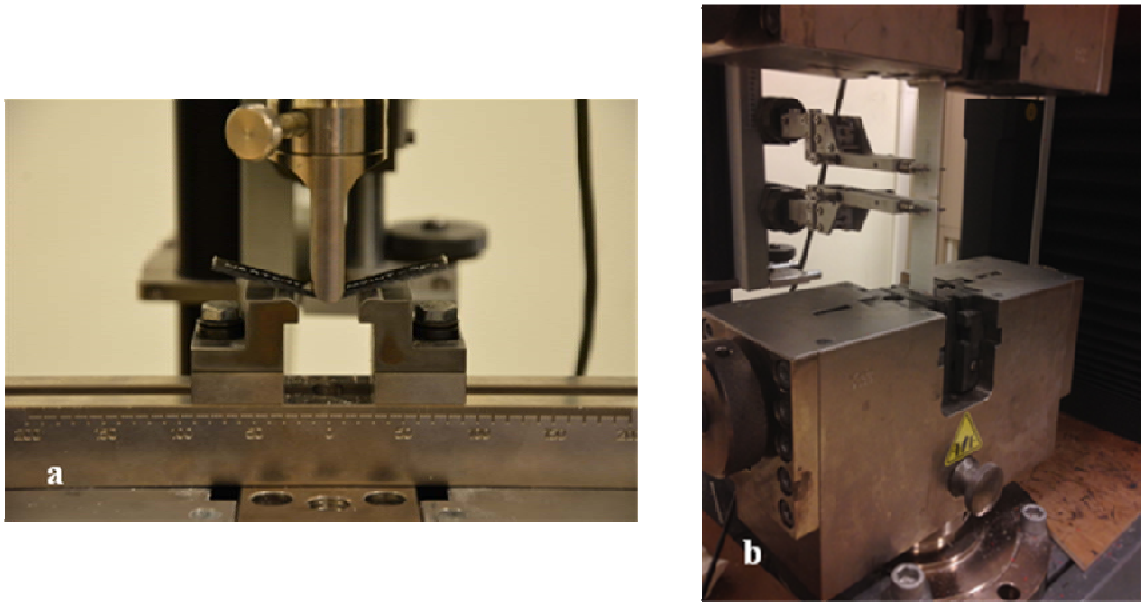


**Figure 4.7** Deformation of a) three point bending and b) tensile test specimens

#### **4.2.4 Surface Characterization**

Fracture surface after tensile failure for both neat and OD-MWNT integrated glass fiber-epoxy specimens were established with LEO Supra VP35 Field Emission Scanning Electron Microscope using secondary electron detector at 2 kV in order to examine the fracture behavior of the samples and also nanotube distribution at the interface between glass-epoxy resin within the composite. Carbon coating was applied onto the specimens by sputter deposition to obtain conductive samples.

## **4.3 Results and Discussion**

### **4.3.1 Composite Production**

Composite samples that were manufactured in this study are summarized in Table 4.1. For G1-B9,  $300 \times 300 \text{ mm}^2$  area was electro-sprayed by using only OD-MWNT (0) (shown in Table 4.1) whereas a  $300 \times 300 \text{ mm}^2$  area was left blank as neat composite for comparison purposes. During the production of G1-B10 and G1-B11, electro-spray process was performed in the y direction with OD-MWNTs under different conditions as summarized in Table 4.1 and the whole panel consisted of four or three  $100 \times 300 \text{ mm}^2$  areas, respectively, including a blank area which is the neat part for comparison purposes. Same amount of CNT solution was deposited on each surface of the glass mat consisted of 12 layers in order to ensure the CNT content on every surface was the same, 400 or 800  $\text{mg/m}^2$ , which resulted in 0.01 wt% or 0.02 wt% CNT content in each section of the composite as summarized Table 4.1. The overall volume fraction of primary reinforcing glass fibers in the composite plates was determined by the burning test as approximately 40 %.

### **4.3.2 Static Tensile and Three Point Bending Test Results under UTM**

Tensile stress and elastic modulus results for OD-MWNT (0) integrated composite with its corresponding neat specimens (without OD-MWNTs) and (prepared from G1-B9) are shown in Figure 4.8 and Table 4.2. CNT incorporated panels contain 0.01 wt% OD-MWNTs in the overall composite (with respect to both resin and glass fiber), which corresponds to 0.03 wt% with respect to the epoxy resin. All of the stress-strain curves in the following correspond to the representative one among the tested three specimens for each produced samples.

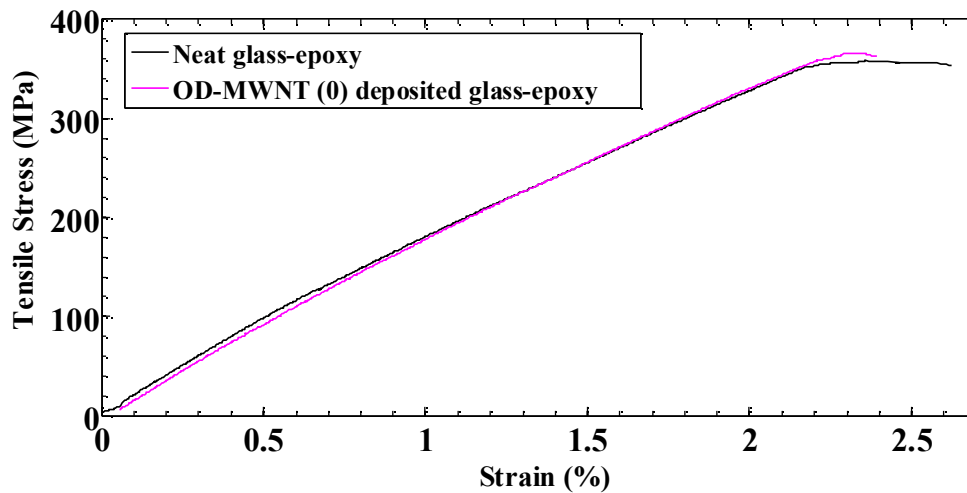


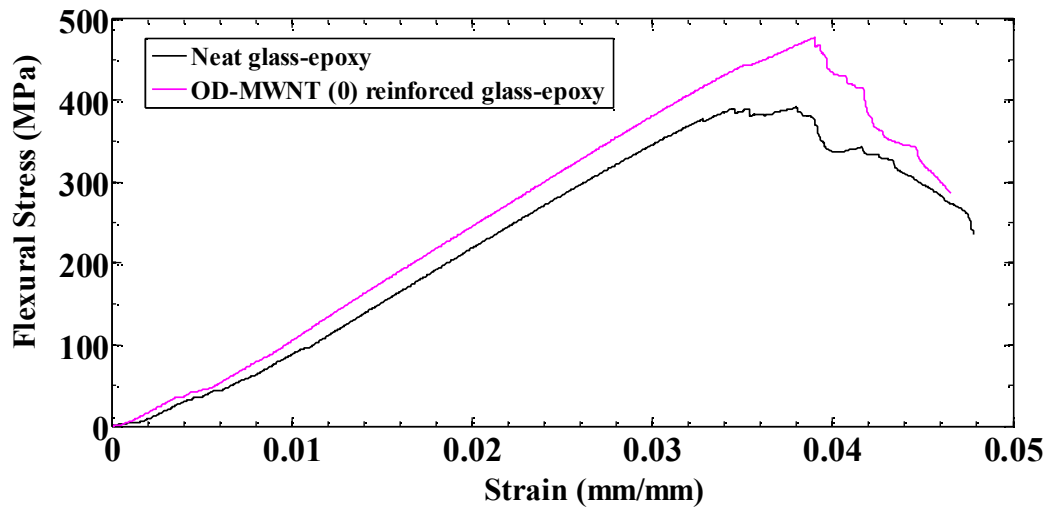
Figure 4.8 Tensile stress versus strain results of G1-B9 specimens

Table 4.2 Average tensile strength and Young's modulus obtained from G1-B9

Experiments	Average $\sigma_{max}$ (MPa)	Change %	Average $E_T$ (GPa)	Change %
Neat Glass- Epoxy	362.27 (+/- 4.89)		16.87 (+/- 0.66)	
OD-MWNT (0) Glass-Epoxy	379.26 (+/- 14.52)	4.70	16.86 (+/- 39)	- 0.10

Flexural properties determined with three point bending test are effective parameters in order to characterize the nanotube-matrix and nanotube-fiber interfacial interactions through the thickness direction for the nanotube reinforced GFRP composite materials. On the other hand as expected tensile properties were not affected by the CNT incorporation into the glass fiber reinforced epoxy composites according to the Table 4.2, because in plane tensile loads applied along  $0^\circ$  directional edge of the specimens were dominated by glass fiber reinforcement.

Three point bending test was performed on all specimens in order to determine and compare flexure stress and strain behaviors of neat and CNT incorporated composite samples prepared in this study as seen in Figure 4.9, Figure 4.10 and Figure 4.11 for each production summarized in Table 4.1.



**Figure 4.9** Flexure stress versus strain results of G1-B9 specimens including 0.01 wt. % of nanotubes within overall composite.

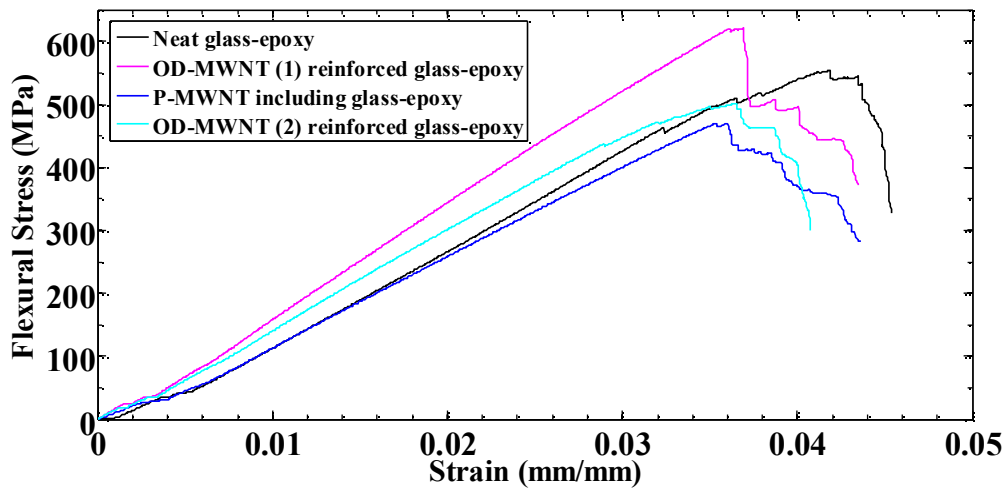


**Figure 4.10** Flexure stress versus strain results of G1-B10 specimens including 0.01 wt. % of nanotubes within overall composite.

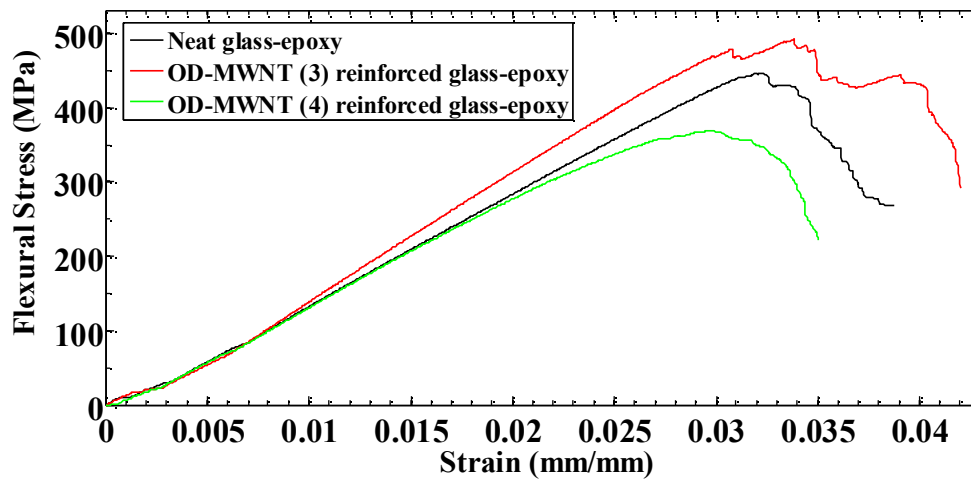


**Figure 4.11** Flexure stress versus strain results of G1-B11 specimens including 0.02 wt. % of nanotubes within overall composite.

Average flexure strength and modulus results of all of specimens were reported in Table 4.3 such that the change in mechanical properties were additionally examined as a function of dispersion concentration and the amount of nanotube deposition over the specified area.

**Table 4.3** Average flexure strength and Young's modulus results for overall specimens

Productions		Dispersion Concentration (wt %)	CNT content in the final composite (wt %)	Solvent	Average $\sigma_{max}$ (MPa)	Change %	Average $E_B$ , (GPa)	Change %
<b>G1-B9</b>	Neat Glass- Epoxy				397.37 (+/- 18.28)		13.07 (+/- 1.00)	
	OD-MWNT (0) / Glass-Epoxy	0.005	0.010	NMP/H <sub>2</sub> O	479.42 (+/- 3.37)	20.63*	14.04 (+/- 0.90)	7.50*
<b>G1-B10</b>	Neat Glass- Epoxy				524.33 (+/- 26.53)		15.30 (+/- 0.50)	
	P-MWNT / Glass-Epoxy	0.005	0.010	NMP/H <sub>2</sub> O	472.83 (+/- 19.43)	-10*	14.03 (+/- 0.62)	-8.50*
	OD-MWNT (1) / Glass-Epoxy	0.005	0.010	NMP/H <sub>2</sub> O	598.98 (+/- 19.83)	14.23*	18.42 (+/- 1.40)	20.47*
	OD-MWNT (2) / Glass-Epoxy	0.010	0.010	NMP/H <sub>2</sub> O	506,30 (+/- 36)	-3.40*	16 (+/- 1.40)	4.50*
<b>G1-B11</b>	Neat Glass- Epoxy				431.55 (+/- 9.50)		16.23 (+/- 0.86)	
	OD-MWNT (3) / Glass-Epoxy	0.010	0.020	NMP/H <sub>2</sub> O	476.75 (+/- 16.87)	10.50*	17.68 (+/- 0.87)	8.90*
	OD-MWNT (4) / Glass-Epoxy	0.010	0.020	NMP	345.40 (+/- 20.40)	-20*	14.32 (+/- 1.50)	-12*

\*: with respect to neat composite sample from the same production of each sample

In accordance with flexural stress- strain curves and Table 4.3 above, OD-MWNT(0) containing composite sample from the production G1-B9 (prepared by electro-spraying from a 0.005 wt. % of O-MWCNT containing dispersion in NMP/H<sub>2</sub>O) in x and y directions shows significant improvement, nearly 20 % in average strength and 7.5 % in average Young's modulus in comparison with the neat samples from the same composite production (G1-B9). Such a significant increase in flexural strength and Young's modulus values upon the incorporation of as low as 0.01 wt% OD-MWNTs in the overall composite indicates that an efficient stress transfer can be achieved through the interface, which was tailored with the incorporation of chemically oxidized MWNTs that were uniformly incorporated with the aid of a good dispersion by the electro-spray process.

In order to verify the reproducibility of these results observed in composite samples from production G1-B9 and investigate the effect of the presence of oxygenated groups in the CNT structure and the concentration of electro-sprayed CNTs on the mechanical properties of final composites, a new production, G1-B10, was performed. The composite panel produced in G1-B10 composed of four different sections with 100x300 mm<sup>2</sup> area each. The first section was the neat composite, the second section was prepared by electro-spray deposition of 400 mg/m<sup>2</sup> pristine MWNTs (P-MWNTs) from a 0.005 wt% NMP/H<sub>2</sub>O dispersion, the third section contained 400 mg/m<sup>2</sup> OD-MWNT(1) electro-sprayed from a 0.005 wt% NMP/H<sub>2</sub>O dispersion and the fourth section contained 400 mg/m<sup>2</sup> OD-MWNTs electro-sprayed from a 0.01 wt% NMP/H<sub>2</sub>O dispersion. As summarized in Table 4.3, the incorporation of P-MWNTs negatively affected both flexural strength and Young's modulus of the compared to the neat composite sample. Such a considerable decrease in flexural properties of P-MWCNT deposited composite specimens can be clearly explained by the fact that pristine MWNTs always result in a poor dispersion in NMP or NMP/H<sub>2</sub>O mixture as discussed in the previous chapter. The incorporation of visually detectable large agglomerates of MWNTs in the dispersion used in the electro-spray process into the composite interface could create stress concentration points and thus poor stress transfer through the polymer-fiber interface, resulting in deficiency in interfacial properties. On the other hand, OD-MWNT(1) incorporated sample in G1-B10 production prepared by electro-spraying of a 0.005 wt% dispersion in NMP/H<sub>2</sub>O to obtain 400 mg/m<sup>2</sup> deposition showed an improvement of 14 % in flexural strength and 20% in Young's modulus values. The fact that the

improvement in the flexural strength of this sample from production G1-B10 was lower (14% vs. 20%) than that of the previous sample with the same CNT content from the production G1-B9 could be explained by the difference in the electro spray direction of MWNTs. In G1-B9 nanotubes were electro sprayed onto the specified glass fiber area electro sprayed by applying a two axis spraying process (x & y) whereas in G1-B10 nanotubes were electro sprayed only in the y-direction. In order to understand the effect of OD-MWNT concentration on the final composite properties, OD-MWNT (2) reinforced composite samples (from G1-B10) were prepared, in which the nanotube dispersion concentration to be sprayed was doubled and increased from 0.005 wt% to 0.01 wt% compared to the previous sample to achieve 400 mg/m<sup>2</sup> deposition of nanotubes on each surface, resulting in 0.01 wt% nanotubes in the whole composite. In this case, flexural properties were slightly decreased and Young's modulus only slightly increased compared to the neat composite sample from the same production, which clearly indicates that the nanotube concentration plays a key role in the uniform deposition of nanotubes on the glass fiber surface by the electro spray process. Increased nanotube concentration was assumed to have caused stability issues since it was clearly observed that the spray pattern was not uniform during the electro spray process.

In G1-B11, nanotube dispersion concentration was increased up to 0.01 wt. % in NMP/H<sub>2</sub>O or NMP, while the amount of nanotubes deposited on each surface was increased from 400 to 800 mg/m<sup>2</sup>, corresponding to 0.02 wt% oxidized nanotubes in the final composite material. Although it was expected to observe a much higher improvement in mechanical properties than that of the previous composite samples, there was a moderate improvement in the flexural strength and Young's modulus of the OD-MWNT (3) integrated composite sample. This improvement was lower than the previous productions. Clearly increasing dispersion concentration negatively affected the dispersion stability and the uniformity of the nanotube deposition during electro spray process due to exceeding the critical nanotube concentration. This was expected to cause agglomeration nanotubes, which cannot be tolerated within the overall composite structure. On the other side OD-MWNT (4) composite sample prepared by using an NMP-based nanotube dispersion show 20 % and 12 % reduction in average flexure strength and modulus values respectively. The consecutive results can be explained by the fact that using only large amount of NMP as solvent has a destructive effect on the glass fibers within the composite which leads to significant

deficiency in mechanical response of the nanotube deposited specimens due to insufficient stress transfer through the weak interfacial interactions.

### 4.3.3 Fracture Surface Characterization

In order to investigate and verify the uniform distribution of oxidized MWNTs, fracture surfaces of both neat and OD-MWNT (0) incorporated composite specimens were analyzed after tensile failure under the scanning electron microscope (SEM) as represented in Figure 4.12.

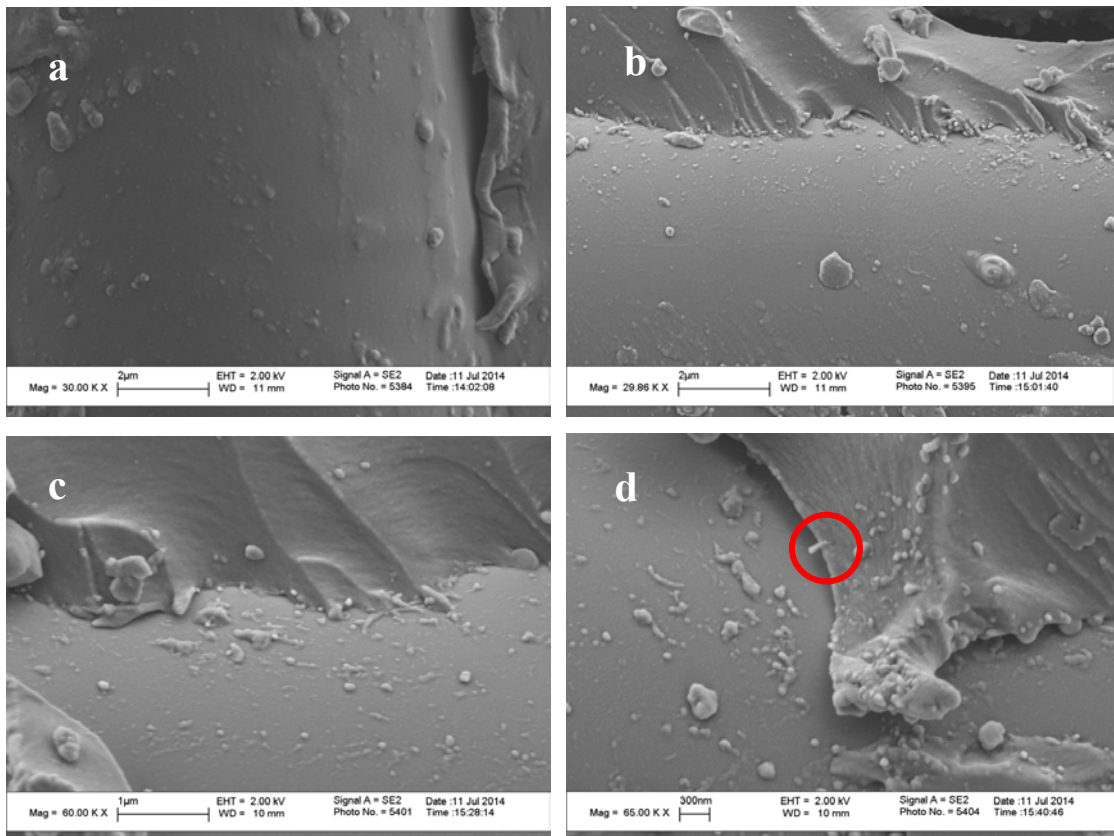


**Figure 4.12** SEM images of the fiber-matrix interface of a) neat; b, c and d) OD-MWNT (0) deposited composite specimens

SEM images in Figure 4.12-b, c and d clearly reveal the presence of electrospray deposited nanotubes at the fiber-matrix interface for the composite sample with CNT deposited from 0.005 wt. % concentrated NMP/H<sub>2</sub>O dispersion mixture resulting in 0.01 wt. % in the overall composite. The presence of these nanotubes evidences that

CNTs were originally deposited on the glass fiber mat surface have established efficient interactions with the fiber surface and they have not migrated or agglomerated during the shear intensive vacuum infusion process. These finely dispersed CNTs that are effectively interacting with each component at the interface are expected to act as additional stress transfer regions between fiber and matrix, leading to considerable improvement in interfacial properties within the glass fiber-epoxy composites which were proved by flexural test results.

#### **4.4 Conclusions**

CNTs were deliberately incorporated into the polymer matrix-fiber interface in FRPCs by using electrospray process, which enabled uniform deposition of CNTs onto the glass fiber mat surface from dispersion prior to the composite manufacturing process by vacuum infusion. Although the incorporation of P-MWNTs resulted in a dramatic decrease in the mechanical properties of final composite structures, incorporation of chemically oxidized CNTs at a content of as low as 0.01 wt. % in the overall composite resulted in significant improvement of flexural properties compared to their corresponding neat analogues without CNTs. Key process parameters such as the spray direction, CNT concentration and solvent type in the dispersion to be sprayed, and final CNT content in the overall composite were studied for optimum mechanical performance. Within the scope of this study, the optimum results in flexural strength and modulus were achieved by spraying oxidized MWNTs in the both x and y direction from a dispersion mixture containing 0.005 wt. % of nanotube concentration in NMP/H<sub>2</sub>O mixture, resulting in 0.01 wt. % of nanotubes in the overall composite structure which was represented as OD-MWNT (0) in Table 4.1. As also revealed by SEM analysis of fractured composite surfaces, the mechanism of the mechanical reinforcement was attributed to the uniform distribution of oxidized MWNTs with tailored chemical interactions at the fiber-matrix interface with each component, resulting in prevention or retardation of crack initiation or propagation through the interface. As a result of tailored chemical functionality and novel electrospray deposition method proposed in this study, such a high efficiency of mechanical reinforcement, up to 20 % improvement in flexural strength with as low as 0.01 wt. % oxidized MWNTs in the final composite material, will be reported for the first time.

## CHAPTER 5

### 5 INTERFACE ANALYSIS of POLY(ST-CO-GMA) NANOFIBER INTEGRATED FRPCs

#### 5.1 Introduction

Nano structures have received significant attention in the last decade as fillers for fiber reinforced epoxy based composite materials because of their ability to improve both physical and mechanical properties of manufactured composite structures. Being a well established fact that the externally applied force on a composite structure is transferred from matrix to the reinforcing fibers through matrix-fiber interfaces, it is expected that the adhesive interfacial bonding should directly influence the rigidity, strength, and fracture behavior of composites [75]. Nano structures can be used viable interfacial materials to create strong interfacial bonding between the matrix and the primary reinforcement of composite materials. Due to their large surface area, nano-fillers contribute to the improvement of interfacial interactions through enabling efficient cross-linking with the epoxy resin [76]. Moreover, interfacial sliding features of the nano- fillers within the composites enhances damping properties [8] with improved interfacial interactions between fiber and polymer matrix.

One of the most widely preferred production methods for forming continuous nanofibers is electrospinning process. Electrospun nanofibers produced from copolymers have recently received noticeable interest in order to develop functional

polymeric or composite materials with improved properties such as thermal stability, biodegradability and mechanical strength etc. For instance, Kenawy et al. [77] studied electrospinning of elastic poly(ethylene-co-vinyl alcohol) (PEVA) nanofiber mat and stiff poly(glycolide) (PGA) blend. Huang and Chang [78] have enhanced the thermal stability of poly methyl methacrylate (PMMA) by copolymerization of methyl methacrylate (MMA) with methacrylic acid (MAA). The reason behind this improvement could be explained considering the higher glass transition and degradation temperature of poly(methacrylic acid) (PMAA) with respect to PMMA. Electrospun nano fibers have also been under investigation for some time as a secondary reinforcement in glass or carbon fiber reinforced composites since continuous electrospun nanofibers forming extended chain arrangements with highly crystalline structure has an effect on macromolecular properties of polymeric composites such as interfacial adhesion between the constituents. Particularly in Airbus Military patent application, Barrero et al. [4] developed a novel methodology which involved electrospinning process in order to integrate nanofibers of epoxy resin and also nanofibers doped with carbon nanotubes onto each carbon fiber plies by a two axes electrically moving device. Finally, the electromagnetic characteristics of the aero-structures are significantly improved especially for the protection against lightning impact.

In the light of the further improvements needed in nano-enhanced composites, this work focuses on the integration of poly(styrene-co-glycidyl methacrylate) P(St-co-GMA) nano- fibers (with epoxide functionalities which can directly interact with the epoxy resin) within the glass fiber reinforced epoxy composite materials by using electrospinning technique with the aim of improving the structural and mechanical performances of the final composite through enhancing interfacial interaction between the primary constituent materials. Composite laminates with and without (neat) electrospun nano-fibers between each laminas are produced using resin transfer molding method. Mechanical test specimens are cut from each type of laminates and tested under tensile and bending loads by using a universal testing machine (UTM) to investigate interfacial characteristics and load transfer between fibers and epoxy matrix. We have also performed dynamic mechanical-thermal analysis (DMTA) test on the relevant test specimens to further investigate the effect of nano-layers on the interfacial properties within the composites as a function of temperature.

## 5.2 Experimental

### 5.2.1 Electrospun Poly[Styrene-co-Glycidylmethacrylate] Nanofibers

The copolymer is synthesized following the procedure reported in the reference [79]. The synthesized copolymer is dissolved in N, N-dimethylformamide (DMF) to prepare copolymer solution with the concentration of 30 wt %. It was observed in several trial experiments that the polymer concentration less than this amount led to either bead formation or failure in nano-fiber formation. Having stirred the copolymer solution overnight using magnetic stirrer, the solution is loaded into 5 mL syringe, and 4 mL copolymer solution is electrospun over un-impregnated glass fiber reinforcement with an applied voltage of 15 kV, a flow rate of 3 $\mu$ L/h and tip-to-ground distance of 10 cm.

To be able to reveal the effect of interlayer on the mechanical response of composites, we have manufactured two composite plates having different arrangements of nano-fiber integration in between the plies. The laminate selected for the first experiment is [0/90]<sub>6S</sub> E-glass fiber. The fiber used is Metyx LT300 E10A 0/90 biaxial E-glass stitched fabric with 161 gsm in the 0° orientation, and 142 gsm in the 90° orientation, summing to 329 gsm total. Nano-fibers are electrospun over 0° directional surface of every second fiber layers (having the dimensions of 620mm x 320mm) covering the area of 300 mm x 320mm as shown in Figure 5.1. Totally we used 12 biaxial glass layers in order to fabricate nearly 4 mm- thick composite laminate.



**Figure 5.1** Electrospun P(St-co-GMA) nanofiber over  $0^\circ$  directional surface of glass fiber layer deposited through  $90^\circ$  direction

In the second experiment, to save the amount of material used and the time to prepare the electro spun fiber integrated composites, composite laminate having electro spun fibers integrated regions are manufactured by using six biaxial E-glass layers, namely,  $[0/90]_{3S}$ . In this experiment, unlike the first one, nano fibers are electrospun on each  $0^\circ$  direction surface of glass fiber layers using the same processing condition as the first experiment. The glass fiber substrates were covered with electrospun nano-fiber mats having volume fractions of approximately 4.5% and 9 % (1.8 % and 3.6 %) of the primary reinforcement (within the overall composite) for the first and second experiments, respectively.

### **5.2.2 Electrospun Poly[Styrene-co-GMA] Interlayered Composites**

A sophisticated laboratory-scale RTM apparatus which can produce a flat panel with the dimensions of 620 mm x 320 mm x 4 mm has been used to impregnate electrospun nano-fiber integrated glass fiber layers. The electrospun fiber integrated glass fiber layers are stacked forming a symmetrical arrangement, and then placed into the RTM mold cavity such that  $90^\circ$  direction surface of glass fiber layer face towards the mold surfaces and  $0^\circ$  direction of the plies is aligned along the resin flow direction. The mold is closed and injected with Araldite LY 564 epoxy resin with XB 3403 hardener produced by Huntsman Corporation by means of dry air pressure increased gradually up

to 2 bars during the entire impregnation process. It should be noted that in the second experiment, recalling that 6 layers of glass fiber is used; the thickness of the mold cavity is reduced by using a spacer plate of 2.5 mm metal thereby producing approximately 1.6 mm-thick composite plate. The panels undergo an initial cure at 65 °C for 24 hours with a post cure at 80 °C for 24 hours and glass fiber volume fraction are kept constant. The volume fractions of glass fiber into the composite laminates were calculated by burning test as nearly 40 % of overall composites for both experiments. The first and second experiments lead to composite plates with the thickness of 4 mm and 1.6 mm, respectively.

### **5.2.3 Mechanical Characterization**

Mechanical properties of manufactured composites were investigated by Zwick Roell Z100 Universal Testing Machine (UTM) and Netzsch Dynamic Mechanical Analysis (DMA) 242C at Sabanci University. Both panels in this study are processed into tensile, bending and DMA specimens and tested in accordance with the relevant standards, namely, ASTM D790 for flexural test, and ASTM D3039 for tensile test. All test samples are cut off the panels such that the length of the specimens is along the 0° direction. The dimensions of specimens for tensile and flexural are respectively 250 mm × 25 mm and 80 mm × 15 mm. The span length for tensile test samples is taken to be 150 mm while for flexural test samples, it is 128 mm and 25.6 mm for the first and second experiments, respectively. Tensile test is performed with the head displacement rate of 2mm/min. Flexural tests are conducted with cross head motion of 6.83 and 0.683 mm/min for the first and second experiments, respectively. To have reliable and repeatable results, at least three test specimens are cut from the neat and nanofiber integrated parts of the composites and are tested under both tensile and bending loadings. The average strength and modulus values are calculated and reported. Fractured specimens of three point bending and tensile tests are respectively illustrated in Figure 5.2 and Figure 5.3 respectively. To have reliable and repeatable results at least three test specimens cut from the neat and nanofiber integrated parts of the composites are tested for both tensile and bending tests. Therefore, the average strength and modulus values are calculated and reported.

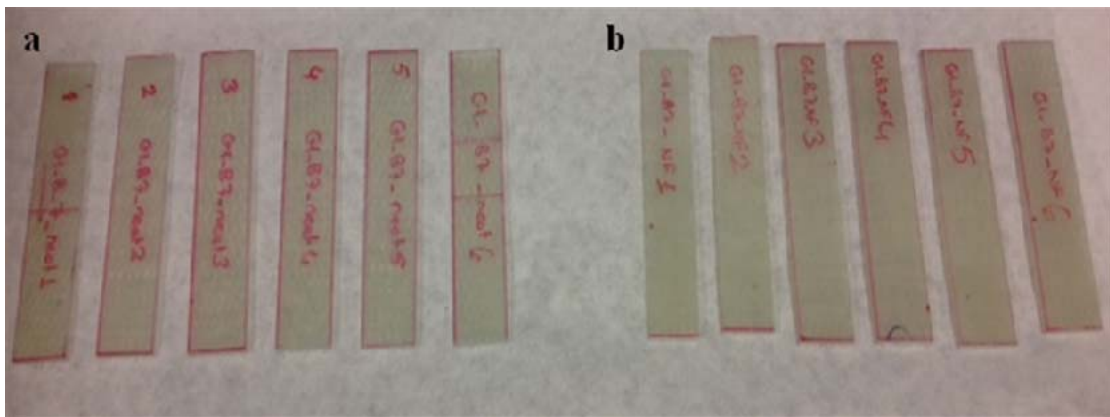


**Figure 5.2** Three point bending specimens; a) neat samples, b) copolymer integrated samples.

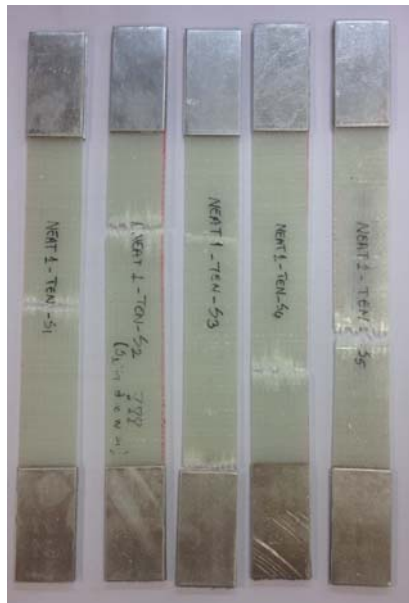


**Figure 5.3** Tensile fracture specimens

DMA is also conducted under three-point bending mode in order for characterization of interfacial adhesion between fiber and matrix. The neat and nanofiber integrated composite specimens were also processed in accordance with the testing mode and existing range between maximum and minimum values of the storage modulus. The dimensions of the specimens are 40 mm x 10 mm x 1.8 mm thickness as can be seen in the Figure 5.4. The maximum dynamic force, amplitude and constant static force utilized are 4 N, 120  $\mu$  and 0.01 N, respectively. All of the composite specimens are tested under three point bending mode at 2 Hz of frequency with the temperature range

between 20 and 120 °C. In addition to mechanical test characterization results, glass transition temperature and transitions between the glassy state and rubbery state are also analyzed using DMA test results.

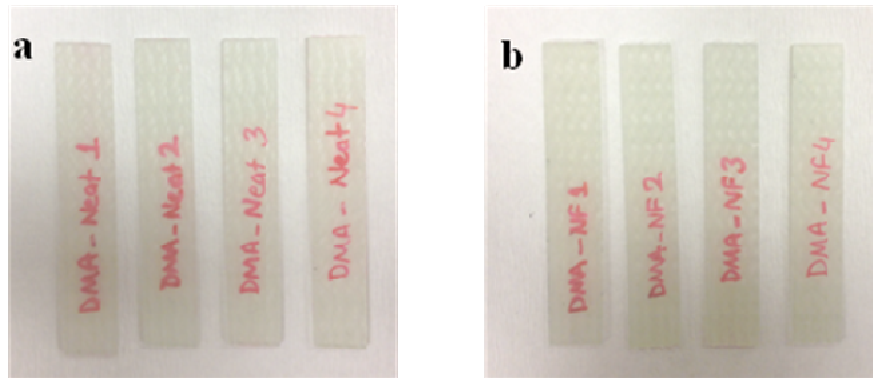


**Figure 5.4** DMA samples; a) neat samples, b) copolymer included samples.

#### **5.2.4 Surface Characterization**

Nanofiber formation on the glass fiber is investigated with LEO Supra VP35 Field Emission Scanning Electron Microscope using secondary electron detector at 2 kV. Carbon coating is applied onto the specimens by sputter deposition to obtain conductive samples.

### **5.3 Results and Discussion**

#### **5.3.1 Morphological Analysis of Electrospun Nanofiber**

Figure 5.5 present SEM micrographs clearly showing the morphology of nanofiber produced through electrospinning polymer solution with 30 wt. % concentration under the applied electric field on the glass fiber. The diameter of electrospun nanofibers changes between 600-1200 nm and high copolymer concentration provides an increase in the viscosity of the solution, thus reducing the bead formation.

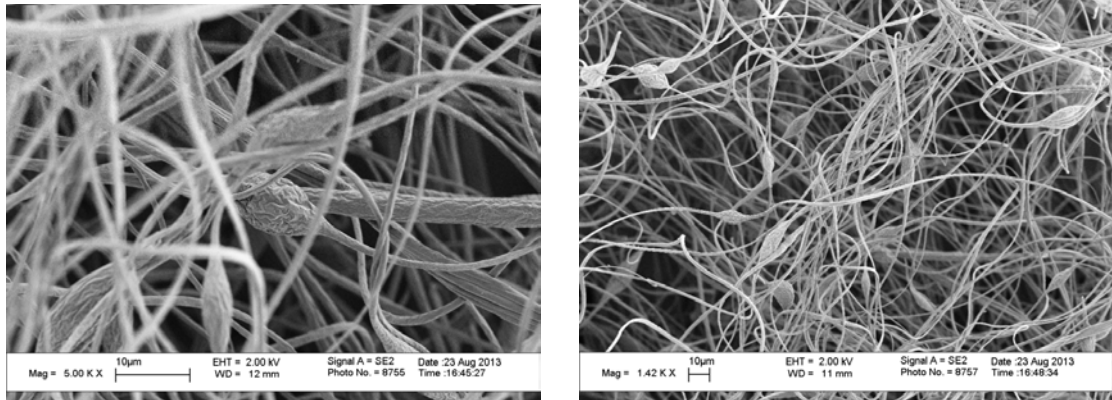


**Figure 5.5** Nanofiber morphologies electrospun from 30% copolymer solution concentration

### 5.3.2 Static Flexural and Tensile Test Results

Three point bending tests were performed to investigate the effect of Poly (St-co-GMA) electrospun interlayer on the flexural performance of composite. Hence, both neat and Poly (St-co-GMA) electrospun fiber integrated composite specimens are tested to determine their flexural strength and Young's modulus. Figure 5.6 presents deformation of the specimen under bending load. Table 5.1 shows average flexural strength and Young's modulus results of the three point bending test specimens. Flexural stress-strain curves corresponding to both neat and nanofiber enhanced specimens for first and second experiment were illustrated comparatively in Figure 5.7.



**Figure 5.6** Three point bending test specimen under loading

**Table 5.1** Average flexural strength and Young's modulus values of two different composite plates with 30 % Poly (St-co-GMA) and different production configuration.

Experiments		Thickness (mm)	Average $\sigma_{max}$ (MPa)	Average Change in $\sigma_{max}$ (%)	Average $E_B$ (GPa)	Average Change in $E_B$ (%)
Experiment 1 (%30 solution)	Neat Glass-Epoxy	4.00	533.41 (+/- 21.40)	5.82	18.72 (+/- 0.50)	0.26
	Copolymer Glass-Epoxy		564.45 (+/- 16.47)		18.773 (+/- 0.49)	
Experiment 2 (%30 solution)	Neat Glass-Epoxy	1.60	488.15 (+/- 23.35)	15.40	15.39 (+/- 0.11)	10.35
	Copolymer Glass-Epoxy		563.35 (+/- 53.83)		16.98 (+/- 1.42)	

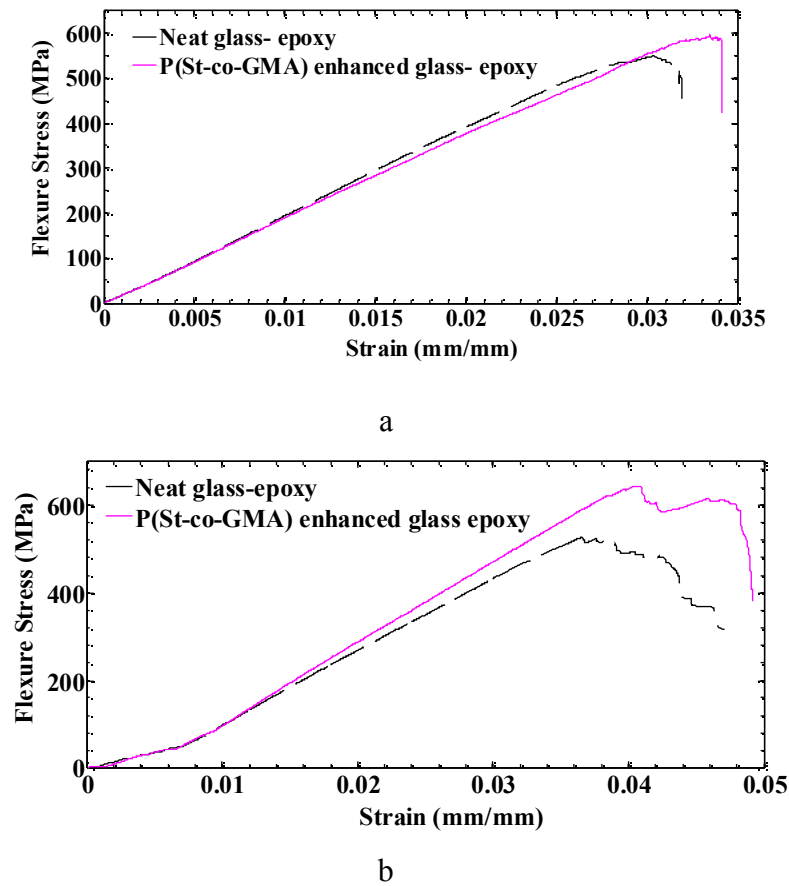


**Figure 5.7** Three point bending test results for a) 1<sup>st</sup> and b) 2<sup>nd</sup> experiment

As can be seen from Figure 5.7 and also from Table 5.1, there is a notable increase in both flexural strength and modulus of P(St-co-GMA) nano fiber integrated specimens produced in the second experiment in comparison with the corresponding neat glass-epoxy composite specimens. The significant difference between the increases in the mechanical performance of the specimens of both the first and the second experiment indicates the toughening and crack arresting effect of interlayers in between the plies of the primary reinforcement within the produced composites. Recalling that in the first experiment, the interlayer is present on every second ply while in the second one; all plies are covered by interlayer. Any crack formed under the bending load between the plies can propagate towards the next one if there is no interlayer. Therefore, it is prudent to expect that the increase in the flexural strength of nano fiber integrated composite with respect to the associated neat one should be small as one may clearly substantiate this conclusion referring to the relevant results.

Furthermore Table 5.2 and Figure 5.8 present the results of tensile test performed on both neat and P(St-co-GMA) integrated specimens for only the second experiment.

**Table 5.2** Average tensile strength and Young’s modulus of composites for 2<sup>nd</sup> experiment with 30 % Poly (St-co-GMA)

Experiments		Average $\sigma_{max}$ (MPa)	Average Change in $\sigma_{max}$ (%)	Average $E_T$ (MPa)	Average Change in $E_T$ (%)
Experiment 2 (%30 solution)	Neat Glass- Epoxy	371.03 (+/- 16.60)		179.93 (+/- 3.34)	
	Copolymer Glass-Epoxy	368.60 (+/- 14.70)	- 0.65	178.46 (+/- 13.10)	- 0.81

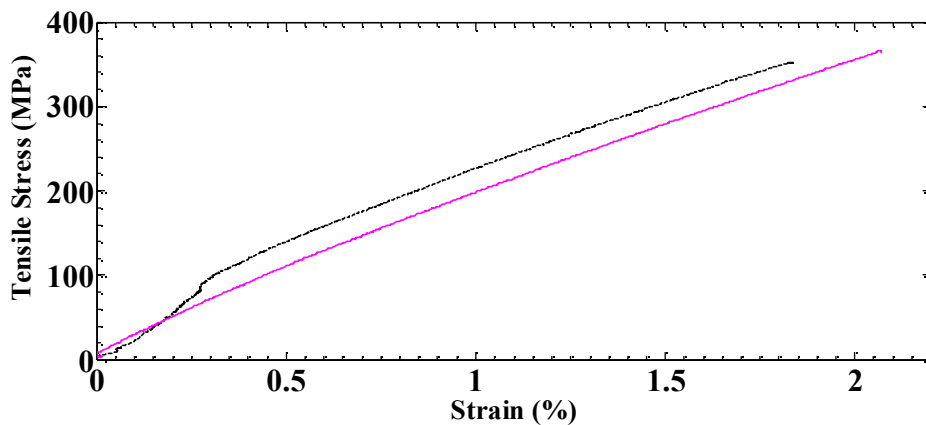


**Figure 5.8** Static tensile test results for 2<sup>nd</sup> experiment

Referring to results in Table 5.2 and Figure 5.8, literally, there is a no change in tensile properties between neat and nano-fiber integrated glass fiber reinforced epoxy composite specimens. This is a highly expected result noting that the glass fiber is the major constituent in carrying the external load coming onto the composite, and also the current result can be also interpreted such that the interlayer is not degrading effect on tensile properties of composite structure through not acting as defects at the interface regions of the composite laminas.

### 5.3.3 Dynamic Mechanical and Thermal Analysis (DMTA)

The dynamic storage modulus ( $E'$ ) is an important parameter related to the stiffness of the materials, which can be estimated through measuring energy stored due to the elastic behavior. Figure 5.9 indicates that the storage modulus values of both neat and P(St-co-GMA) nanofiber integrated composite samples change with increasing temperature from 20 to 120 °C.

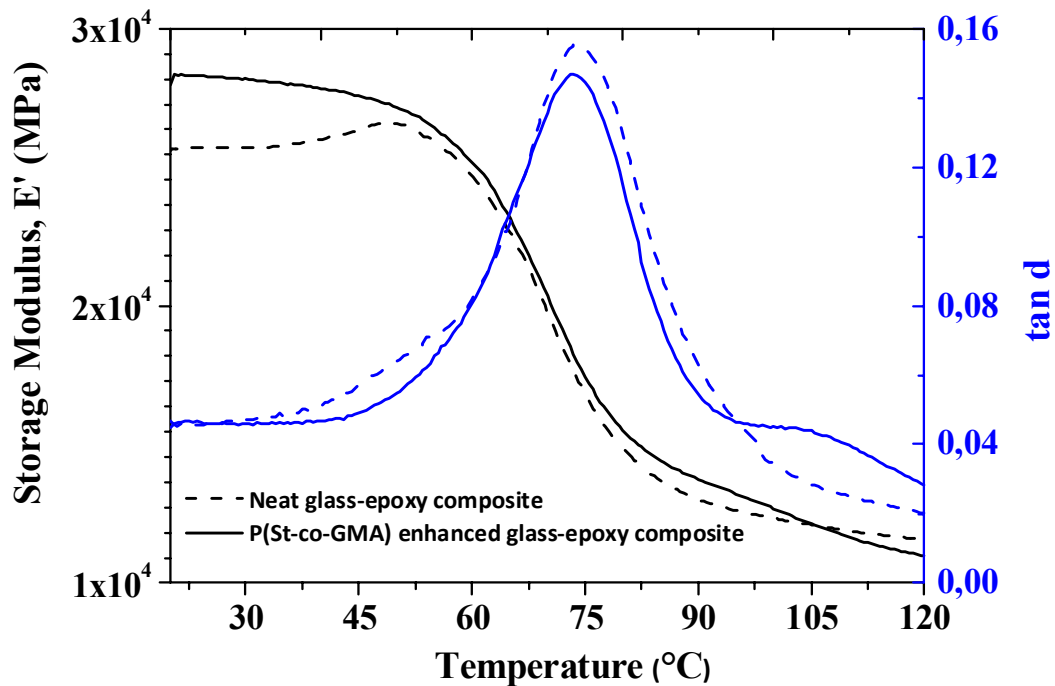


**Figure 5.9** DMA results for neat and P(St-co-GMA) nanofiber reinforced glass-epoxy composites.

According to the Figure 5.9, one can note that the storage modulus ( $E'$ ) of both types of specimen shows a significant decrease with increasing temperature especially after glass transition temperature ( $T_g$ ) which occurs approximately at 75 °C which was obtained from the peak point of tan delta plot. This reduction in  $E'$  was based on the increasing molecular chain mobility in the visco-elastic region during the phase transition from the glassy state to the rubbery state of the material. Interfacial interactions between fiber and matrix start to weaken; thus the resistance to elongation, known as “stiffness”, decreases above  $T_g$ . There can be seen a second peak position in tan  $\delta$  results for the nanofiber integrated composites at approximately 98 °C. This corresponds to the  $T_g$  of

the P(St-co-GMA) copolymer such that the nanofiber presence within the composite structure can be proved.

As seen in the Figure 5.9, there is approximately 10 % increase in the dynamic storage modulus ( $E'$ ) for P(St-co-GMA) nanofiber integrated glass-epoxy composites (from 25.732 to 28.276 GPa) at the room temperature. The increase in the storage modulus of nano-fiber integrated composite with respect to the neat one at room temperature directly supports the results of the flexure modulus obtained from the static three point bending tests. Therefore, one can reliably conclude that stiffness of the composite increases as a result of efficient stress transfer from the glass fiber to epoxy polymer through the help of nanofiber integrated interface due to the compatibility of P(St-co-GMA) including epoxide functionality with epoxy resin.

In a composite material damping properties associate with the molecular chain motions in the glass transition region. Furthermore, the strength of interfacial interactions is inversely proportional to the peak maximum of damping ( $\tan \delta$ ) and energy dissipation. In this study contrary to neat composite samples, copolymer integrated composites show lower damping ratio ( $\tan \delta$ ) at the peak position which assigned to  $T_g$  at approximately 75 °C. This lower amplitude of  $\tan \delta$  is attributed to reduction in the molecular chain mobility resulting from the stronger interfacial interactions. This structurally modified interfaces including P(St-co-GMA) nanofiber interlayers can dominate the applied stress by decreasing the dissipation of energy with greater load transfer from the fiber to the matrix [80]. Therefore, P(St-co-GMA) nanofiber interlayers enable better interfacial bonding by lowering the damping ratio in contrast to the neat glass-epoxy composites.

## 5.4 Conclusions

Two different nano-integrated composite plates are manufactured by changing number of plies in the laminate and the nanofiber integration strategy. P(St-co-GMA) nanofiber formation was visualized using SEM analysis. The tensile and flexural properties of nanofiber interlayered glass-epoxy composite specimens together with their corresponding neat specimens are studied using universal testing machine. DMA test is also performed for determining the storage modulus as well as damping properties of the nano-composite.

For the first experiment, the flexural strength and modulus of the nano-composite have shown marginal increase with respect to that of neat composite, namely, 5.82 % and 0.26 %. As for the second experiment, the improvement obtained in these quantities are notably significant, which is around 15.40 % for flexural strength and 10.35 % for Young's modulus in comparison to the neat composite of the second experiment. The observable difference between the results of the first and the second experiment can be prudently attributed to toughening and crack arresting effect of interlayers between the plies of the primary reinforcement. However, there was relatively no change in tensile properties between neat and nanofiber reinforced glass -epoxy composites for the second experiment due to the dominating effect of the glass fibers on the in-plane tensile properties. This result also indicates that the presence of interlayer does not degrade the tensile properties of composite structure through not acting as defects at the interface regions of the composite laminas. Furthermore, 10 % increase in storage modulus were observed for the P(St-co-GMA) nanofiber reinforced glass-epoxy composites at the room temperature and this storage modulus values decrease especially after  $T_g$  for both neat and nanofiber enhanced composite samples due to increasing molecular chain mobility in the viscoelastic region during the phase transition. Additionally contrary to neat composite samples, lower amplitude of  $\tan \delta$  of copolymer integrated composites is attributed to reduction in the molecular chain mobility resulting from the stronger interfacial interactions lowering the energy dissipation at the interface. Finally, mechanical and thermal improvement can be attributed to the efficient stress transfer from the glass fiber to epoxy polymer through the nanofiber interlayer due to the structural cross-linking ability of P(St-co-GMA) with epoxy resin.

## **CHAPTER 6**

### **6 FUTURE WORK**

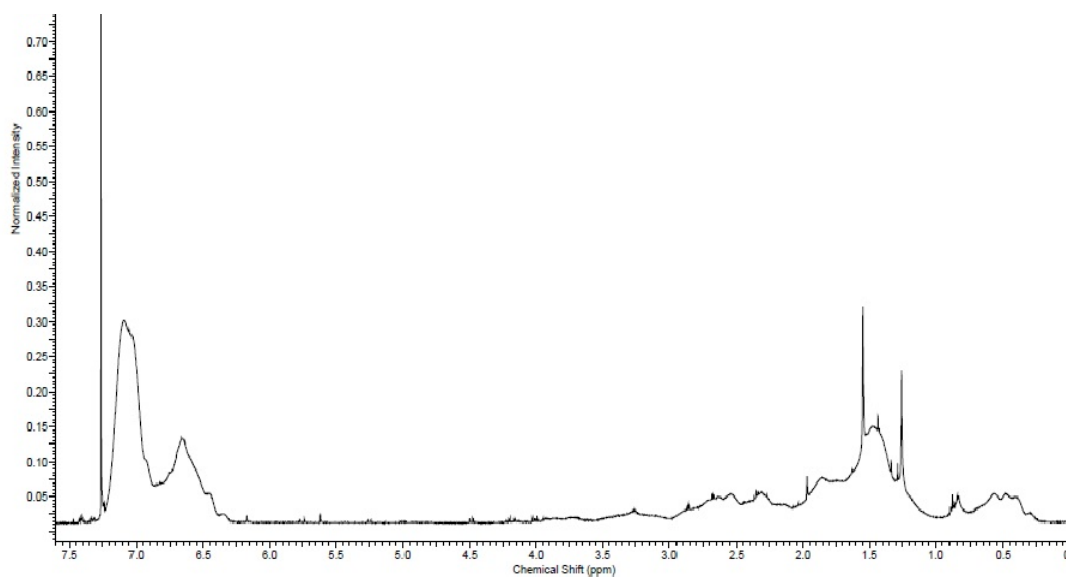
The current thesis works has led to several novel results as detailed within the body of thesis. The future woks to be performed as an extension of what has been presented here should include followings. MWNTs should be bi-functionalized in order to create strong covalent interactions between nanotube-epoxy resin, and also between nanotube-primary glass fiber reinforcement and should be electrosprayed with the processing parameters as described in this thesis , which can result in homogenous distribution of CNTs in the composite. To further investigate the effect of MWNTs on the mechanical performance of composites and on crack propagation across the plies of the composite specimens, fatigue tests and fracture toughness of nanotube integrated composite specimens should be investigated.

## Appendix

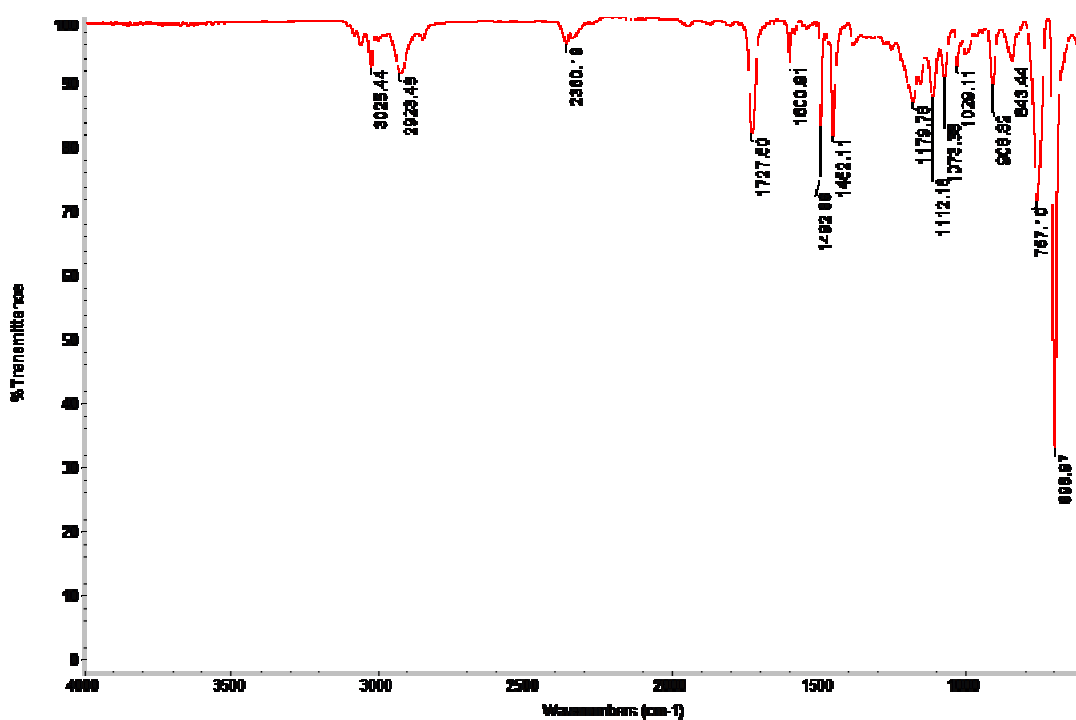
Regarding to P(St-co-GMA) synthesis, we used purified 96 wt. % of Styrene and 4 wt. % of Glycidylmethacrylate (GMA) as monomers which were purchased from Sigma Aldrich Co. while 60 wt. % of tetrahydrofuran (THF) within the reaction mixture and methanol were used as solvents. Firstly monomers were put within the reaction bulb while they were stirring in an ice bath. Then THF was added and the initiator, azobisisobutyronitrile (AIBN), was put into the bulb at the end. As soon as the inlet of the tube was closed with rubbery septum, the nitrogen was purged through the reaction medium during half an hour in order to remove impurities of oxygen species. The reaction mixture was then heated at the constant temperature, 70 °C during 5 days. Finally the viscous solution was poured into the methanol by drop wise in order to precipitate co-polymer while stirring them on the magnetic stirrer. Then the polymer was dried at 50 °C into the vacuum oven overnight. The chemical structure of synthesized P(St-co-GMA) was characterized by using proton nuclear magnetic resonance (H-NMR) and FT-IR as seen in the following figures.



Solution co-polymerization reaction set up of P(St-co-GMA)



NMR spectroscopy of Poly [Styrene-co-GMA] copolymer



FT-IR spectroscopy results of Poly [Styrene-co-GMA] copolymer

## Bibliography

1. M. Prasad, C.V.a.T.J., *Experimental Methods of Determining Fracture Toughness of Fiber Reinforced Polymer Composites under Various Loading Conditions*. Journal of Minerals and Materials Characterization and Engineering, 2011. **Vol. 10 No. 13**: p. 1263-1275.
2. Wernik, J.M. and S.A. Meguid, *Recent Developments in Multifunctional Nanocomposites Using Carbon Nanotubes*. Applied Mechanics Reviews, 2011. **63(5)**: p. 050801-050801.
3. Wernik, J.M. and S.A. Meguid, *Recent Developments in Multifunctional Nanocomposites Using Carbon Nanotubes*. Applied Mechanics Reviews, 2010. **63(5)**: p. 050801.
4. Barrero, R.A., et al., *Method for producing nanofibres of epoxy resin for composite laminates of aeronautical structures to improve their electromagnetic characteristics*, 2010, Google Patents.
5. Ajayan PM, S.O., Colliex C, Trauth D, *Aligned carbon nanotube arrays formed by cutting a polymer resin–nanotube composite*. Science, 1994: p. 265:1212–4.
6. Theodore, M., et al., *Influence of functionalization on properties of MWCNT–epoxy nanocomposites*. Materials Science and Engineering: A, 2011. **528(3)**: p. 1192-1200.
7. Frankland, S.J.V., et al., *Molecular Simulation of the Influence of Chemical Cross-Links on the Shear Strength of Carbon Nanotube–Polymer Interfaces*. The Journal of Physical Chemistry B, 2002. **106(12)**: p. 3046-3048.
8. Zhu, J., et al., *Reinforcing Epoxy Polymer Composites Through Covalent Integration of Functionalized Nanotubes*. Advanced Functional Materials, 2004. **14(7)**: p. 643-648.
9. Bilge, K., et al., *Structural composites hybridized with epoxy compatible polymer/MWCNT nanofibrous interlayers*. Composites Science and Technology, 2012. **72(14)**: p. 1639-1645.
10. De Volder, M.F., et al., *Carbon nanotubes: present and future commercial applications*. Science, 2013. **339(6119)**: p. 535-9.
11. Ajayan, P.M., *Nanotubes from Carbon*. Department of Materials Science & Engineering, Rensselaer Polytechnic Institute, Troy, New York 12180-3590, 1999. **Vol. 99, No. 7**: p. 1788-89, 1793-97.
12. Pulickel M. Ajayan, O.Z.Z., *Applications of Carbon Nanotubes*, in *Carbon Nanotubes*, M. Dresselhaus, G. Dresselhaus, and P. Avouris, Editors. 2001, Springer Berlin Heidelberg. p. 391-425.
13. Dimitrios Tasis, N.T., Alberto Bianco, and Maurizio Prato, *Chemistry of Carbon Nanotubes*. 2006: p. 1105.
14. Dai, H., *Carbon Nanotubes: Synthesis, Integration, and Properties*. Accounts of Chemical Research, 2002. **Vol. 35, No. 12**: p. 1035-44.
15. Melemez, F.F., *An Experimental Study On The Incorporation Of Carbon Nanotubes Into Resin Transfer Molded Composites*. 2013.
16. Szabó, A., et al., *Synthesis Methods of Carbon Nanotubes and Related Materials*. Materials, 2010. **3(5)**: p. 3092-3140.
17. al., C.S.e., *Interference and Interaction in Multiwall Carbon Nanotubes*. 2008.
18. Paul L. McEuen, M.S.F., and Hongkun Park, *Single-Walled Carbon Nanotube Electronics*. IEEE Transactions On Nanotechnology, 2002. **1**.
19. Coleman, J.N., et al., *Small but strong: A review of the mechanical properties of carbon nanotube–polymer composites*. Carbon, 2006. **44(9)**: p. 1624-1652.

20. B. Q. Wei, R.V., P. M. Ajayan, *Reliability and current carrying capacity of carbon nanotubes*. Vol. 79. 2001, Applied Physics Letters: American Institute of Physics.
21. Yu, M.-F., et al., *Strength and Breaking Mechanism of Multiwalled Carbon Nanotubes Under Tensile Load*. Science, 2000. **287**(5453): p. 637-640.
22. Ma, P.-C., et al., *Dispersion, interfacial interaction and re-agglomeration of functionalized carbon nanotubes in epoxy composites*. Carbon, 2010. **48**(6): p. 1824-1834.
23. Hilding, J., et al., *Dispersion of Carbon Nanotubes in Liquids*. Journal of Dispersion Science and Technology, 2003. **24**(1): p. 1-41.
24. Qian, H., et al., *Carbon nanotube-based hierarchical composites: a review*. Journal of Materials Chemistry, 2010. **20**(23): p. 4751-4762.
25. Sadeghian, R., et al., *Manufacturing carbon nanofibers toughened polyester/glass fiber composites using vacuum assisted resin transfer molding for enhancing the mode-I delamination resistance*. Composites Part A: Applied Science and Manufacturing, 2006. **37**(10): p. 1787-1795.
26. Rodriguez, A.J., et al., *Mechanical properties of carbon nanofiber/fiber-reinforced hierarchical polymer composites manufactured with multiscale-reinforcement fabrics*. Carbon, 2011. **49**(3): p. 937-948.
27. Thostenson, E.T., et al., *Carbon nanotube/carbon fiber hybrid multiscale composites*. Journal of Applied Physics, 2002. **91**(9): p. 6034-6037.
28. Garcia, E.J., B.L. Wardle, and A. John Hart, *Joining prepreg composite interfaces with aligned carbon nanotubes*. Composites Part A: Applied Science and Manufacturing, 2008. **39**(6): p. 1065-1070.
29. Bekyarova, E., et al., *Multiscale Carbon Nanotube–Carbon Fiber Reinforcement for Advanced Epoxy Composites*. Langmuir, 2007. **23**(7): p. 3970-3974.
30. Zhang, J., et al., *Functional interphases with multi-walled carbon nanotubes in glass fibre/epoxy composites*. Carbon, 2010. **48**(8): p. 2273-2281.
31. Sager, R.J., et al., *Effect of carbon nanotubes on the interfacial shear strength of T650 carbon fiber in an epoxy matrix*. Composites Science and Technology, 2009. **69**(7–8): p. 898-904.
32. Agarwal, S., J.H. Wendorff, and A. Greiner, *Use of electrospinning technique for biomedical applications*. Polymer, 2008. **49**(26): p. 5603-5621.
33. Bhardwaj, N. and S.C. Kundu, *Electrospinning: A fascinating fiber fabrication technique*. Biotechnology Advances, 2010. **28**(3): p. 325-347.
34. Taylor, G., *Disintegration of Water Drops in an Electric Field*. Proceedings of the Royal Society A: Mathematical, Physical and Engineering Sciences, 1964.
35. Adomaviciute, E. and R. Milasius, *The Influence of Applied Voltage on Poly(vinyl alcohol) (PVA) Nanofiber Diameter*. Fibers Textiles East Eur, 2007. **15**: p. 64-65.
36. Sukigara, S., et al., *Regeneration of Bombyx mori silk by electrospinning—part 1: processing parameters and geometric properties*. Polymer, 2003. **44**(19): p. 5721-5727.
37. Ki, C.S., et al., *Characterization of gelatin nanofiber prepared from gelatin–formic acid solution*. Polymer, 2005. **46**(14): p. 5094-5102.
38. Zong, X., et al., *Structure and process relationship of electrospun bioabsorbable nanofiber membranes*. Polymer, 2002. **43**(16): p. 4403-4412.
39. Doshi, J. and D.H. Reneker, *Electrospinning process and applications of electrospun fibers*. Journal of Electrostatics, 1995. **35**(2–3): p. 151-160.
40. Deitzel, J.M., et al., *The effect of processing variables on the morphology of electrospun nanofibers and textiles*. Polymer, 2001. **42**(1): p. 261-272.
41. Frenot, A. and I.S. Chronakis, *Polymer nanofibers assembled by electrospinning*. Current Opinion in Colloid & Interface Science, 2003. **8**(1): p. 64-75.

42. In-Yup Jeon, D.W.C., Nanjundan Ashok Kumar, Jong-Beom Baek, *Functionalization of Carbon Nanotubes*. p. 91-111.
43. Chou, T.-W., et al., *An assessment of the science and technology of carbon nanotube-based fibers and composites*. Composites Science and Technology, 2010. **70**(1): p. 1-19.
44. Hirsch, A., *Functionalization of Single-Walled Carbon Nanotubes*. Angewandte Chemie International Edition, 2002. **41**(11): p. 1853-1859.
45. Kim, S.W., et al., *Surface modifications for the effective dispersion of carbon nanotubes in solvents and polymers*. Carbon, 2012. **50**(1): p. 3-33.
46. Mickelson, E.T., et al., *Fluorination of single-wall carbon nanotubes*. Chemical Physics Letters, 1998. **296**(1-2): p. 188-194.
47. Chen, J., et al., *Solution Properties of Single-Walled Carbon Nanotubes*. Science, 1998. **282**(5386): p. 95-98.
48. Lim, J.K., et al., *Selective thiolation of single-walled carbon nanotubes*. Synthetic Metals, 2003. **139**(2): p. 521-527.
49. Xing Y, L.L., Chusuei CC, Hull RV, *Sonochemical oxidation of multiwalled carbon nanotubes*. Langmuir, 2005 p. 21(9):4185-90.
50. Del Canto, E., et al., *Critical Investigation of Defect Site Functionalization on Single-Walled Carbon Nanotubes*. Chemistry of Materials, 2011. **23**(1): p. 67-74.
51. Monthieux, M., et al., *Sensitivity of single-wall carbon nanotubes to chemical processing: an electron microscopy investigation*. Carbon, 2001. **39**(8): p. 1251-1272.
52. Banerjee, S., T. Hemraj-Benny, and S.S. Wong, *Covalent Surface Chemistry of Single-Walled Carbon Nanotubes*. Advanced Materials, 2005. **17**(1): p. 17-29.
53. Peng, K., et al., *Room temperature functionalization of carbon nanotubes using an ozone/water vapor mixture*. Carbon, 2011. **49**(1): p. 70-76.
54. Naveed A. Siddiqui, C.Y.L., Peng Cheng Ma , Jang-Kyo Kim, *Carbon Nanotubes with Dual Wall Structure; Properties and Fracture Behavior of Epoxy Nanocomposites*. p. 1-12.
55. Deb, A.K. and C.C. Chusuei, *Aqueous Solution Surface Chemistry of Carbon Nanotubes*. Physical and Chemical Properties of Carbon Nanotubes. 2013.
56. Li, M., et al., *Oxidation of single-walled carbon nanotubes in dilute aqueous solutions by ozone as affected by ultrasound*. Carbon, 2008. **46**(3): p. 466-475.
57. Vennerberg, D.C., et al., *Oxidation Behavior of Multiwalled Carbon Nanotubes Fluidized with Ozone*. ACS Applied Materials & Interfaces, 2014. **6**(3): p. 1835-1842.
58. Li, X., et al., *Noncovalent assembly of carbon nanotube-inorganic hybrids*. Journal of Materials Chemistry, 2011. **21**(21): p. 7527-7547.
59. Yi W, M.A., Chu Q, Sokolov AP, Colon ML, Meador M, Pang Y, *Wrapping of single-walled carbon nanotubes by a pi-conjugated polymer: The role of polymer conformation-controlled size selectivity*. J Phys Chem B 112(39), 2008: p. 12263-9.
60. Iijima, S., *Helical microtubules of graphitic carbon*. Nature 354, 1991: p. 56-58.
61. Andrews R, W.M., *Carbon nanotube polymer composites*. Curr Opin Solid State Mater Sci, 2004;8:31-7.
62. Damian, C.M., et al., *Covalent and non-covalent functionalized MWCNTs for improved thermo-mechanical properties of epoxy composites*. Composites Part B: Engineering, 2012. **43**(8): p. 3507-3515.
63. Banerjee, S., et al., *Ozonized single-walled carbon nanotubes investigated using NEXAFS spectroscopy*. Chem Commun (Camb), 2004(7): p. 772-3.
64. Ziegler, K.J., et al., *Controlled Oxidative Cutting of Single-Walled Carbon Nanotubes*. Journal of the American Chemical Society, 2005. **127**(5): p. 1541-1547.

65. Datsyuk, V., et al., *Chemical oxidation of multiwalled carbon nanotubes*. Carbon, 2008. **46**(6): p. 833-840.
66. Li, W., et al., *Effect of hydroxyl radical on the structure of multi-walled carbon nanotubes*. Synthetic Metals, 2005. **155**(3): p. 509-515.
67. Richter, E. and K.R. Subbaswamy, *Theory of Size-Dependent Resonance Raman Scattering from Carbon Nanotubes*. Physical Review Letters, 1997. **79**(14): p. 2738-2741.
68. Ferrari, A.C., et al., *Raman Spectrum of Graphene and Graphene Layers*. Physical Review Letters, 2006. **97**(18): p. 187401.
69. Davis, D.C., et al., *A strategy for improving mechanical properties of a fiber reinforced epoxy composite using functionalized carbon nanotubes*. Composites Science and Technology, 2011. **71**(8): p. 1089-1097.
70. Zhang, J., et al., *Reducing dispersity of mechanical properties of carbon fiber/epoxy composites by introducing multi-walled carbon nanotubes*. Composites Part B: Engineering, 2013. **54**(0): p. 371-376.
71. Zhou, Y., et al., *Improvement in mechanical properties of carbon fabric-epoxy composite using carbon nanofibers*. Journal of Materials Processing Technology, 2008. **198**(1-3): p. 445-453.
72. Hameed, N., et al., *Morphology, dynamic mechanical and thermal studies on poly(styrene-co-acrylonitrile) modified epoxy resin/glass fibre composites*. Composites Part A: Applied Science and Manufacturing, 2007. **38**(12): p. 2422-2432.
73. Gojny, F.H., et al., *Influence of nano-modification on the mechanical and electrical properties of conventional fibre-reinforced composites*. Composites Part A: Applied Science and Manufacturing, 2005. **36**(11): p. 1525-1535.
74. Barbero, E.J., *Introduction to Composite Materials Design, Second Edition*. 2010: Taylor & Francis.
75. Liao, Y.-T. and K.-C. Lee, *Effect of interface properties on the static and dynamic properties of unidirectional composites*. Journal of Applied Polymer Science, 1992. **44**(5): p. 933-936.
76. Tsai, J.-L. and N.-R. Chang, *Investigating damping properties of nanocomposites and sandwich structures with nanocomposites as core materials*. Journal of Composite Materials, 2011. **45**(21): p. 2157-2164.
77. Kenawy, E.-R., et al., *Electrospinning of poly(ethylene-co-vinyl alcohol) fibers*. Biomaterials, 2003. **24**(6): p. 907-913.
78. Huang, C.-F. and F.-C. Chang, *Comparison of hydrogen bonding interaction between PMMA/PMAA blends and PMMA-co-PMAA copolymers*. Polymer, 2003. **44**(10): p. 2965-2974.
79. Ozden, E., Y.Z. Menciloglu, and M. Papila, *Engineering chemistry of electrospun nanofibers and interfaces in nanocomposites for superior mechanical properties*. ACS Appl Mater Interfaces, 2010. **2**(7): p. 1788-93.
80. Keusch, S. and R. Haessler, *Influence of surface treatment of glass fibres on the dynamic mechanical properties of epoxy resin composites*. Composites Part A: Applied Science and Manufacturing, 1999. **30**(8): p. 997-1002.